Structural Characterization and Control of Organized Polymer Systems by Photoprocesses

TAKANORI HAYASHI

1995

Contents

General Introduction

General Introduction

GI-1. Background and Motivation of This Thesis

There are various organized molecular systems in nature. The organized structures have important roles in various biological processes such as selective transport, selective permeation, energy transfer, energy conversion, and metabolism. These structures are highly organized, and the arrangements of these structures are closely related to their unique functionalities. Recently, varioius artificial organized molecular system having a specific arrangement have been designed, and its unique properties and chemical reactivity have been studied.

The photophysical functionality of these highly organized molecular systems is gathering interest. The photosynthesis of plants is a kind of energy converting system with high efficiency in nature, and vision is a kind of information transfer system. They require organized molecular assemblies. In the field of application, many photofunctional materials have been made. For example, photoresists have been developed for a large scale integrated circuit (LSI) and the information industry is greatly indebted to this technology.

The purpose of this study is to analyze the structure of those organized molecular assemblies by using an excited state intermolecular interaction and to control the ordered structure by photoreaction. In this study, an ultrathin film highly ordered in the direction to the layer thickness was fabricated by using the Langmuir-Blodgett technique, and the film structure was analyzed. A liquid crystal film was prepared from a liquid crystalline polymer and the phase transtion behavior induced by UV irradiation on this film was studied. The thesis is divided into two parts. In part 1, the organized polymer structure made by the Langmuir-Blodgett technique was examined by the fluorescence method. In part 2, the control of the highly oriented structure of the liquid crystalline phase was attempted by using a photochemical reaction, i.e., photoisomerization. Some basic studies were made on the structural characterization and phase transition control

of the organized polymer systems by use of photoprocess: energy transfer and photoisomerization. In the next section, the following terms are briefly explained: 1) excited energy transfer processes, 2) the Langmuir-Blodgett technique to fabricate highly ordered structures, and 3) liquid crystals, especially side chain liquid crystalline polymers and the phase transition behavior controlled by the guest-host effect.

GI-2. Short Survey on Energy Transfer Processes

Energy transfer is defined as the donation of excitation energy from one molecule to another. One of the most general forms of electronic energy transfer can be represented by

$$D^* + A \rightarrow D + A^* \quad ...(1)$$

where D represents a donor molecule, A represents an acceptor molecule and * denotes the electronically excited state. Energy transfer occurs through two processes; one is a radiative process, and the other is a non-radiative process. The radiative transfer process consists of sequential emission of fluorescence or phosphorescence from the donor molecule D^* and the reabsorption of the donor emission by the acceptor molecule A. This process can be represented by

$$D^* \rightarrow D + h\nu \quad ...(2)$$

$$h\nu + A \rightarrow A^* \quad ...(3)$$

The absorption spectrum of the acceptor must overlap with the emission spectrum of the donor and the intervening medium should be transparent to the light at the wavelengths of the absorption and emission bands.

The non-radiative transfer process is a long-range transfer of electronic excitation which occurs even if the separation distance of the donor and the acceptor is several times larger than the collision diameter. At this distance, only the coulombic interaction is important and electron-exchange effects can be negligible. Förster developed a quantitative relation expressed in terms of experimentally obtainable parameters for the rate of resonance energy transfer originating in dipole-dipole interactions between an isolated donor and acceptor

pair.[11] The conditions favoring energy transfer are a large overlap between the absorption band of the acceptor molecule and the emission band of the donor molecule, and a high fluorescence yield of the donor molecule. The efficiency of intermolecular dipole-dipole transitions is expressed in terms of the critical separation distance R_0 at which the probability of transfer is equal to that of spontaneous decay. From Förster's equation, R_0 is given by

$$R_0^6 = [\ 9000(\ln 10)\kappa^2\phi_D / (128\pi^6 n^4 N)\ ] \int_0^\infty F_D(\bar{\nu})\epsilon_A(\bar{\nu})d\bar{\nu} / \bar{\nu}^4 \quad ...(4)$$

in which N is Avogadro's number, n is the refractive index of the medium, κ^2 is an orientation factor, usually assumed to be 2/3 for a random distribution of D and A, ϕ_D is the quantum yield for emission from the donor, $F_D(\bar{\nu})$ is the fluorescence emission spectrum of the donor normalized to unity, $\epsilon_A(\bar{\nu})$ is the molar extinciton coefficient of the acceptor as a function of $\bar{\nu}$. It is important to note that for this mechanism, the spin conservation law is applied to the donor and acceptor molecules individually, and no change in spin is allowed in the donor and acceptor during transfer. Thus singlet-state energy transfer is certainly allowed, although triplet-triplet energy transfer is forbidden.

GI-3. Short Survey on Langmuir-Blodgett Film

The Langmuir- Blodgett (LB) technique is one of the most attractive methods to achieve artificial molecular assemblies. The thickness of the LB film is controlled by the chain length of amphiphilic compounds and the number of the deposited monolayers. The LB technique can also provide highly ordered molecular assemblies with well-defined molecular orientation. One can design LB films having various functionalities in a molecular level by depositing monolayers which have different properties. A great number of studies have been made on LB films.[12,13]

Studies on monolayers began toward the end of the last century.[14,15] In the

beginning of this century, Langmuir developed the experimental and theoretical concepts which underlie our current understanding of monolayers, by studying a well defined series of fatty acid salts.[16] The first detailed description of sequential monolayer deposition was given by Blodgett in the 1930's.[17,18] Langmuir demonstrated that the thickness of a monolayer is one molecule and that the molecules are oriented at the water surface, with the polar functional group immersed in the water and the long nonpolar chain directed nearly vertically up from the surface.

Gaines[19] summarized these early works comprehensively and divided the substances, which are capable of forming Langmuir-Blodgett films, into two classes;

(1) Simple, nonpolymeric substances which are substantially insoluble, but whose molecules have sufficient attraction to the subphase to permit them to spread and disperse at the surface.

(2) Polymeric materials which are positively adsorbed at the liquid-gas interface.

The contamination of the water subphase should be removed carefully because the existance of surfactants also gives a great influence on the formation of monolayer. The substance is dissolved in an adequate solvent such as benzene or chloroform and spread onto the water surface quietly. Then a suitable substrate is normally dipped and raised vertically through the monolayer. The most common deposition mode is to stack in a head-to-head and tail-to-tail configuration, which is called the Y-type deposition. However, some monolayers do not stack on this manner. When the deposition occurs only with down modes, this is called the X-type deposition. When the deposition occurs only with up modes, it is called the Z-type deposition. These three deposition types are shown in Figure GI-1.

Many experimental techniques have been used to study LB films. For example, ellipsometry, electron spin resonance, infra-red dichroism, surface potential, and polarized resonance Raman spectroscopy are used for the characterization experiments.[20] For a more complete assessment of the film

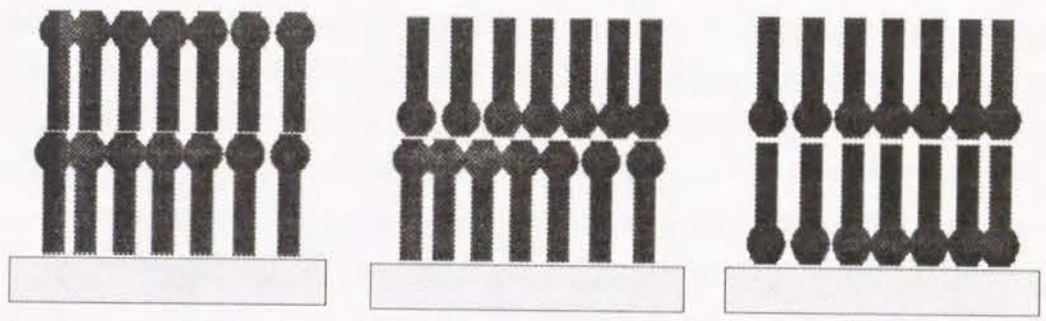

Figure GI-1. Three different types of deposition onto solid substrate. The deposition which occurs only at down-modes is called the X type. The deposition which occurs both at up- and down-modes is called the Y type, and the one which occurs only at up-modes is called the Z type. A circle represents hydrophilic part of the molecule and a rectangular represents hydrophobic part of the molecule. A commonly used deposition mode is the Y type, where the molecules stack vertically with a head-to-head and tail-to-tail configuration.

structure, electron diffraction, transmission electron microscopy,[21] X-ray diffraction,[22,23] neutron diffraction,[24] and surface plasmon[25] are also introduced to the experiment.

LB films are of great interest as model systems in fundamental research. Kuhn and his colleagues studied photophysical and photochemical processes such as excited energy transfer, migration, and electron transfer with various molecular arrangements containing chromophoric groups.[26-28] They constructed molecular assemblies of functional units with an energy donating molecule (D) and an appropriate energy acceptor molecule (A). D and A could be fixed at any intended distance by choosing an appropriate number of spacer layers and an appropriate number of carbon atoms in the fatty acid used as the spacer. Notable achievement has been made in the successful series of experiments for investigation of the Förster type of energy transfer. Related works have been carried out by Kilsreiter,[29] Leitner.[30] Yamazaki demonstrated by time-resolved fluorescence spectroscopy that the chromophoric guest molecules tend to aggregate in the fatty acid monolayer.[31]

Although conventional LB films are prepared from low molecular-weight compounds such as long alkyl chain fatty acids, these LB films are usually poor in thermal and mechanical stability. To solve these problems, various polymeric LB films have been widely examined.[32,33] There are two types of polymer LB films. One is the polymerization of amphiphilic monomers after spreading onto the water surface or depositing onto the substrate.[34-36] Another is the deposition of preformed polymeric monolayers. The latter type of LB film was firstly reported by Tredgold.[37] Since then several polymeric LB films[38-41] have been examined. Swallen et al. studied the molecular orientation in the monolayers and LB films of poly(octadecyl methacrylate) by infrared spectroscopy.[42] Schouten[43] et al. studied the monolayer behavior of poly(methyl methacrylate) with various tacticities. Miyashita synthesized a series of polyacrylamide derivatives and studied their properties as LB films.[44]

The aggregation of chromophores can be prevented by the introduction

of chromophoric groups into polymer LB films.[45] Therefore, it is possible to attain a homogeneous distribution of chromophore for studying the structure of polymer LB films.

GI-4. Short Survey on Liquid Crystalline Polymer and Phase Transition

Low molecular weight liquid crystalline compounds have been known for more than 100 years.[46,47] However, liquid crystalline polymers have attained prominence only in the last quarter century. In 1975, de Gennes predicted theoretically that polymers which have rigid longitudinal mesogenic element and flexible element become nematic liquid crystal.[48] The interests to liquid crystalline polymers greatly increased in the latter half of the 1970's, and a number of thermotropic polyesters have been synthesized since then.[49]

Liquid crystalline polymers can be classified into two types; in one type of a liquid crystalline polymers, the mesogenic groups are located in the polymer main chain. These polymers are known as main chain liquid crystalline polymers. Because of high orientation of polymer backbone in the liquid crystalline state, the main chain liquid crystalline polymers have high elasticity and high strength. It is a promising material in the field of engineering plastics. In the other type of liquid crystalline polymers, the mesogenic groups are attached to the polymer main chain with a linkage of carbon chains[50-52] or siloxane chains[53-55] in a side-chain-like manner. Such polymers are known as side chain liquid crystalline polymers. Polymers with mesogenic side chains are usually thermotropic. Although the liquid crystalline properties of the polymers are related to those of the low molecular weight analogues, the differences are due mainly to high melt viscosity and the interaction of the polymer backbone chain and the mesogenic groups. The high viscosity impedes structural rearrangements caused by external fields. Moreover, the polymer backbone chain tends to take a random-coil configuration, and the mesogenic side groups tends to organize in liquid crystalline phases causing a certain interaction between the main chain and side

chains. This interaction may be loosened to some extent by inserting spacer groups between the backbone chain and the mesogenic groups.[50,52] Side chain liquid crystalline polymers have the advantages of orientation control and phase control, which may enable the developement of novel functional materials such as thermosensor, optical filter,[11] selective permeation membrane,[57] and heat writable film.[58]

One of the important aspects of the liquid crystal is that the position of the director is greatly influenced by an electric or magnetic field. Highly oriented liquid crystalline polymer films with mesogenic side chains can be used to store information. The "writing" is stored at temperatures below the polymer Tg but may be erased by heating or applying an electric field to different direction. A polysiloxane with highly polar cyanobiphenyl in the side chains can be used as an electro-optical storage system.[59] Because of polydispersity, these materials exhibit a wide biphasic region above 80℃. An opaque randomly oriented polymer layer in the biphasic region can be converted to homeotropically transparent areas by an alternating electric current. Wide application perspectives for these polymers are promising as optical components in linear and non-linear optics. Furthermore, novel optical memory materials can be materialized.

Recently, liquid crystalline display devices utilizing a guest-host effect are widely accepted.[60-63] The addition of a non-mesomorphic solute to a nematic liquid crystal impedes the liquid crystalline formation.[64-70] If the structure of the guest molecule is not very different from that of the mesogen, they can coexist forming a single liquid crystal phase. In this case, the temperature range of the liquid crystalline state depends on the structure and concentration of the guest molecules.[71-73] If the structure of guest molecules is greatly changed by an external stimulation, these guest molecules disturb the liquid crystal formation considerably and cause the phase transition from nematic liquid crystalline phase to isotropic phase. Thus, phase transition can be controlled by the structural change of the guest molecules. An effective method to induce a structural change of guest molecules is to use photoisomerization.[74-77] Figure GI-2 shows the general

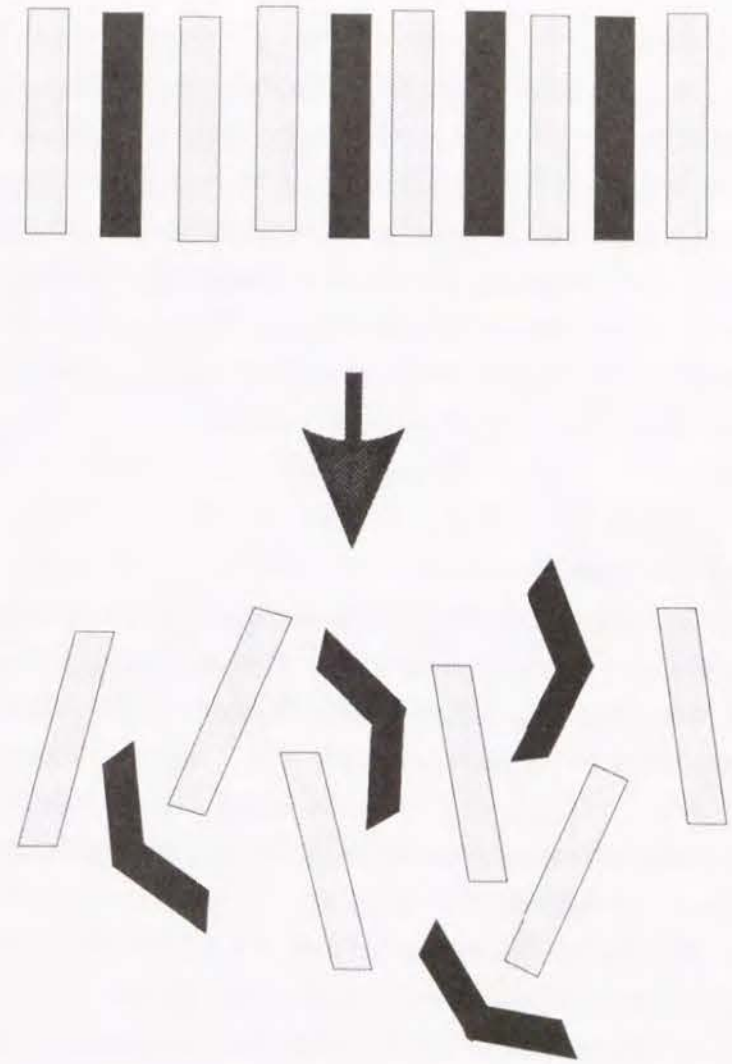

Figure GI-2. The guest-host effect of liquid crystalline structure. Gray rectangles represent liquid crystal (LC) and black rectangles represent photosensitive molecules (PM). When PM absorbs light at a specific wavelength, it changes its shape and disturbs the liquid crystal formation. This phase transition can be made reversible by choosing appropriate photosensitive molecules.

concept of controlling liquid crystal formation by photoisomerization. When the photosensitive guest molecules take a trans form, they do not interfere with the liquid crystal formation. However, once the trans form of guest molecules is photoisomerized to a cis form by specific UV irradiation, they greatly interfere with the liquid crystal formation. An advantage of photoisomerization is reversibility. One can "write" information by a specific UV light and erase it by a UV light of another wavelength or heating. To improve the ability of storage, a photosensitive polymer with mesogenic side chains is promising as a recording material.

GI-5. Outline of This Thesis

This thesis concerns highly organized polymer systems studied by analyzing and utilizing photoprocesses. The main subjects are the structural relaxation process and the phase transition behavior of the systems. The thesis is divided into two parts.

Part I (Chapter 1 - 6) describes the thermal stability of polymeric Langmuir-Blodgett films and in situ study of a polymer monolayer on the water surface by using the fluorescence method.

In Chapter 1, poly(vinyl pentanal acetal) (PVPe) and its derivatives were synthesized as amphiphiles and deposited onto a solid substrate as a LB film. Then, the thermal stability of the PVPe LB film was examined by the interlayer energy transfer from energy donor to acceptor moieties labeled to the polymer chain. The theoretical calculation based on Förster kinetics was applied to this phenomenon and the experimental data was fitted with the calculation curve by assuming a Gaussian distribution of chromophores in the direction normal to the layer plane. The diffusion constant (D) and the apparent activation energy (ΔE) of polymer segments were also evaluated by fitting with the experimental data.

In Chapter 2, poly(vinyl butanal acetal) (PVB), poly(vinyl octanal acetal) (PVO), and their derivatives were synthesized as the amphiphiles for LB deposition. The distribution of energy donating and accepting polymer segments

was measured by the energy transfer method as a function of time and temperature. The critical temperature, (T_C), at which the rapid increase of transfer efficiency starts, was discussed in comparison with the glass transition temperature (Tg) of the corresponding polymers in the bulk state. A numerical calculation by Monte Carlo method was applied to the experimental results to yield the diffusion constants and activation energies for the polymer diffusion.

In Chapter 3, the thermal stability of various kinds of Langmuir-Blodgett films, poly(vinyl octanal acetal) (PVO), poly(diisopropyl fumarate) (PDiPF), poly(dicyclohexyl fumarate) (PDcHF), and poly(isobutyl methacrylate) (PiBMA) was examined by the energy transfer method. These films were sandwiched by a pair of energy donating and accepting PVO layers as the probes. The structural relaxation of the other polymeric Langmuir-Blodgett films as well as poly(vinyl alkanal acetal) was discussed in relation to their glass transition temperatures of the corresponding polymer bulk. In this case, the misciblity between the examined layer and probe layers was an important factor. The effects of molecular weight and the initial spatial arrangement of LB layers on the structural relaxation were also examined.

In Chapter 4, the author applied this energy transfer method to a fatty acid multilayer. The structure of the Langmuir-Blodgett film composed of cadmium stearate and poly(vinyl octanal acetal) was investigated by the energy transfer method. The direct observation of the thermal relaxation process of composite film was also carried out by a transmission electron microscopy. The former method was very sensitive to the alteration of layer distance, i. e., to the microscopic structural relaxation of the layered structure. On the other hand, the latter method was useful to understand the macroscopic structural relaxation of the film.

In Chapter 5, photoreactive Langmuir-Blodgett films were made of poly(vinyl octanal acetal-*co*-vinyl cinnamate) (P(VO-VC)) and UV-irradiated to induce photocrosslinking of the polymer layers. The effect of photocrosslinking on the durability of P(VO-VC) layers against chemical treatment was examined by UV absorption spectra and solubility experiment. Furthermore, the difference

in thickness between the UV exposed and unexposed regions was measured by surface plasmon spectroscopy. The curing effect on the thermal relaxation of the layered structure was studied by the energy transfer method.

In Chapter 6, in situ studies of the structures and properties of monolayer films on the water surface were done by the fluorescence method. Poly(vinyl alkanal acetal)s were synthesized, and a part of the side chains was labeled with pyrene chromophores. Fluorescence intensity and lifetime of pyrenes were measured and the influence of the atmosphere on the emission intensity and the lifetime of the monolayer on the water surface was examined. The dynamic behavior of the monolayer was determined by measuring the excimer formation of pyrenes. Time-resolved measurements were employed to examine the mobility of the monolayer.

Part II (Chapter 7,8) describes the control of phase transition by photoisomerization of photosensitive group in the system.

In Chapter 7, a low molecular weight liquid crystal was mixed with a photoisomerizable molecule. The conditions of induced phase transition were examined for two different liquid crystal mixtures. One was a mixture of the low molecular weight liquid crystal with the low molecular weight azo compound, and the other was a mixture of the low molecular weight liquid crystal with the azo polymer. The effects of the concentration of guest molecules and of UV irradiation on these mixtures were examined. The mixture was examined with its feasibility as a photo-recording material.

The phase separation between liquid crystal and azobenzene compounds gave rise to inhomogeneity, a serious defect as the recording material. In Chapter 8, liquid crystalline copolymers containing 4'-cyanobiphenyl-4-oxyundecylacrylate (CBO-11-A) groups and phenylazophenyloxy-undecylacrylate (ABO-11-A) groups in various proportions were synthesized as non-aggregating samples. The liquid crystalline behavior of the copolymers was examined with respect to azo concentrations. Isothermal phase transition of the copolymers was induced by the photoisomerization of azobenzene moiety by irradiation of 365 nm light. The response time of this phase transition was measured by using a strong

laser pulse (351 nm).

References

(1) Parker, C.A. *Photoluminescence of Solutions*; Elsevier, Amsterdam, 1968.

(2) Birks, J. B. *Photophysics of Aromatic Molecules*; Wiley, New York, 1970.

(3) Phillips, D. *Polymer Photophysics*; Chapman and Hall, London, 1985.

(4) Guillet, J. *Polymer Photophysics and Photochemistry*; Cambridge University Press, Cambridge, 1985.

(5) Govindjee, R. *Bioenergetics of Photosynthesis*; Academic Press, 1975.

(6) Kaneko, M.; Yamada, A. *J. Phys. Chem.* **1977**, *81*, 1213.

(7) Dolphin, D. *The Porphyrins, Vol. 1*; Academic Press, New York, 1978.

(8) Willson, C.G.; Ito, H.; Frechet, J. M. J.; Tessier, T. G.; Houlihan, F. M. *J. Electrochem. Soc.* **1986**, *133*, 181.

(9) Bowden, M. J.; Thompson, L. F.; Farenholtz, S. R.; Doerries, E. M. *J. Electrochem. Soc.* **1981**, *128*, 1304.

(10) Smith, D. K. *Photographic Science and Engineering* **1968**, 263.

(11) Förster, Th. *Naturforsch.* **1949**, *4A*, 321.

(12) Ulman, A. *An Introduction to Ultrathin Organic Films from Langmuir-Blodgett to Self-Assembly*; Academic Press, San Diego 1991.

(13) Roberts, G. G. *Adv. Phys.* **1985**, *34*, 475.

(14) Rayleigh, Lord, *Proc. Soc.* **1890**, *47*, 364.

(15) Pockels, A. *Nature* **1891**, *43*, 437.

(16) Langmuir, I. *J. Am. Chem. Soc.* **1917**, *39*, 1848.

(17) Blodgett, K. B. *J. Am. Chem. Soc.* **1935**, *57*, 1007.

(18) Blodgett, K. B. *Phys. Rev.* **1939**, *55*, 391.

(19) Gaines, Jr. G. L. *Insoluable Monolayers at Liquid-Gas Interfaces*; Wiley-Interscience, New York, 1966.

(20) Robert, G. G.; Pitt, C. W. *Thin Solid Films*, **1983** *99*,

(21) Peterson, I. R.; Russell, G. J.; Roberts, G. G. Thin Solid Films **1983**, *109*, 371.

(22) Matsuda, A.; Sugi, M.; Fukui, T.; Iizima, S. *J. Appl. Phys.* **1977**, *48*, 771.

(23) Ohnishi, T.; Ishitani, A.; Ishida, H.; Yamamoto, N.;Tsubomura, *H. J. Phys. Chem.* **1978**, *82*, 1989.

(24) Nicklow, R. M.; Pomerantz, M.; Segmuller, A. *Phys. Rev. B* **1981**, *23*, 1081.

(25) Brown, C. A.; Burns, F. C.; Knoll, W.; Swalen, J. D. *J. Phys. Chem.* **1983**, *87*, 3616.

(26) Kuhn, H.; Möbius, D.; Bücher, H. *Physical Methods of Chemistry*; Weissberger, A. and Rossiter, B. Eds.; Wiley, New York 1972.

(27) Kuhn, H. *Thin Solid Films* **1983**, *99*, 1.

(28) Kuhn, H. *Thin Solid Films* **1989**, *178*, 1.

(29) Killesreiter, H. *Ber. Bunsenges Phys. Chem.* **1978**, *82*, 503.

(30) Leitner, A.; Lippitisch, M.E.; Draxler, S.; Riegler, M.; Aussenegg, F. R. *Thin Solid Films* **1985**, *132*, 55.

(31) Yamazaki, I.; Tamai, N.; Yamazaki, T.; murakami, A.; Mimuro, M.; Fujita, Y. *J. Phys, Chem.* **1988**, *92*, 5035.

(32) Miyashita, T. *Prog. Polym. Sci.* **1993**, *18*, 263.

(33) Breton, M. *J. Macromol. Sci., Rev. Macromol. chem.* **1981**, *C21*, 61.

(34) a) Miyashita, T.; Yoshida, H.; Matsuda, M. *Thin Solid Films* **1987**, *155*, L11. b)Miyashita, T.; Yoshida, H.; Murakata, T.; Matsuda, M. *Polymer* **1987**, *28*, 311. c) Miyashita, T.; Matsuda, M. *Thin Solid Films* **1989**, *168*, L47. d) Miyashita, T.; Sakaguchi, K.; Matsuda, M. *Polymer* **1990**, *31*, 461. e) Miyashita, T.; Sakaguchi, K.; Matsuda, M. *Langmuir* **1992**, *8*, 336. f) Miyashita, T.; Yoshida, H.; Ito, H.; Matsuda, M. *Nippon Kagaku Kaishi* **1987**, 2169.

(35) Laschewsky, A.; Ringsdorf, H. *Macromolecules* **1988**, *21*, 1936.

(36) a) Wegner, G. *Z. Naturforsch., Teil B* **1969**, *24*, 824. b) Wegner, G. *Pure Appl. Chem.* **1977**, *49*, 443. c) Lieser, G.; Tieke, B.; Wegner, G. *Thin Solid Films* **1980**, *68*, 77. d) Bubeck, C.; Tieke, B.; Wegner, G. *Ber. Bunsenges, Phys. Chem.* **1982**, *86*, 495.

(37) a) Tredgold, R. H.; Winter, C. S. *J. Phys. D: Appl. Phys.* **1982**, *15*, L55. b) Tredgold, R. H. *Thin Solid Films* **1987**, *152*, 223.

(38) Shigehara, K.; Hara, M.; Nakahama, H.; Miyata, S.; Murata, Y.; Yamada, A. *J. Am. Chem. Soc.* **1987**, *109*, 1237.

(39) Naito, K. *J. Colloid Interface Sci.* **1989**, *131*, 218.

(40) Duda, G.; Schouten, A.J.; Arndt, T.; Lieser, G.; Schmidt, G. F.; Bubeck, C.; Wegner, G. *Thin Solid Films* **1988**, *159*, 221.

(41) Watanabe, M.; Kosaka, Y.; Oguchi, K.; Sanui, K.; Ogata, N. *Macromolecules* **1988**, *21*, 2997.

(42) Mumby, S. J.; Swalen, J. D.; Rabolt, J. F. *Macromolecules* **1986**, *19*, 1054.

(43) a) Brinkhuis, R. H. G.; Schouten, A. J. *Macromolecules* **1991**, *24*, 1487. b) Brinkhuis, R. H. G.; Schouten, A. J. *Macromolecules* **1991**, *24*, 1496.

(44) Miyashita, T.; Mizuta, Y.; Matsushita, M. *Br. Polym. J.* **1990**, *22*, 327.

(45) Ohmori, S.; Ito, S.; Yamamoto, M.; Yonezawa, Y.; Hada, H. *J. Chem. Soc. Chem. Commun.* **1989**, 1293.

(46) Reinitzer, F. *Monatch.* **1888**, *9*, 421.

(47) Lehmann, O. *Flüssige Kristalle*; Engelmann, Leipzig. 1904.

(48) de Gennes, P. G. *C. R. Acad. Sci.*; Paris, **1975**, *B281*, 101.

(49) Jin, J. I.; Antoun, S.; Ober, C.; Lenz, R. W. *Brit. Polym. J.* **1980**, 132.

(50) Finkelmann, H.; Rehage, G. *Liquid Crystal Polymers II/III 60/61 of Advances in Polymer Science Series*; Gordon, M. Ed.; Springer-Verlag, New York, 1984; p99.

(51) Ober, C. K.; Jin, J. I.; Lenz, R. W. *ibid.* p103.

(52) Shibaev, V. P.; Plate, N. A. *ibid.* p173.

(53) Finkelmann, H.; Rehage, G. *Makromol. Chem. Rapid Commun.* **1980**, *1*, 31.

(54) Gemmel, P. A.; Gray, G.W.; Lacey, D. *Mol. Cryst. Liq. Cryst.* **1985**, *122*, 205.

(55) Ringsdorf, H.; Schneller, A. *Makromol. Chem. Rapid Commun.* **1982**, *3*, 557.

(56) Tsutsui, T.; Tanaka, R. *Polym.* **1981**, *22*, 117.

(57) Terada, I.; Washizu, S.; Kajiyama, T.; Takayanagi, M.; Koide, N.; Iimura, K. *Rept. Progr. Polym. Phys. Japan.* **1983**, *26*, 227.

(58) Shibaev, V. P.; Kostromin, S.G.; Plate, N. A.; Ivanov, S. A.; Vetrov, V. Y.; Yakkovlev, I. A. *Polym. Commun.* **1983**, *24*, 364.

(59) Coles, H. J.; Simon, R. *Recent Advances in Crystalline Polymers*; Chapoy, L. L. Ed.; Elsevier Applied Science publishers, Ltd., Barking UK, 1984; Chapt. 22, p323.

(60) Heilmeier, G. H.; Zanoni, L. A. *Appl. Phys. Lett.* **1968**, *13*, 91.

(61) Heilmeier, G. H.; Castellano, J. A.; Zanoni, L. A. *Mol. Cryst. Liq. Cryst.* **1969**, *8*, 293.

(62) Morita, M.; Imamura, S.; Yatabe, K. *Jpn. J. Appl. Phys.* **1975**, *14*, 315.

(63) White, D. L.; Taylor, G. N. *J. Appl. Phys.* **1974**, *45*, 4718.

(64) Martire, D. E. *The Molecular Physics of Liquid Crystals*; Luckhurst, G. R. and Gray, G. W. Eds.; Acad. Press, London, New York, San Francisco, 1979; Chapt. 10.

(65) Oweimreen, G. A.; Lin, G. C.; Martire, D. E. *J. Phys. Chem.* **1979**, *83*, 2111.

(66) Oweimreen, G. A.; Martire, D. E. *J. Chem. Phys.* **1980**, *72*, 2500.

(67) Oweimreen, G. A.; Hasan, M. *Mol. Cryst. Liq. Cryst.* **1983**, *100*, 357.

(68) Oweimreen, G. A.; Shibab, A. K.; Halhouki, K.; Sikander, S. F. *Mol. Cryst. Liq. Cryst.* **1986**, *138*, 327.

(69) Esnault, P.; Volino, F.; Gauthier, M. M.; Ciroud-Godquin, A. M. *Mol. Cryst. Liq. Cryst.* **1986**, *139*, 217.

(70) Kozielski, M. Bauman, D.; Drozdowski, M.; Salamon, Z. *Mol. Cryst. Liq. Cryst.* **1987**, *142*, 1.

(71) Haase, W.; Trinquet, O.; Quotschalla,U.; Foitzik, J. K. *Mol. Cryst. Liq. Cryst.* **1987**, *148*, 15.

(72) Salamon, Z.; Bauman, D. *Mol. Cryst. Liq. Cryst. Lett.* **1982**, *82*, 115.

(73) Kuball, H. -G.; Altschuh, J.; Kulbach, F.; Schönhofer, A. *Helv, Chim. Acta* **1978**, *61*, 571.

(74) Ringsdorf, H.; Urban, C. *Makromol. Chem.* **1992**, *193*, 1235.

(75) Cabrera, I.; Krongauz, V.; Ringsdorf, H. *Angew. Chem. Int. Ed. Engl.* **1987**, *26*, 1178.

(76) Eich, M.; Wendorff, J. H. *Makromol. Chem., Rapid Commun.* **1987**, *8*, 67.

(77) Ikeda, T.; Horiuchi, S.; Karanjit, D.B.; Kurihara, S.; Tazuke, S. *Macromolecules* **1990**, *23*, 36.

Part I

Structural Characterization of Ultra-thin Polymer Films

Chapter 1

Fluorescence Study of Polymer Diffusion and Its Analysis with an Approximate Calculation for a Layered Structure of Poly(vinyl pentanal acetal) Langmuir-Blodgett Films

1-1. Introduction

The Langmuir-Blodgett technique is an effective method to fabricate artificial molecular assemblies. It enables one to control the thickness of the layers by modifying the chain length of amphiphilic molecules, and to arrange the multilayer structures by changing the substance at the molecular level. It also may permit fabrication of a highly ordered film with molecular orientation. In the LB film, one can expect to observe new aspects of chemical, physical, electrical, and biological processes. Over the past few decades, a considerable number of studies have been made on LB films.[1-3]

In the field of photophysics and photochemistry, Kuhn et al. have studied fundamental photophysical processes.[4] They proved that basic photo-processes such as energy transfer and electron transfer can be controlled by the nano-scale structure fabricated by the LB technique. They showed that the Förster theory[5] for the excitation energy transfer can explain the phenomenon in the real systems. This means that the reverse is also possible; the layered structure of LB films can be probed by the energy transfer.

Recently, to improve the stability of LB films, polymer LB films have been examined extensively.[6-15] Ringsdorf et al. studied the structural stability of LB films prepared from macrolipids which consist of two-chain surfactants interconnected by hydrophilic polymer chains.[9] The X-ray reflection measurement indicated that the thermal stability is improved markedly by the adjustment of the molecular flexibility. Rabolt et al. also examined the stability of polymeric LB film by polarized infrared spectroscopy.[11] The hydrophobic side chain attached to

a hydrophilic main chain showed a high degree of orientation. The orientation was disordered by heating, but it was mostly recovered during the cooling process.

Poly(vinyl alkanal acetal) has been studied as a representative of amorphous polymeric LB materials,[16-19] because it shows excellent properties on the deposition process; the transfer ratio of the monolayer onto various kinds of substrates was kept unity over a wide range of the conditions, and the resulting LB films showed clear evidence that the deposition was successfully carried out. Furthermore, this polymer is useful as a base polymer to which various functional and probing moieties can be introduced.[20]

In this chapter, the diffusion process of polymer segments in the amorphous polymer LB films is discussed. A theoretical calculation for the relaxation processes based on Förster kinetics[5] is applied to the experimental results to evaluate the diffusion coefficient quantitatively.

1-2. Experimental Section

1-2-1. Materials

Poly(vinyl pentanal acetal) (PVPe) and its derivatives were synthesized by acetalization of commercial Poly(vinyl alcohol) (PVA) (Wako Chemicals, dp=2000) with pentanal and chromophoric aldehydes, according to the procedure of Ogata et al.[10] PVA powder (0.5g), pentanal, and chromophoric aldehyde were mixed in 10 ml of chloroform containing two drops of hydrochloric acid. The reaction mixture was stirred for 24 h at 40℃. PVA powder dissolved in the solution as the acetalization proceeded. After the reaction, the solution was diluted with 40 ml of chloroform, and poured into 1 L of methanol containing a trace amount of sodium hydroxide. The polymer was purified by reprecipitation from benzene into methanol three times and then freeze-dried from benzene solution in vacuo. The chemical structures of the resulting polymers are shown in Chart 1-1.

Three kinds of PVPe were prepared: unlabeled PVPe for the spacing and protection layer, phenanthrene labeled polymer (PVPe-P) for the energy donating layer, and anthracene labeled polymer (PVPe-A) for the energy accepting layer.

Table 1-1 represents the compositions of pentanal unit (x) and chromophoric unit (y) which were determined from the elemental analysis and UV absorption spectra.

1-2-2. Sample Preparation

Pure water for the subphase was ion-exchanged, distilled and then finally passed through a purification system (Barnstead Nanopure II). A benzene-methanol (9:1) solution of each polymer (0.01 wt%) was spread on pure water at 19℃ in a Teflon-coated trough. The surface film was compressed at a rate of 10 mm min^{-1}, and transferred vertically onto a substrate at 20 mN m^{-1} for PVPe, 17.5 mN m^{-1} for PVPe-P, 18 mN m^{-1} for PVPe-A, respectively.

A non-fluorescent quartz plate (10 mm x 40 mm) was used as a substrate for the fluorescence measurements. It was cleaned in sulfuric acid containing a small amount of potassium permanganate, dipped in 10% hydrogen peroxide solution, and then washed with water repeatedly. To make the quartz plate hydrophobic, it was soaked in a toluene solution of trimethylchlorosilane (10%) for 30 min. Under these conditions, a good transfer ratio was obtained in both the up and down modes, yielding a Y-type built-up film.

Figure 1-1 illustrates the structure of the LB films for energy-transfer measurements. The sample films were fabricated on a quartz plate in the following sequence: (1) four layers of PVPe for the precoating layers, (2) two layers of PVPe-P for the energy donating layers, (3) n layers (n=0,4,8) of PVPe for the spacer between the donating layers and the accepting layers, (4) two layers of PVPe-A for the energy accepting layers, (5) (10-n) layers of PVPe for the protecting layers. To fix the composition of the film, the total number of layers was kept constant to be 18 layers by adjusting the number of the protecting layers. Therefore, sample films which have different spacing layers between the donor and acceptor layers but the same compositions of PVPe, PVPe-P, and PVPe-A can be obtained. The thickness of each layer is estimated to be 0.9 nm.[10] These are abbreviated as PVPe-PnA where n is the number of spacing layers.

Chart 1-1

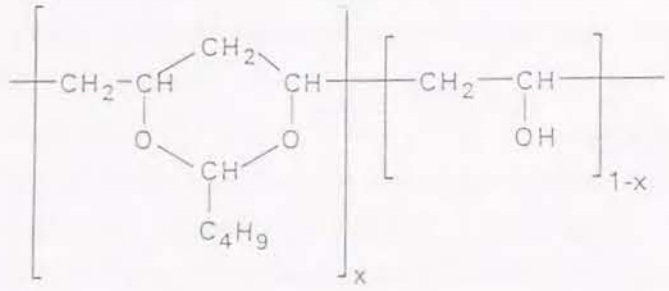

PVPe

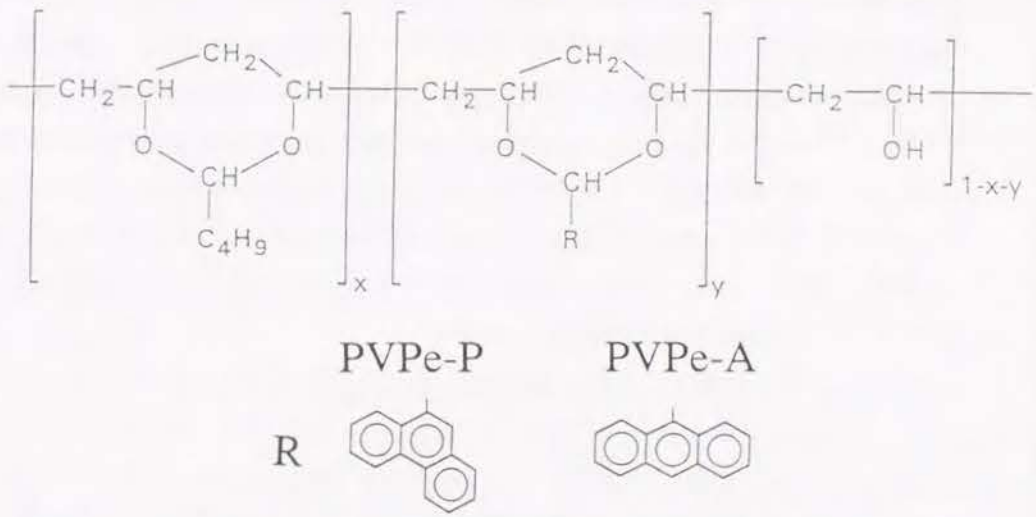

PVPe-P PVPe-A

R

Table 1-1. Compositions of Synthesized Polymers and Glass Transition Temperatures

samples	x(%)	y(%)	1-x-y(%)	Tg(°C)
PVPe	66	-	34	54
PVPe-P	65	8	27	77
PVPe-A	62	2	36	64

PVPe	10-n layers
PVPe-A	2 layers of energy acceptor
PVPe	n layers
PVPe-P	2 layers of energy donor
PVPe	4 layers
Hydrophobic quartz plate	

Figure 1-1. Schematic illustration of the multilayer structure of the PVPe LB films for the energy-transfer measurement. The figure n means the number of spacing layers: 0, 4, and 8.

1-2-3. Measurements

UV-absorption spectra were measured by a Shimadzu UV-200S spectrophotometer. The glass transition temperature (Tg) was obtained from differential scanning calorimetry (Rigaku Thermoflex DSC-8230). The fluorescence spectra were recorded by a Hitachi 850 fluorescence spectrophotometer equipped with a thermoregulated sample chamber. Heating and cooling rates were fixed to be 0.5℃ min^{-1} in the range 20-100℃. A personal computer was used for the calculation of energy transfer efficiency on the way of the relaxation process.

1-3. Results and Discussion

To probe the structural relaxation of the PVPe LB films, energy transfer efficiencies between phenanthrene (P) and anthracene (A) layers were measured. The donor chromophore P was selectively excited at 298 nm, and the transfer efficiency was evaluated using the fluorescence intensity ratio I_A/I_P on the spectrum, where I_A is the intensity of A emission at 438nm and I_P is that of P at 350nm. This method enables one to detect a small change in the distances between P and A chromophores, without considering the errors of intensity measurements among samples.

Figure 1-2 shows an example of spectral change of PVPe-P8A sample at a constant temperature: 60℃. A drastic change of the spectrum was observed, indicating thermal relaxation of the layered structure at the elevated temperature.

Figure 1-3 shows the thermal stability of PVPe-PnA films by plotting the ratio I_A/I_P as a function of temperature. The energy transfer efficiency was measured at every 5℃ both in the heating and cooling process. The closer the distance between P and A, the higher the energy transfer efficiency observed, resulting in the larger value of I_A/I_P, as seen in PVPe-P4A and PVPe-P8A. On the contrary, the ratio I_A/I_P decreases when P and A begin to separate from each other, as seen in PVPe-P0A which has a contact pair of P and A layers at the beginning. In both cases, thermal relaxation of the layers could be observed at temperatures

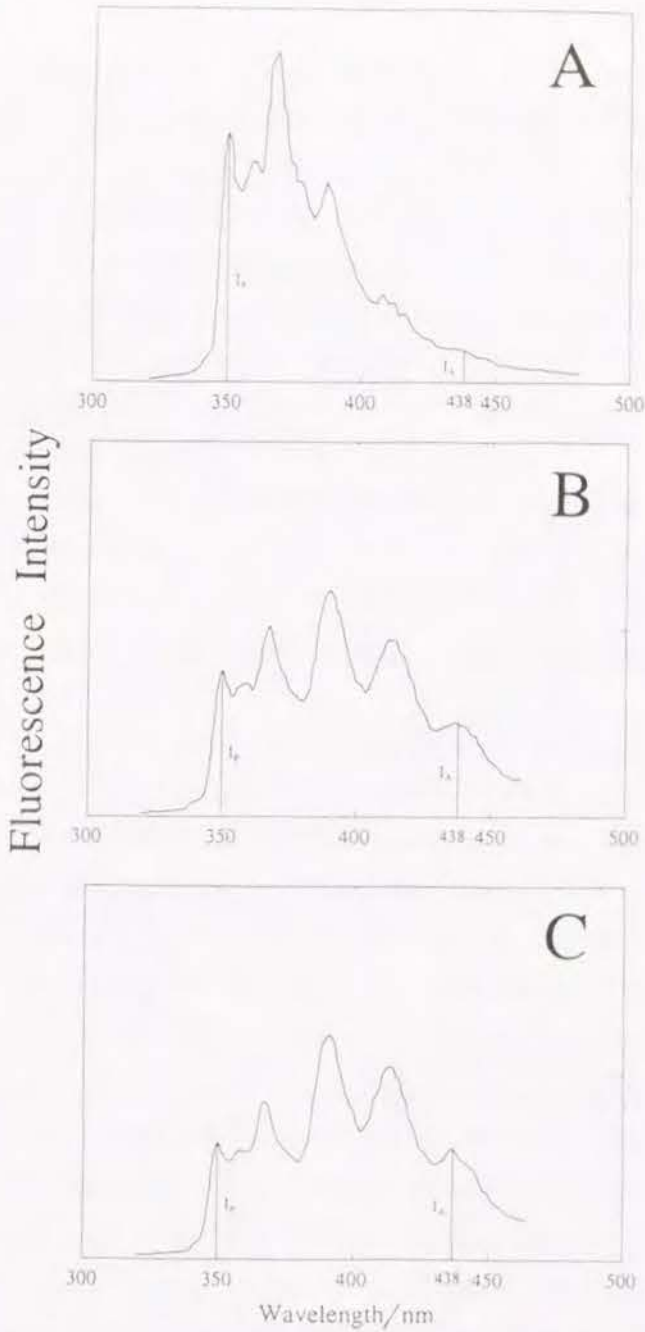

Figure 1-2. Spectral change of PVPe-PnA films with time at a constant temperature, 60℃: (A) initial stage, (B) after 1h, (C) after 3h. The excitation wavelength is 298 nm.

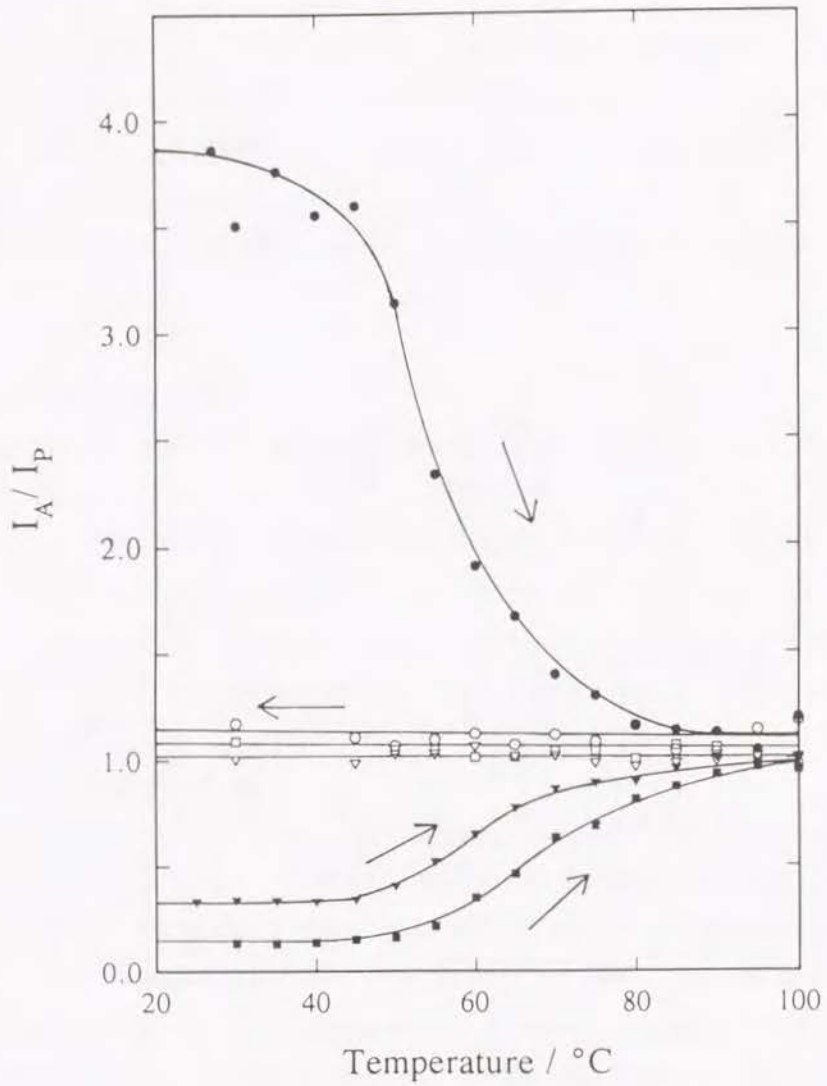

Figure 1-3. Effect of heating on the energy transfer efficiency of PVPe-PnA LB films: (○) PVPe-P0A, (▽) PVPe-P4A, (□) PVPe-P8A. Closed symbols indicate the values for the heating process, and open symbols those for the cooling process.

above 50℃. Compared with poly(vinyl octanal acetal) (PVO), the changes start at higher temperatures. It is probably due to the difference of the Tgs of PVO and PVPe, which are 25℃ and 54℃, respectively. The films were completely disordered when the temperature rose to 100℃. After heating the film up to 100℃, the ratio I_A/I_P reached a plateau region and kept its value even when the temperature decreased. Therefore, this thermal relaxation process can be regarded as an irreversible process. Moreover, the energy transfer efficiencies of all samples showed similar values between 0.9 and 1.1 regardless of the number of spacer layers at the initial stage.

Figure 1-3 provides a qualitative but general view of the phenomenon. To make a quantitative discussion on the diffusion process of the polymer segments, the energy transfer efficiency was examined for PVPe-P0A, PVPe-P4A, and PVPe-P8A and the ratio I_A/I_P was monitored as a function of time at constant temperatures between 40 and 80℃.

The energy transfer efficiency of PVPe-P0A which had no spacing layers decreased with time as shown in Figure 1-4A. From this experiment, it is obvious that P and A chromophores diffuse to the surrounding layers, and consequently are separated from each other compared with the initial state. On the other hand, P and A in PVPe-P4A and PVPe-P8A tend to approach each other compared with the initial state as shown in Figure 1-4B, 1-4C. The initial slope of the I_A/I_P curves is increased with the increase of temperature owing to the rapid relaxation. Above 60℃, all three samples reached a plateau region, the I_A/I_P value being around 0.9-1.1. A cast film which consisted of the same components as the LB samples were prepared on a quartz plate by a spin-coating method. The ratio I_A/I_P of the cast film was found to be 1.07, which is quite similar to the equilibrium value of the LB films after heating. From these results, it can be concluded that the layered structure of the LB films was completely disordered and mixed through the thermal treatment.

The movement of chromophores in the LB films was simulated by a modeling of diffusion process. The energy transfer efficiency of a pair of chromophores is given by the following equations:

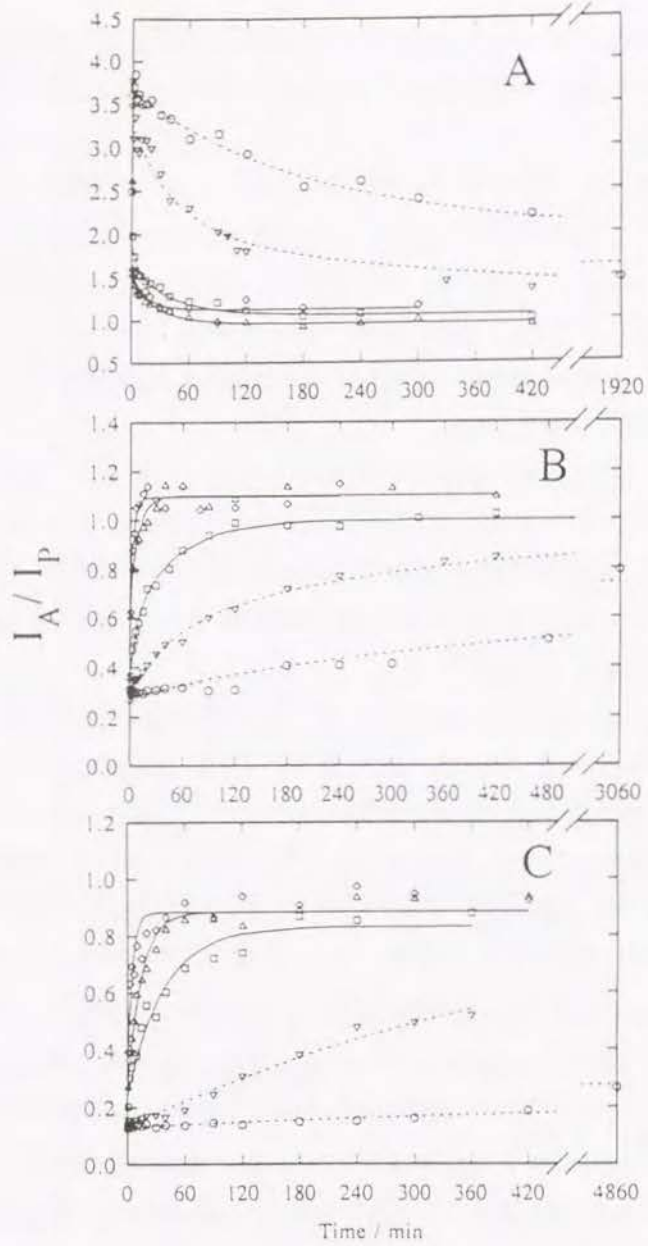

Figure 1-4. Energy-transfer efficiencies as a function of time at different temperatures for (A) PVPe-P0A, (B) PVPe-P4A, and (C) PVPe-P8A: (○) 40℃, (▽) 50℃, (□) 60℃, (△) 70℃, (◇) 80℃.

$$T_e = k_T / (k_D + k_T) \quad ...(1\text{-}1)$$

$$k_D = 1 / \tau_D \quad ...(1\text{-}2)$$

$$k_T = (1 / \tau_D) (r_0 / r)^6 \quad ...(1\text{-}3)$$

where k_D is the fluorescence emission probability of excited donor in a unit time, k_T is the probability of Förster-type energy transfer per unit time, τ_D is the unquenched lifetime of donor, r is the distance between donor and acceptor, and r_0 is the critical transfer radius at which donor has an equal probability of energy transfer to other decay processes (2.12 nm).[21] Equations 1-4 and 1-5 are derived from eq 1-1.

$$T_e = 1 / [1 + f(r)^{-1}] \quad ...(1\text{-}4)$$

$$f(r) = (r_0 / r)^6 \quad ...(1\text{-}5)$$

In the case of plural donors and acceptors, energy transfer efficiencies are determined by the following procedures. Firstly, taking plural acceptors into consideration, $f(r)$ is added up for all acceptors as follows.

$$T_e = 1 / \{ 1 + [1 / \Sigma f(r)] \} \quad ...(1\text{-}6)$$

Then, the average of T_e for all donors is calculated.

$$T_e = < 1 / \{ 1 + [1 / \Sigma f(r)] \} > \quad ...(1\text{-}7)$$

To estimate the diffusion rate of chromophores by structural relaxation, a Gaussian function, $P(x)$, was employed as a model of chromophore distribution in the direction of the film thickness (plane normal).

$$P(x) = (c_0 / \sigma\sqrt{2\pi}) \exp (-x^2 / 2\sigma^2) \quad ...(1\text{-}8)$$

where x is a displacement of a chromophore from the distribution center, c_0 is the concentration of chromophore, and σ^2 is the variance of distribution, which is related to the diffusion constant D as follows:

$$\sigma^2 = 2Dt \quad ...(1\text{-}9)$$

Unfortunately, the analytical form of eq 1-7 cannot be obtained for a Gaussian distribution of both P and A. Therefore, an approximate equation was derived under the assumption that each chromophore is placed on a layer, considering the population in a Gaussian form by eq 1-8. This means that the displacement x is given by an integer, which represents the number of layers from

the substrate. Figure 1-5 shows a schematic illustration of the thermal relaxation process.

Let us assume that the nearest A from a certain P predominantly determines its energy transfer efficiency. From this point of view, energy transfer efficiency is given as follows.

$$T_e = \int_{r_1}^{\infty} 2\pi rc \exp(-\pi r^2 c) \{ 1 / [1 + 1 / g(r)] \} dr \quad ...(1\text{-}10)$$

$$g(r) = f(r) + \int_{r}^{\infty} 2\pi rc\, f(r) dr \quad ...(1\text{-}11)$$

where c is the concentration in a given layer, r is the distance between P and A chromophores, and r_1 is the excluded distance of P and A due to their molecular size. Here r_1 = 0.6 nm was employed from the limiting area of acetal unit: 0.36 nm^2. The probability that the nearest acceptor appears at r from the center can be represented by $2\pi rc \exp(-\pi r^2 c)$. The influence of acceptors further than the nearest one must be small. Therefore, the contribution to the energy transfer efficiency was taken into account by the second term of eq 1-11, which represents the sum of energy transfer rates to A's appeared simply with the presence probability: $2\pi rc$. Using these equations, the energy transfer efficiency T_e was calculated for various distributions.[22] Now, it becomes possible to fit the experimental data, $T_{e\ expt}$, with this theoretical curve $T_{e\ calc}(\sigma^2)$ as follows:

$$T_{e\ expt} = k\, T_{e\ calc}(\sigma^2) \quad ...(1\text{-}12)$$

$$\sigma^2 = 2Dt + \sigma_0^2 \quad ...(1\text{-}13)$$

where k is the correction factor for the amplitude, and σ^2 in eq 1-9 is modified taking into account the initial dispersion, σ_0^2. The author obtained the diffusion constant (D) of each samples which has a different number of spacers. Table 1-2 shows the best fit values of D, k, and σ_0^2 using the least-square fitting method. Owing to the experimental condition, it was difficult to neglect errors when the temperature was too high or too low. For example, the relaxation of PVPe-P0A at 80℃ was too fast to get a reliable value of D, while the relaxation of PVPe-P8A at 40℃ was too slow and did not reach the final state within the experimental

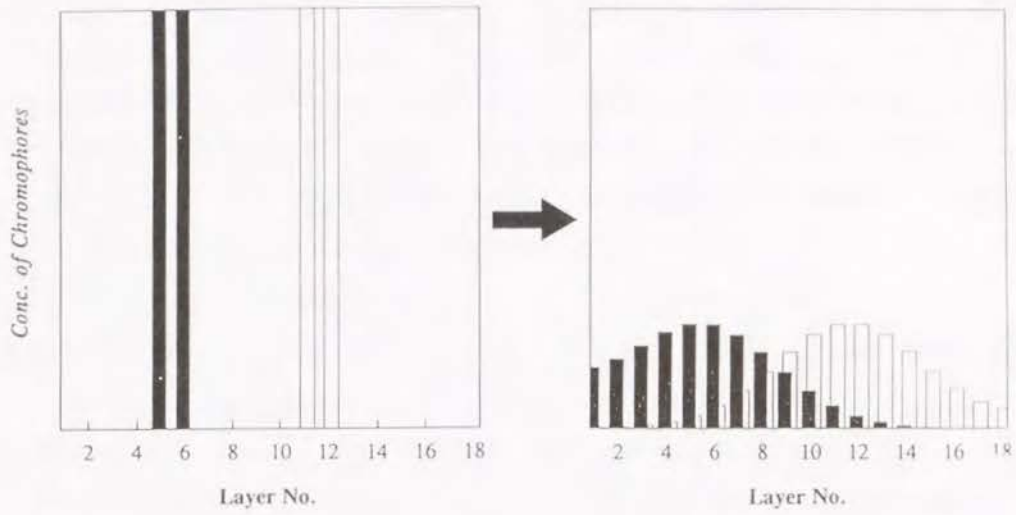

Figure 1-5. Schematic illustration for the thermal relaxation process of the layered structure.

Table 1-2. Fitting parameters for energy-transfer efficiency.

	PVPe-P0A			PVPe-P4A			PVPe-P8A		
Temp (℃)	k	$Dx10^{-18}$ (cm^2s^{-1})	σ_0^2 (nm^2)	k	$Dx10^{-18}$ (cm^2s^{-1})	σ_0^2	k	$Dx10^{-18}$ (cm^2s^{-1})	σ_0^2
40	1.2	1.2	0.051	0.7	1.3	3.6	-	-	-
50	1.1	4.5	0.023	0.8	7.5	3.3	0.8	5.9	8.9
60	0.9	36.0	2.7	0.8	48.0	3.4	0.7	78.0	15.0
70	0.8	53.0	3.7	0.9	180.0	3.7	0.7	210.0	13.0
80	-	-	-	0.9	610.0	2.2	0.7	620.0	14.0

k is the correction factor for the amplitude, D is the diffusion constant, and σ_0 is the initial dispersion.

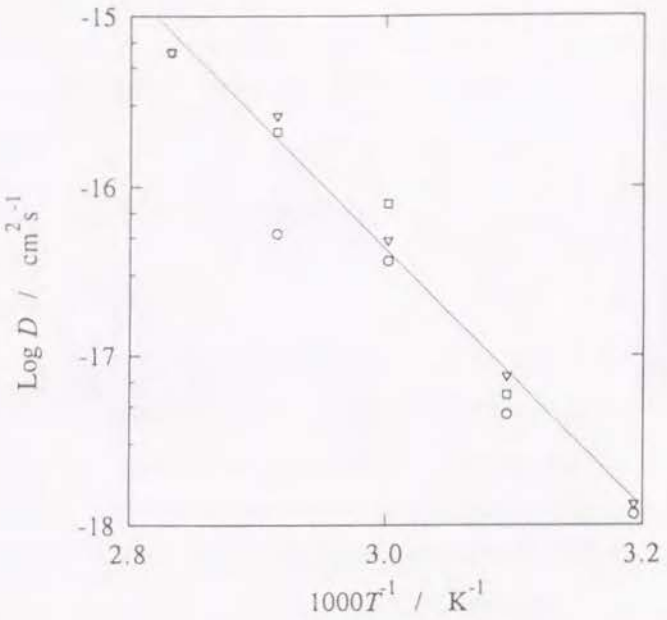

Figure 1-6. Arrhenius plot of diffusion constant of chromophores: (○) PVPe-P0A, (▽) PVPe-P4A, (□) PVPe-P8A.

time range. Therefore, these data are not shown in Table 1-2. Although there are some variations in the values of D, k, and σ_0^2 depending on the number of spacing layers, they are probably caused by the experimental restrictions.

The initial variance σ_0^2 shows a slight preexistent relaxation before the thermal treatment. This dispersion is partly due to the disordering after the dipping process. Especially PVPe-P8A shows a large value of σ_0^2 because of the larger error arising from the smaller I_A value. Therefore, chromophoric layers have the standard deviations σ_0 of 1.5 to 3.5 nm in the as-deposited LB films. It should be noted that the expected thickness of chromophoric layers is 2 nm, because these are transferred as a Y-type film, i. e., as a double layer. Figure 1-4 shows the calculated curves. Good agreement with experimental data was

obtained.

The diffusion constant of the chromophores (D) represents the structural relaxation rate of the multilayers. For the sake of further discussion, the relation between temperatures and the diffusion coefficients was plotted in Figure 1-6. A linear relationship was seen between the logarithms of D and the reciprocal of temperature. From the slope of the straight line, the apparent activation energy, ΔE, for the relaxation is calculated to be about 150 kJ mol^{-1} by

$$D = D_0 \exp (-\Delta E / RT) \quad \text{...(1-14)}$$

The D value observed is in the order of 10^{-16} - 10^{-18} cm^2 s^{-1}. These values are similar to the values reported for the diffusion phenomena of bulk polymers.[23-25] The polymer chains in the ultrathin LB films behave like those in a polymer bulk, but this point must be clarified in details. Polymer diffusion in LB films is being studied by changing M_W, stereoregularity of the polymer, etc.

1-4. Conclusion

LB films containing fluorescence probes were prepared from poly(vinyl pentanal acetal), and the thermal relaxation of the layered structure was measured by the energy transfer between phenanthrene and anthracene chromophores. This experiment enabled one to evaluate the very small diffusion coefficient of polymer segments as a function of temperature. The values observed were rather consistent with those for polymer diffusion in bulk. Furthermore, the relaxation was closely related to Tg of the sample polymers. It should be noted that fluorescence spectroscopy provides us with a unique and powerful technique for probing dynamic processes occurring in the nanometer dimension.

References and Notes

(1) Kuhn, H. *Thin Solid Films* **1989**, *178*, 1.

(2) Ringsdorf, H.; Schmidt, G.; Schneider, J. *Thin Solid Films* **1987**, *152*, 207.

(3) Wegner, G. *Ber. Bunsenges. Phys. Chem.* **1991**, *95*, 1326.

(4) Kuhn, H.; Möbius, D.; Bücher, H. *Physical Methods of Chemistry;* Weissberger, A.; Rossiter, B. W., Ed., Wiley: New York, 1972; Vol 1, Part 3B, p 577.

(5) Förster, Th. Z. *Naturforsch.* **1949**, *4A*, 321.

(6) (a) Schouten, A. J.; Wegner, G. *Makromol. Chem.* **1991**, *192*, 2203. (b) Arndt, T.; Schouten, A. J.; Schmidt, G. F.; Wegner, G. *Makromol. Chem.* **1991**, *192*, 2215.

(7) O'Brien, K. C.; Lando, J. B. *Langmuir* **1985**, *1*, 453.

(8) Shigehara, K.; Murata, Y.; Amiya, N.; Yamada, A. *Thin Solid Films* **1989**, *179*, 287.

(9) (a) Laschewsky, A.; Ringsdorf, H.; Schmidt, G.; Schneider, *J. Am. Chem. Soc.* **1987**, *109*, 788. (b) Erdelen, C.; Laschewsky, A.; Ringsdorf, H.; Schneider, J.; Schuster, A. *Thin Solid Films* **1989**, *180*, 153.

(10) (a) Oguchi, K.; Yoden, T.; Sanui, K.; Ogata, N. *Polym. J.* **1986**, *18*, 887. (b) Watanabe, M.; Kosaka, Y.; Sanui, K.; Ogata, N.; Oguchi, K.; Yoden, T. *Macromolecules* **1987**, *20*, 452. (c) Watanabe, M.; Kosaka, Y.; Oguchi, K.; Sanui, K.; Ogata, N. *Macromolecules* **1988**, *21*, 2997.

(11) (a) Schneider, J.; Ringsdorf, H.; Rabolt, J. F. *Macromolecules* **1989**, *22*, 205. (b) Schneider, J.; Erdelen, C.; Ringsdorf, H.; Rabolt, J. F. *Macromolecules* **1989**, *22*, 3475.

(12) Mumby, S. J.; Swalen, J. D.; Rabolt, J. F. *Macromolecules* **1986**, *19*, 1054.

(13) Shimomura, M.; Song, K.; Rabolt, J. F. *Langmuir* **1992**, *8*, 887.

(14) Jark, W.; Russell, T. P.; Comelli, G.; Stöhr, J. *Thin Solid Films* **1991**, *199*, 161.

(15) Naito, K. *J. Colloid Interface Sci.* **1989**, *131*, 218.

(16) (a) Ito, S.; Okubo, H.; Ohmori, S.; Yamamoto, M. *Thin Solid Films* **1989**, *179*, 445. (b) Ohmori, S.; Ito, S.; Yamamoto, S.; Yonezawa, Y.; Hada, H. *J. Chem. Soc. Chem. Commun.* **1989**, 1293. (c) Ohmori, S.; Ito, S.; Yamamoto, M. *Macromolecules* **1990**, *23*, 4047.

(17) Ohmori, S.; Ito, S.; Yamamoto, M. *Macromolecules* **1991**, *24*, 2377.

(18) Ueno, T.; Ito, S.; Ohmori, S.; Onogi, Y.; Yamamoto, M. *Macromolecules* **1992**, *25*, 7150.

(19) Ito,S.; Ueno, T.; Yamamoto, M. *Thin Solid Films* **1992**, *211*, 614.

(20) Wegner, G. *Thin Solid Films* **1992**, *216*, 105.

(21) Berlman, I. B. *Energy Transfer Parameters of Aromatic Compounds*, Academic Press, New York, 1973.

(22) In the text, author described procedures only for the intralayer energy transfer for the sake of simplicity. When D and A locate in different planes, T_e can be calculated by a modified form of eq 10.

$$T_e = \int_0^\infty 2\pi l c \exp(-\pi l^2 c) \{ 1 / [1 + 1 / h(l)] \} dl \quad \ldots(20)$$

$$h(l) = r_0^6 / (l^2 + r_2^2)^3 + \pi c r_0^6 / 2 (l^2 + r_2^2)^2 \quad \ldots(21)$$

where l is the distance from the center of a plane to A chromophores in the plane, and r_2 is the layer distance between donating layers and accepting layers. Eqs 10 and 20 were taken into account for all layers.

(23) (a) Pekcan, Ö.; Winnik, M. A.; Droucher, M. D. *Macromolecules* **1990**, *23*, 2673. (b) Zhao, C.; Wang, Y.; Hruska, Z.; Winnik, M. A. *Macromolecules* **1990**, *23*, 4082.

(24) Yukioka, S.; Nagato, K.; Inoue, T. *Polymer* **1992**, *33*, 1171.

(25) Nealey, P. F.; Cohen, R. E.; Argon, A. S. *Macromolecules* **1993**, *26*, 1287.

Chapter 2

Fluorescence Study of Polymer Diffusion and Its Analysis with the Monte Carlo simulation for a Layered Structure of Poly(vinyl alkanal acetal) Langmuir-Blodgett Films

2-1. Introduction

The Langmuir-Blodgett (LB) technique is a promising method to realize nano-architectures of organic materials.[1] Extensive investigations on LB films have been made on the design and fabrication of functional organic films. Recently much attention has been paid to the polymer LB film,[2-6] because it may overcome the drawbacks of conventional fatty acid films, associated with their poor thermal and mechanical stability.[7-9]

The structural relaxation and stability of the amorphous polymer LB films have been studied by the fluorescence method.[10-14] Previously, the thermal relaxation of the layered structure of poly(vinyl octanal acetal) LB films was studied by the energy transfer method to detect the structural disordering in the nanoscale order. A pair of layers containing the energy donor and acceptor chromophores were incorporated in spectroscopically inert layers, and the transfer efficiency from an excited donor to acceptors was monitored in the course of heating. The change of transfer efficiency clearly showed that the layered structure was irreversibly disordered and mixed by the thermal treatment. Sensitive detection is possible even for the weak fluorescence from a monolayer containing fluorescent probes with a content of only a few percent. By using this method, the aging effect of the layered structure[11], and the thermal relaxation of the structure under elevated temperatures[14] have been examined.

In this study, the distribution of energy donating and accepting polymer segments is measured by the energy transfer method as a function of time and temperature, yielding the diffusion constants and activation energies of the polymer

diffusion.

2-2. Experimental Section

2-2-1. Materials

Poly(vinyl alkanal acetal)s were synthesized by acetalization of commercial poly(vinyl alcohol) (Wako Pure Chemical Industries, DP=2000). Details have been described in Chapter 1.[10,15] The polymer was labeled with phenanthrene (P) or anthracene (A) chromophores by the reaction with the corresponding chromophoric aldehydes (Aldrich).

Table 2-1 shows the fraction of chromophoric unit and alkyl unit in the acetalized polymers, PVB, PVPe, and PVO, where butanal, pentanal, and octanal were employed as the alkyl group, respectively. These fractions were determined by UV absorption of the phenanthrene unit and anthracene unit, and from the carbon fraction measured by elementary analysis. Unlabeled polymers were used as the spacing layer, while the polymers labeled with P and A were used for the energy donating and accepting layers, respectively.

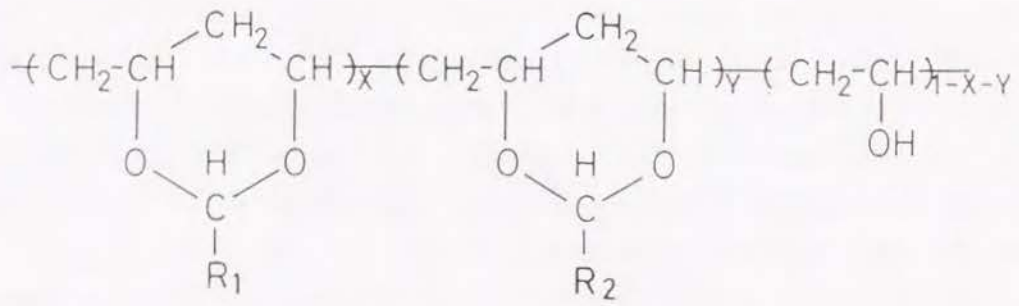

R1 :

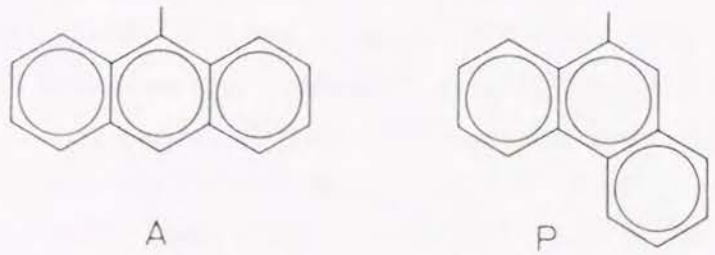

A P

R2 : $-C_3H_7$、$-C_4H_9$、$-C_7H_{15}$

Table 2-1. Compositions of Poly(vinyl alkanal acetal) and Surface Pressures at the LB Deposition

Sample	X (%)	Y (%)	1-X-Y (%)	Surface Pressure ($mN\ m^{-1}$)
PVB	0	70	30	20
PVB-P	7	58	35	16
PVB-A	2	62	36	17
PVPe	0	66	34	20
PVPe-P	8	65	27	18
PVPe-A	2	62	36	18
PVO	0	73	27	23
PVO-P	12	57	31	18
PVO-A	7	55	38	20

Table 2-2. Thickness of Spacer Layers, Critical Temperature (Tc) of LB Films, and Glass Transition Temperature (Tg) of the Bulk Polymer

Sample	Thickness (nm)	Tc (℃)	Tg (℃)
PVB-P8A	6.8	60	63
PVPe-P8A	7.2	50	54
PVO-P8A	8.2	35	25

2-2-2. Film Preparation

The deposition of LB films was performed with a high transfer ratio both in the up and down modes yielding a Y-type LB film. Details have been described in Chapter 1.

Figure 2-1 shows the layer structure of sample film. For example, a PVO film consists of 18 layers, in which two layers of PVO-P and two layers of PVO-A were incorporated. These chromophoric layers were separated by spacing layers whose number of layers, n was 0, 4, and 8. These samples are abbreviated as PVO-PnA. Both outsides of the chromophoric layers were covered with at least two layers of PVO as the protection layers. Since the total number of layers was kept constant to be 18, the samples have the same compositions of PVO, PVO-P, and PVO-A, regardless of n. The thickness of one layer is known to be 0.85 nm for PVB, 0.90 nm for PVPe, and 1.02 nm for PVO.[9]

2-2-3. Measurements

Fluorescence spectra were recorded by a Hitachi 850 fluorescence spectrophotometer equipped with a thermoregulated sample chamber. The spectral change under heating and cooling cycles was observed with a rate of 0.5℃ min^{-1} in the range of 25-100℃. The glass transition temperatures (Tg) of the prepared polymers were measured with a Metler thermosystem model FP-85.

2-2-4. Theoretical Calculation

The diffusion in the LB film results in a distribution of chromophores in the direction normal to the film plane. In this chapter assumed a Gaussion function is assumed for the distribution which is characterized by the distribution center x_0 and the variance σ^2.

$$c(x) = (c_0/\sigma(2\pi)^{1/2})\exp(-(x-x_0)^2/2\sigma^2) \qquad ...(2\text{-}1)$$

where c(x) is the concentration of chromophores at the displacement x, and c_0 is related to the total number of chromophores placed in the system. The variance σ^2 is given by a function of time and diffusion constant D as follows,

Protection Layer (PVB, PVP, PVO)	10-n
Energy Accepting Layer (PVB-A, PVP-A, PVO-P)	2
Spacing Layer (PVB, PVP, PVO)	n
Energy Donating Layer (PVB-P, PVP-P, PVO-P)	2
Precoating Layer (PVB, PVP, PVO)	4
Quartz Plate	

Figure 2-1. Schematic illustration of layered structure of the LB films.

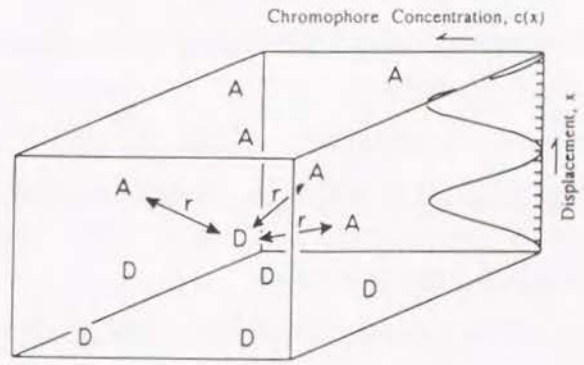

Figure 2-2. Schematic illustration of chromophore distribution in a LB film.

$$\sigma^2 = 2\ D\ t. \qquad ...(2\text{-}2)$$

A numerical calculation is performed to obtain the energy transfer efficiency under a given distibution of chromophores which is produced in a computer using random numbers. At first, acceptors (A) are placed randomly within the space of film thickness, but keeping a Gaussian distribution in the axis normal to the plane. Donors (D) are also placed with a Gaussin distribution around the deposited plane. Figure 2-2 is a schematic illustration of chromophore distribution in a LB film. According to Förster theory,[16] the energy transfer rate constant from a certain donor i to an acceptor j is given by

$$k_{Tij} = (r_0/r_{ij})^6 / \tau_0 \qquad ..(2\text{-}3)$$

where r_{ij} is the distance of separation between i and j. r_0 is the critical transfer radius at which a donor D has the rate of transfer equal to the original deactivation rate: $1/\tau_0$. These parameters for the P and A pair can be obtained experimentally as R_0 = 2.12 nm and τ_0 = 43 ns.[17] The energy transfer takes place to all of acceptors, so the rate must be presented by the sum of eq. 2-3.

$$k_{Ti} = (1/\tau_0)\ \Sigma_j (r_0/r_{ij})^6 \qquad ...(2\text{-}4)$$

The survival probability $p_i(t)$ of the excited donor i at a time t is calculated as follows,

$$p_i(t) = \exp(-t/\tau_0 - k_{Ti}t) \qquad ...(2\text{-}5)$$

Observed p(t) for the system, which corresponds to the fluorescence decay curve, is given by the average of $p_i(t)$ over all donor molecules.

$$p(t) = (1/n_D)\ \Sigma_i\ p_i(t) \qquad ...(2\text{-}6)$$

where n_D is the number of donors. Integration of eq. 2-6 gives the fluorescence quantum yield q_D of donor under the steady-state excitation.

$$q_D = k_f \int_0^\infty p(t)\ dt \qquad ...(2\text{-}7)$$

where k_f is the emission probability of the excited donor. Therefore, the energy transfer efficiency T_e is evaluated by

$$T_e = (q_{D0} - q_D) / q_{D0} \qquad ...(2\text{-}8)$$

where q_{D0} is the quantum efficiency of donor without energy transfer.

All of these eqs. 2-3 - 2-9 are numerically calculated for a given coordinate of D and A chromophores. This procedure is repeated at least 100 times for the different coordinates of D and A under the Gaussian distribution, then the averaged efficiency, T_{av}, is employed as the theoretical prediction of energy transfer efficiency for a variance σ^2. These calculations were performed for various variances in a range of 0-100 nm^2, and in an area of 20 x 20 nm^2, which is large enough compared with the critical radius r_0: 2.12 nm.

2-3. Results and Discussion

Figure 2-3 shows an example of spectral changes under the heating process. The fluorescence spectra of PVO-P4A consist of P emission at 350 and 367 nm and A emission at 393, 416, and 438 nm. The P chromophores were selectively excited at a wavelength of 298 nm, but the efficient energy transfer from P to A yields both of the P and A emission on the spectra. The transfer efficiency is given by $(I_{P0}\text{-}I_P)/I_{P0}$, where I_P is the fluorescence intensity of the P emission and I_{P0} is that in the absence of energy transfer to the A layers. However, the intensity measurements from film to film result in an error of at least 5 %. Therefore, the intensity ratio, I_A/I_P (I_A is the intensity of A emission at 438 nm and I_P is the intensity of P at 350 nm) is adopted as a measure of the transfer efficiency. As Figure 2-3 shows, thermal treatment of the LB films causes drastic changes in the spectra, which is observed only for the first rise of temperature, and once the sample is heated to 100℃, it shows no appreciable change in the subsequent cooling and heating cycles. The value I_A/I_P after heating is similar to those of other samples, regardless of the number of spacing layers, i.e., regardless of the spatial arrangement at the initial stage. These findings indicate that the layered structure is irreversibly disordered and the chromophores are mixed by the heating process.

Figure 2-4 shows the plots of I_A/I_P on the course of the first heating of PVB-P8A, PVPe-P8A , and PVO-P8A. The ratio is normalized by the maximum value

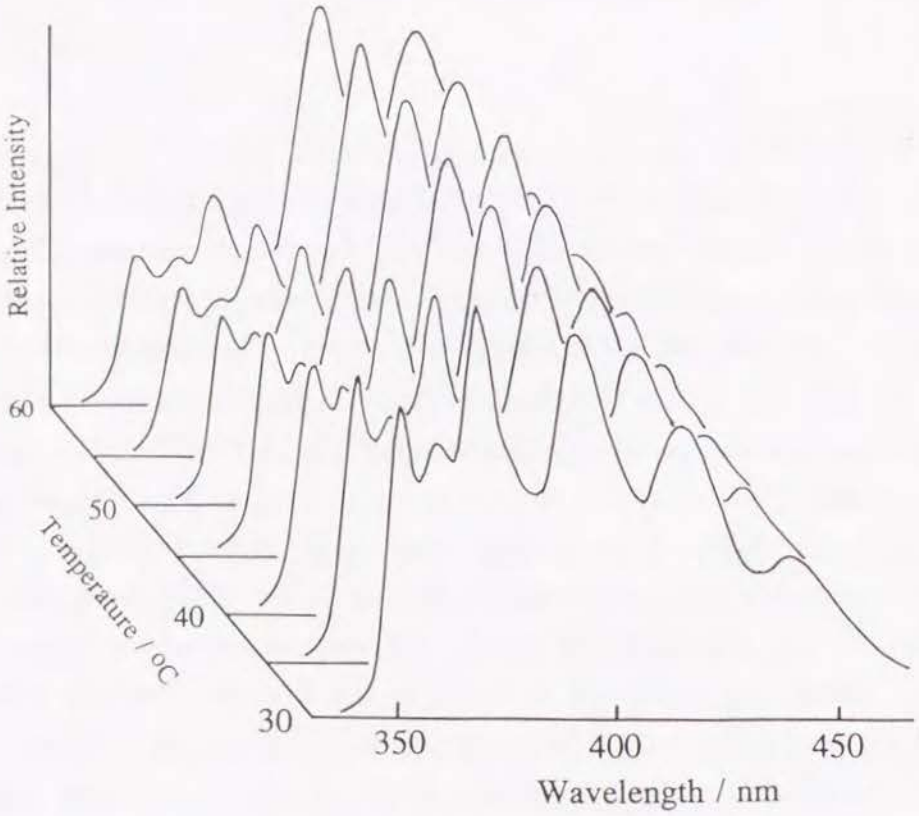

Figure 2-3. Spectral change of a PVO-P4A film by thermal treatment.

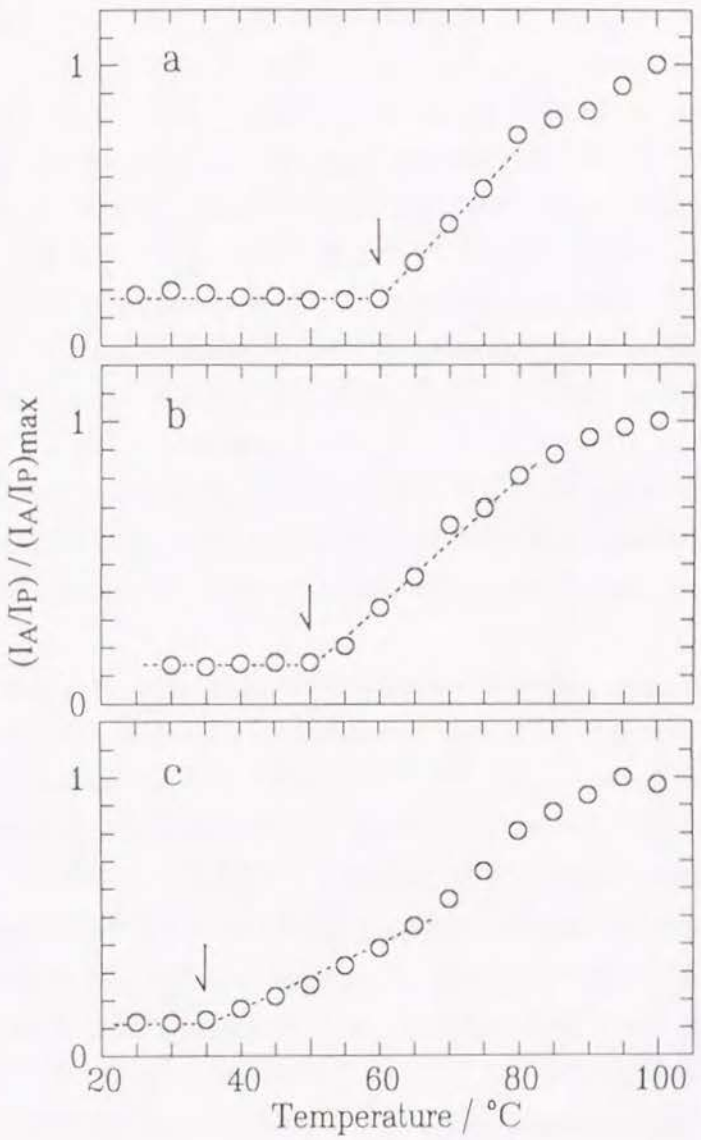

Figure 2-4. Plots of I_A/I_P observed on the course of the first heating: (a) PVB-P8A, (b) PVPe-P8A, and (c) PVO-P8A.

to compensate the difference of acceptor concentrations among the samples. At the beginning, the chromophoric layers were separated by eight layers of the spacing polymer; Table 2-2 shows the thickness . However, the transfer efficiency markedly increased with the thermal treatment. This shows that the donor-acceptor layers become closer than the initial locations.

The arrows in Figure 2-4 show critical temperatures, Tc, at which the rapid increase of transfer efficiency starts. Table 2-2 also shows these values. These temperatures depend on the length of the polymer side chains. PVB films begin the relaxation at ca. 60℃, but PVO films show a much lower Tc than that of PVB films. Compared with the glass transition temperatures, Tg, of the polymer bulk, it is clear that Tc is closely related to Tg. As the length of the side-chain becomes longer from PVB to PVO, the value of Tg decreases due to the flexibility of the alkyl chains. This affects the rate of disordering of the LB films. It is reasonable that the polymer chains have a similar flexibility and mobility both in a polymer bulk and in an ultrathin LB film. In the next step, the author will try to evaluate the diffusion constant D from the time-dependent efficiencies of the energy transfer.

The sample was placed in a thermoregulated chamber of a spectrometer and the energy transfer efficiency was monitored as a function of time. Figure 2-5 shows the results for PVPe-P4A and PVO-P4A at various temperatures. Obviously, the higher the temperature applied, the faster the relaxation occurred. For a quantitative analysis, the theortical calculation mentioned above was performed, where the transfer efficiency T_{av} for both PVPe-P4A and PVO-P4A samples were calculated in a range of variance of 0-100 nm^2 (Figure 2-6). The saturated values for both samples at large variances differ from one another because of the difference of the acceptor concentrations and of the film thickness. However, the features of these curves are quite similar and also bear resemblance to the experimental curves shown in Figure 2-5. These theoretical curves were fitted with the experimental data using the least squares method. In the fitting procedure, eq. 2-2 was modified taking into account the initial dispersion σ_0^2 of chromophores before heating.

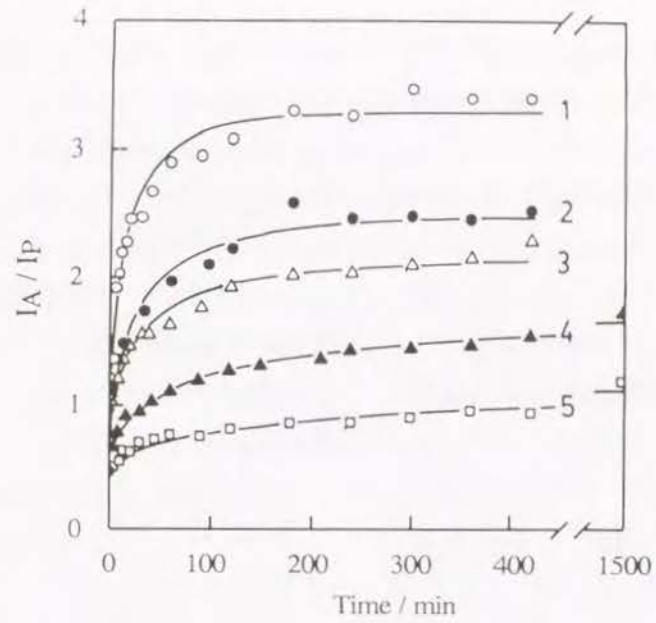

Figure 2-5. I_A/I_P as a function of time at various temperatures: PVO-P4A, 1: 75℃; 2: 60℃; 3: 50℃; 4: 40℃; 5: 30℃.

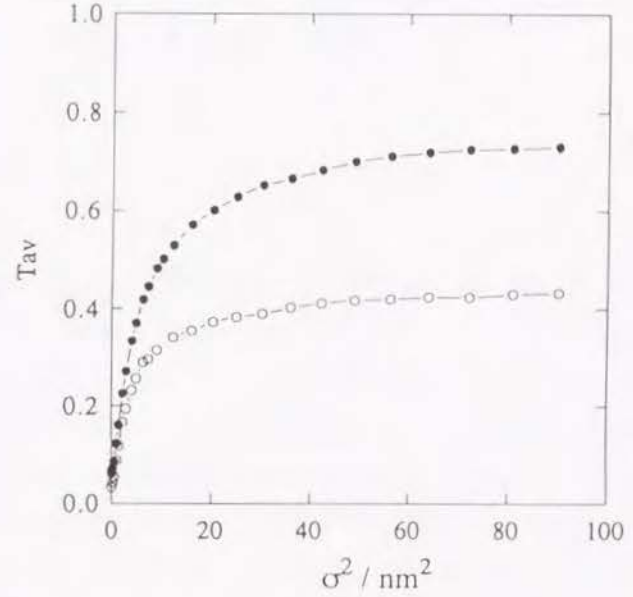

Figure 2-6. Calculated energy transfer efficiency as a function of variance for (●) PVO-P4A and (○) PVPe-P4A.

$$\sigma^2 = 2\,D\,t + \sigma_0^2 \qquad ...(2\text{-}9)$$

Since the monolayer was deposited as a Y-type film, a pair of monolayers have to be considered as a structure unit of the layered system with a thickness of ca. 2 nm. The initial distribution expressed by the best fit value of the standard deviation σ_0, is estimated to be 2-3 nm, i.e., the layered structure is slightly relaxed even in the as-deposited films.

The diffusion constants evaluated are presented by an Arrhenius plot in Figure 2-7. A linear relationship of the logarithms of D against the reciprocal of temperatures is expected under a limited temperature range. From the slope of this plot, an apparent activation energy, E_{ap}, is calculated by the next relation.

$$D = D_0 \exp(-E_{ap}/RT) \qquad ...(2\text{-}10)$$

The observed values of D are in the order of 10^{-18}-10^{-15} $cm^2\ s^{-1}$, values of the same order having been reported for the diffusion of bulk polymers.[18-21] As Figure 2-7 shows the PVO films have larger D and lower E_{ap} than those of PVPe. Since the same poly(vinyl alcohol) (DP=2000) was used for the polymer synthesis, the

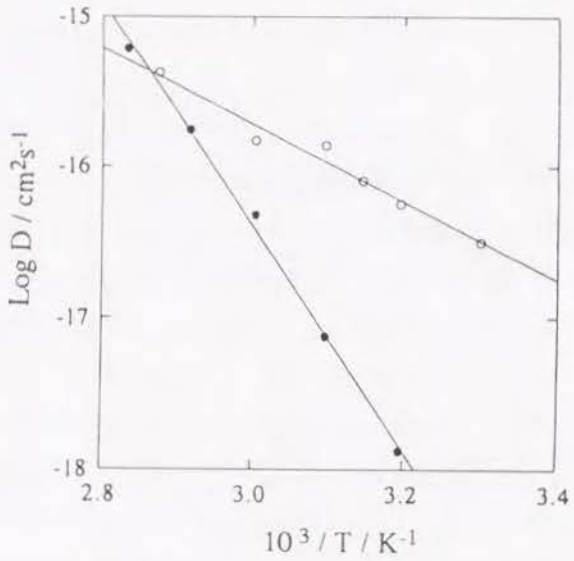

Figure 2-7. Arrhenius plots of diffusion constants: (●) PVO-P4A and (○) PVPe-P4A.

molecular weight of PVO is larger than that of PVP, because of the longer side chains attached. However, Figure 2-7 also shows that the mobility of PVO is larger than that of PVPe. To explain this fact, the different values of Tg should be taken into account. The temperature range covered is higher than Tg for PVO (Tg = 25℃), however, it is in the same range for PVPe (Tg = 54℃). Generally speaking, the temperature dependence of polymer diffusion can be described by the WLF equation which was developed to discribe the rheological properties of amorphous polymers. The equation predicts that the apparent activation energy increases rapidly with decreasing temperature. The larger mobility observed for PVO is probably due to the much higher temperatures than the sample's Tg.

The values of E_{ap} were 35 kcal mol^{-1} for PVPe and 12 kcal mol^{-1} for PVO. These values are a few times smaller than those reported for various kinds of polymers in the bulk states.[22] The reason for this disagreement is that the diffusion of polymer segments from a two-dimensional form to a three- dimensional random coil may take place with a lower activation energy than the diffusion in a polymer bulk due to the thin layer structure. This point must be confirmed by a viscoelastic study for the polymer bulk.

2-4. Conclusion

Ultrathin polymer films of poly(vinyl alkanal acetal) were made by the Langmuir-Blodgett (LB) technique, which enables one to fabricate layered structure with a thickness of only 1 nm per layer. The polymer monolayer on a water surface was successively deposited on a solid substrate as a two-dimensional form, but after the deposition, thermal relaxation of the layered structure occurred at elevated temperatures. The structural change in the nanometer dimension could be sensitively and quantitatively probed by use of energy transfer between fluorescent chromophores incorporated into each layer. The diffusion constants observed as a function of temperature were in the order of 10^{-18} - 10^{-15} $cm^2\ s^{-1}$. The thermal properties of the LB films are well characterized by the glass transitions of the bulk polymers.

References

1) Kuhn, H.; Möbius, D.; Bücher, H. *Physical Methods of Chemistry*, A. Weissberger, B. W. Rossiter Eds., Wiley: New York, 1972, Vol 1, Part 3B, p. 557.

2) Wegner, G. *Thin Solid Films* **1992**, *216*, 105.

3) (a) Laschewsky, A; Ringsdorf, H.; Schmidt, G.; Schneider, J. *J.Am. Chem. Soc.* **1987**, *109*, 788. (b) Ringsdorf, H.; Schmidt, G.; Schneider, J. *Thin Solid Films* **1987**, *152*, 207. (c) Biddle, M. B.; Lando, J. B.; Ringsdorf, H.; Schmidt, G.; Schneider, *J. Colloid Polym. Sci.* **1988**, *266*, 806. (d) Jark, W.; Russell, T. P.; Comelli, G.; Stöhr, J.; Erdelen, C.; Ringsdorf, H.; Schneider, J. *Thin Solid Films* **1991**, *199*, 161.

4) Schaub, M.; Mathauer, K.; Schwiegk, S.; Albouy, P. A.; Wenz, G.; Wegner, G. *Thin Solid Films* **1992**, *211*, 397.

5) (a) Mumby, S. J.; Swalen, J. D.; Rabolt, J. F.; *Macromolecules* **1986**, *19*, 1054. (b) Schneider, J.; Ringsdorf, H.; Rabolt, J. F. *Macromolecules* **1989**, *22*, 205. (c) Schneider, J.; Erdelen, C.; Ringsdorf, H.; Rabolt, J. F. *Macromolecules* **1989**, *22*, 3475.

6) Penner, T. L.; Schildkraut, J. S.; Ringsdorf, H.; Schuster, A. *Macromolecules* **1991**, *24*, 1041.

7) (a)*Langmuir-Blodgett Films 4*, Fukuda, K.; Sugi, M. Eds., Elsevier, London, 1989. (b) *Langmuir-Blodgett Films 5*, Barraud, A.; Palacin, S. Eds., Elsevier, Amsterdam, 1992.

8) (a) Tredgold, R. H.; Winter, C. S. *J. Phys. D.; Appl. Phys.* **1982**, *15*, L55. (b) Tredgold, R. H.; Winter, C. S. *Thin Solid Films* **1983**, *99*, 81. (c) Tredgold, R. H. *Thin Solid Films* **1987**, *152*, 223.

9) Sasanuma, Y.; Kitano, Y.; Ishitani, A.; Nakahara, H.; Fukuda, K. *Thin Solid Films* **1991**, *199*, 359.

10) (a) Ito, S.; Okubo, H.; Ohmori, S.; Yamamoto, M. *Thin Solid Films* **1989**, *179*, 445. (b) Ohmori, S.; Ito, S.; Yamamoto, M.; Yonezawa, Y.; Hada, H. *J. Chem. Soc. Chem. Commun.* **1989**, 1293. (c) Ohmori, S.; Ito, S.; Yamamoto, M. *Macromolecules* **1990**, *23*, 4047.

11) Ohmori, S.; Ito, S.; Yamamoto, M. *Macromolecules* **1991**, *24*, 2377.

12) Ueno, T.; Ito, S.; Ohmori, S.; Onogi, Y.; Yamamoto, M. *Macromolecules* **1992**, *25*, 7150.

13) Ito, S.; Ueno, T.; Yamamoto, M. *Thin Solid Films* **1992**, *211*, 614.

14) Hayashi, T.; Okuyama, T.; Ito, S.; Yamamoto, M. *Macromolecules* **1994**, *27*, 2270.

15) (a) Watanabe, M.; Kosaka, Y.; Oguchi, K.; Sanui, K.; Ogata, N. *Macromolecules* **1988**, *21*, 2997. (b) Oguchi, K.; Yoden, T.; Kosaka, Y.; Watanabe, M.; Sanui, K.; Ogata, N. *Thin Solid Films* **1988**, *161*, 305.

16) Förster, Th. *Z. Naturforsch.* **1949**, *4a*, 321.

17) Berlman, I. B. *Energy Tansfer Parameters of Aromatic Compounds*, Academic, New York, 1973.

18) Kausch, H. H.; Tirrell, M. *Annu. Rev. Mater. Sci.* **1989**, *19*, 341.

19) (a) Zhao, C.; Wang, Y.; Hruska, Z.; Winnik, M. A. *Macromolecules* **1990**, *23*, 4082. (b) Wang, Y.; Winnik, M. A. *J. Chem. Phys.* **1991**, *95*, 2143. (c) Wang, Y.; Winnik, M. A. *Macromolecules* **1993**, *26*, 3147.

20) Yukioka, S.; Nagato, K.; Inoue, T. *Polymer* **1992**, *33*, 1171.

21) Nealey, P. F.; Cohen, R. E.; Argon, A. S. *Macromolecules* **1993**, *26*, 1287.

22) Ferry, J. D. *Viscoelastic Properties of Polymers*, 3rd Ed, Wiley, New York, 1980.

Chapter 3

Thermal Relaxation Process of Several Polymeric Langmuir-Blodgett Films Measured by the Energy Transfer Method

3-1. Introduction

An amphiphilic substance that has both hydrophobic long alkyl chain and hydrophilic portion in one molecule is able to form a monolayer at the air-water interface. The monolayer becomes densely packed under compression at a constant pressure below the collapsing pressure. The monolayer can be transferred onto a substrate, yielding a highly ordered multilayer in the direction of the film thickness. Recently, many polymeric Langmuir-Blodgett (LB) films have been examined because of their good mechanical and heat stabilities compared with the one made of long chain fatty acids.[1-4] Structures of polymeric LB films have been studied extensively by using X-ray,[5-9] IR,[10-13] electron microscopy,[14] and other measurements.[15-17] One of the effective approaches to this problem is the use of fluorescence spectroscopy. The extremely high sensitivity of light detection can provide important information about the structure of the LB film. Sufficient signals can be obtained from only a few mol% of chromophores in a polymer monolayer.

In the previous chapters,[18,19] the energy transfer technique for studying the structural relaxation process of poly(vinyl alkanal acetal) LB films was applied. The aging effect at room temperature and the thermal relaxation of the LB film at an elevated temperature have been examined previously. The energy transfer efficiency was simulated by Förster kinetics on the basis of a diffusion model[19], and the diffusion constant and its apparent activation energy were determined.

In this chapter, the author examined the thermal properties of various polymer LB films by using the energy transfer method,[20,21] and made clear the structural relaxation behavior of the polymer LB films caused by heating, with

particular regard to the effects of the glass transition temperature, polymer miscibility, and their molecular weights.

3-2. Experimental Section

3-2-1. Materials

Poly(vinyl octanal acetal) (PVO) and its derivatives were synthesized according to the procedure reported by Ogata et al.[22] Poly(vinyl alcohol) (PVA; dp 2000, Wako Pure Chemical Industries, Ltd.) was reacted with octanal (Wako Pure Chemical Industries, Ltd.) for the synthesis of PVO. Fluorescent probes were introduced in PVO to make the probe polymers (PVO-P and PVO-A) with chromophoric aldehydes: phenanthrenecarbaldehyde or anthracenecarbaldehyde (Aldrich Chemical Company, Inc.). The synthesis of PVO derivatives was described elsewhere.[23] Poly(di-isopropyl fumarate) (PDiPF), poly(di-cyclohexyl fumarate) (PDcHF), and Poly(di-*t*-butyl fumarate) (PDtBF) were also prepared for the LB film. The low molecular weight polymers are denoted PDiPF(S) (M_W: 13,000) and PDcHF(S) (M_W: 8,000) to distinguish them from the high molecular weight polymers denoted PDiPF(H) (M_W: 400,000) and PDcHF(H) (M_W: 350,000). The synthesis of poly(dialkyl fumarate) is reported by Otsu et al.[24,25] Poly(isobutyl methacrylate) (PiBMA) was purchased from Tokyo Kasei Co. These polymers were purified by the benzene-methanol reprecipitation twice. The molecular weights of the samples were determined by gel permeation chromatography (GPC).

3-2-2. Sample Preparation

A dilute solution of these polymers (0.01 wt%) in benzene (Dojin Spectrograde) was spread onto the surface of pure water in a Teflon-coated trough (Kenkosha model SI-1) equipped with a Wilhelmy-type film balance. The surface film was compressed at a rate of 10 mm min^{-1} and transferred vertically onto a substrate at a constant pressure.

A nonfluorescent quartz plate (10 mm x 40 mm) was prepared for the

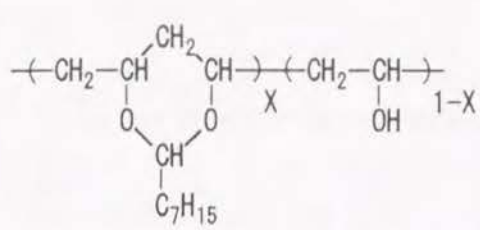

PVO

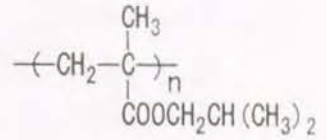

PiBMA

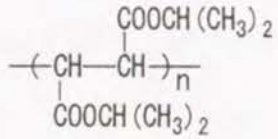

PDiPF

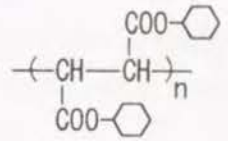

PDcHF

fluorescence measurements. It was cleaned and made hydrophobic by trimethylchlorosilane. A transfer ratio to the substrate was almost 1.0 in both the up and down modes, yielding a Y-type built-up film.

Figure 3-1 illustrates the structure of the LB films for energy transfer measurements. The films were fabricated in the following sequence:

(1) Two layers of a sample polymer (PVO, PDiPF, PDcHF, PiBMA) for the precoating layers.

(2) Two layers of PVO-P for the energy donating layers.

(3) n layers (n = 4 or 6) of the sample polymer (PVO, PDiPF, PDcHF, PiBMA) which is the same polymer as the precoating layers.

(4) Two layers of PVO-A for the energy-accepting layers.

(5) (8-n) layers of the sample polymer (PVO, PDiPF, PDcHF, PiBMA) for the protecting layers.

Thus, two probe layers, PVO-P and PVO-A were embedded into the matrix of sample polymer. In order to fix the compositions of the LB film, the total number of layers was kept to be 14 layers by adjusting the number of the protecting layers. These LB films are abbreviated as PVO-PnA, PiBMA-PnA, PDiPF-PnA, PDcHF-PnA, where n is the number of spacing layers.

3-2-3. Measurements

The molecular weight of the samples were estimated by GPC (Tosoh HLC-802UR) with THF at 38℃ as the eluent on the basis of calibration with standard polystyrene. The glass transition temperature (Tg) was obtained from the differential scanning calorimetry (MAC Science DSC-3100). The film thickness of PDiPF-PnA LB layer was measured by ellipsometry (Mizojiri Kogaku) and the thickness of PDiPF-PnA LB film was measured by surface plasmon spectroscopy. The fluorescence spectrophotometer equipped with a thermoregulated sample chamber was used for the energy transfer measurement. Heating and cooling rates were fixed to be 0.5 ℃ min^{-1} in the range 20 - 100℃.

Protecting Layer	PVO, PiBMA, PDiPF, PDcHF	8-n (n=4,6)
Energy Accepting Layer	PVO-A	2
Spacing Layer	PVO, PiBMA, PDiPF, PDcHF	n (n=4,6)
Energy Donating Layer	PVO-P	2
Precoating Layer	PVO, PiBMA, PDiPF, PDcHF	2
Substrate	quartz	

Figure 3-1. Schematic illustration of the multilayer structure of the polymer LB films for the energy transfer measurement. The number of spacing layers is denoted by n = 4 or 6.

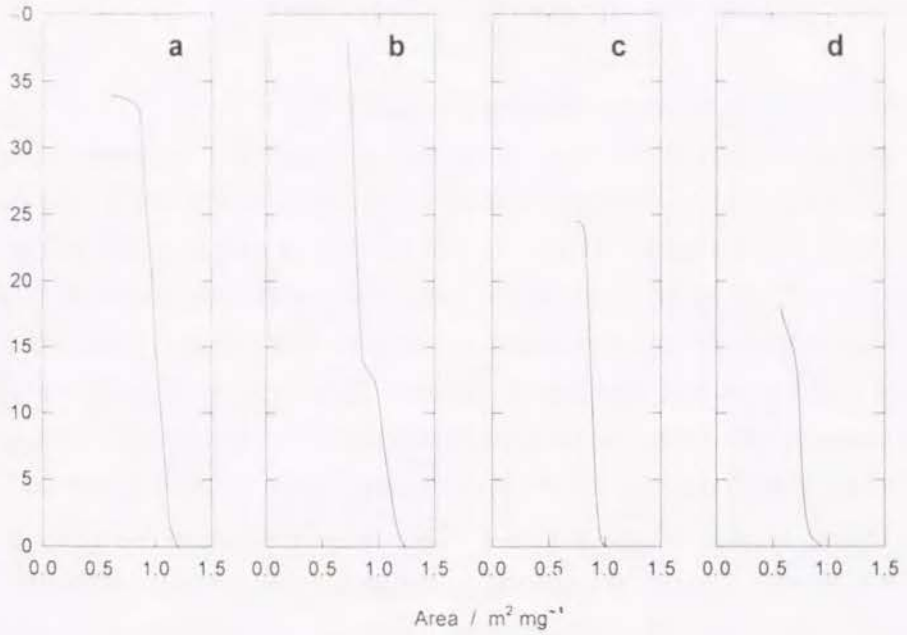

Figure 3-2. Surface pressure-area isotherms of (a) PVO, (b) PiBMA, (c) PDiPF, and (d) PDcHF.

3-3. Results and Discussion

3-3-1. Surface pressure-area isotherms of polymer LB films

Figure 3-2 shows the surface pressure - area (F-A) isotherms of examined polymers. PVO monolayer was deposited onto a quartz plate at 20 mN m^{-1}. The surface pressure of PiBMA (Figure 3-2(b)) shows an inflection at 13 mN m^{-1}. Naito reported that the film is stable at the surface pressures before the inflection.[21] He observed collapsed features of the monolayer after the inflection by X-ray analysis. The PDiPF monolayer is also able to be deposited on a substrate uniformly at 20 mN m^{-1}. Its surface pressure increases sharply at the area of 0.9 m^2 mg^{-1}. PDcHF monolayer collapses at 15 mN m^{-1} as shown in Figure 3-2(d). The bulky side chain seems to interfere the close packing of the monolayer. A similar phenomenon was also observed in the F-A isotherms of PDtBF that had more bulky side chains. The PDtBF monolayer collapsed only at 10 mN m^{-1}, so this material was not used in the following experiments.

3-3-2. Measurement of energy transfer efficiency

The energy transfer efficiency is strongly influenced by the distance between donor (D) and acceptor (A), because the transfer rate is determined by the inverse sixth power of the separation distance. When the layered structure of the film becomes disordered owing to structural relaxation, the distance between D and A changes from the initial value to a smaller one, then, the energy transfer efficiency increases. Consequently, the relation between the energy transfer efficiency and the temperature reflects structural relaxation behavior of the LB film. Figure 3-3 shows a spectral change of PDiPF(H)-P4A caused by thermal treatment. The dashed line shows the data measured at 30 ℃ and the solid line was measured at 100 ℃. A drastic spectral change was observed for this sample. With elevating temperature, the intensity of anthracene emission at 438 nm (I_A) markedly increased while the intensity of phenanthrene emission at 350 nm (I_P) decreased. This clearly indicates the structural relaxation by heat treatment. All the samples that were measured in this study showed similar drastic changes in the emission

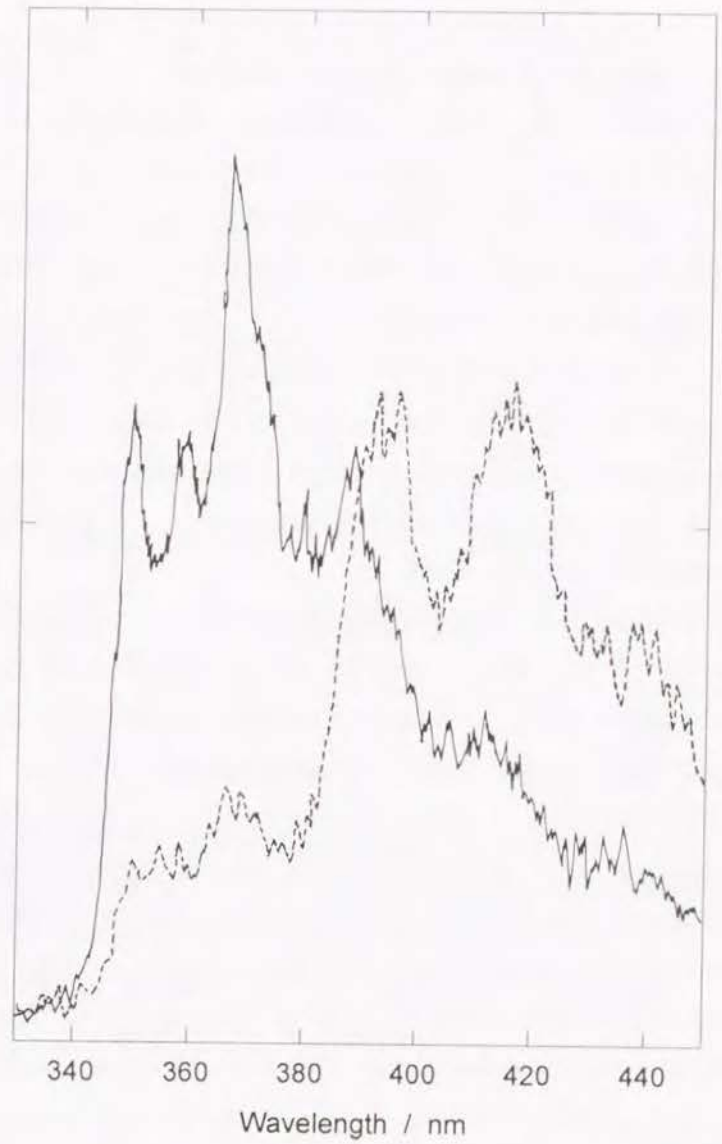

Figure 3-3. Spectral change of PDiPF(H)-P4A by heating up to 100℃: (a) at room temperature (solid line) and (b) at 100℃ (dashed line).

spectra. In order to minimize the experimental error for each samples, I_A/I_P was adopted as a measure of the energy transfer efficiency, and its change was measured as a function of temperature.

3-3-3. Thermal behavior of various polymer LB films

Figure 3-4 shows the thermal stability of various polymer LB films by plotting the ratio I_A/I_P as a function of temperature. The results for PVO-P4A, PiBMA-P4A, PDiPF(H)-P4A, and PDcHF(H)-P4A were shown in Figure 3-4(a) through 3-4(d), respectively. The energy transfer efficiency was measured at every 5℃ on the heating process and every 10℃ on the cooling process. The heating and cooling rates were fixed to 0.5℃ min^{-1}. The closer the distance between P and A, the higher the energy transfer efficiency (I_A/I_P) becomes. The I_A/I_P value increased irreversibly with the rise of temperature for all the samples. The arrows in Figure 3-4 show critical temperatures, T_C, at which the rapid increase of transfer efficiency starts.

The data of thermal properties are summarized in Table 3-1. The initial distance between P and A is estimated by the thickness of each polymeric monolayer and the number of spacing layers. The transition point of polymer bulk measured by DSC (T_{DSC}) and the critical temperature (T_C) of the LB films mentioned above are listed in Table 3-1. I_A/I_P(100℃) represent the values of the transfer efficiency at 100℃ in the first run. By comparing T_C with T_{DSC}, it is clear that there is a close relation between these two temperatures. In the case of PVO and PiBMA, T_{DSC} corresponds to the glass transition temperature. Therefore, the rapid structural relaxation occurs by a large scale segmental motion, and this relaxation leads to complete destruction of the LB film structure, giving a mixed state of the polymer chains. This is the reason why the I_A/I_P values of PVO-P4A and PiBMA-P4A became a constant value around 100℃. The I_A/I_P value of PVO-P4A kept constant during successive heating and cooling cycles owing to their miscibility, while the I_A/I_P value of PiBMA-P4A increased during succesive cooling cycles because of the phase separation. On the other hand, the I_A/I_P value

Table 3-1. The Layer Thickness, the Thermal Properties of the Samples and Energy Transfer Efficiency at 100℃, I_A/I_P(100℃)

Sample	Initial Distance[1] (nm)	DSC Transition (℃)	T_c[2] (℃)	I_A/I_P(100℃)[3]
PVO-P4A	40.8	25	35	2.5
PVO-P6A	61.2	25	45	2.1
PiBMA-P4A	44.0	53	45	4.7
PiBMA-P6A	66.0	53	50	4.5
PDiPF-P4A	32.4	75	65	3.5
PDiPF-P6A	48.6	75	70	1.8
PDcHF-P4A	-	75	60	3.2
PDcHF-P6A	-	75	70	1.9

1) The initial distance between donor and acceptor layers. The film thickness for PVO and PiBMA was measured by ellipsometry and that for PDiPF was measured by surface plasmon.
2) The temperature at which the rapid increase of I_A/I_P begins.
3) The I_A/I_P value at 100 ℃ in the first run.

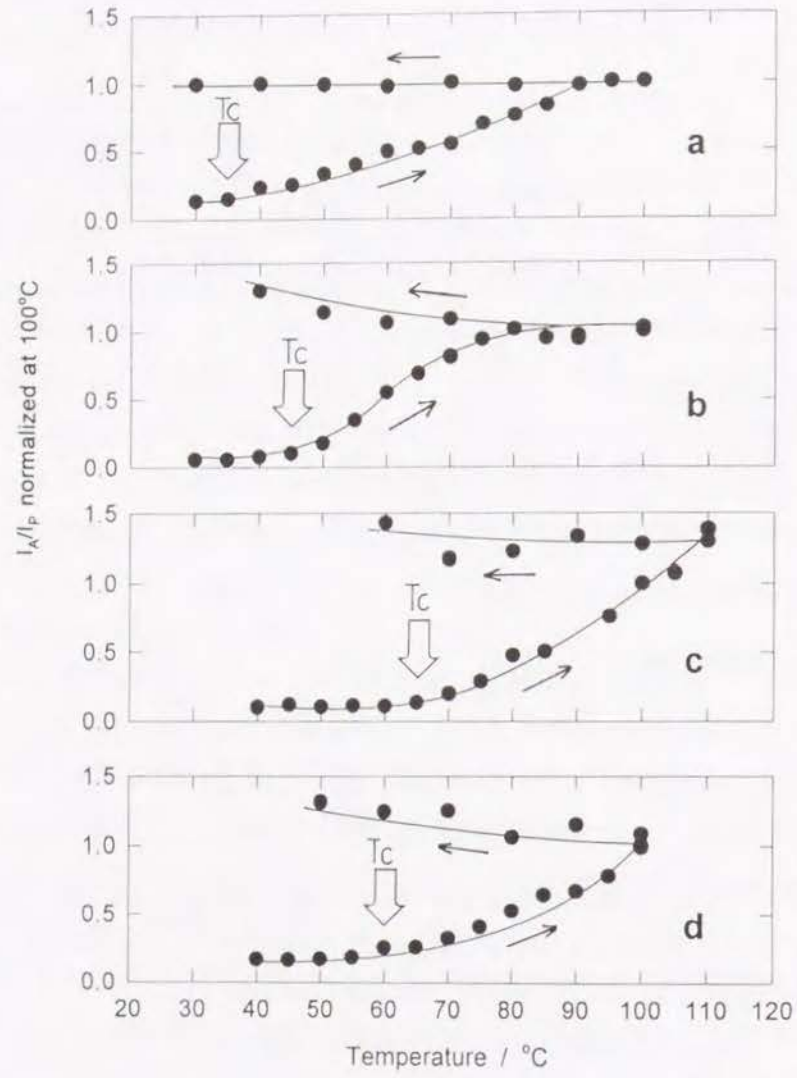

Figure 3-4. Effect of heating and cooling on the energy transfer efficiency of polymer LB films: (a) PVO-P4A, (b) PiBMA-P4A, (c) PDiPF(H)-P4A, (d) PDcHF(H)-P4A. The energy transfer efficiency, I_A/I_P is normalized for each sample at100℃.

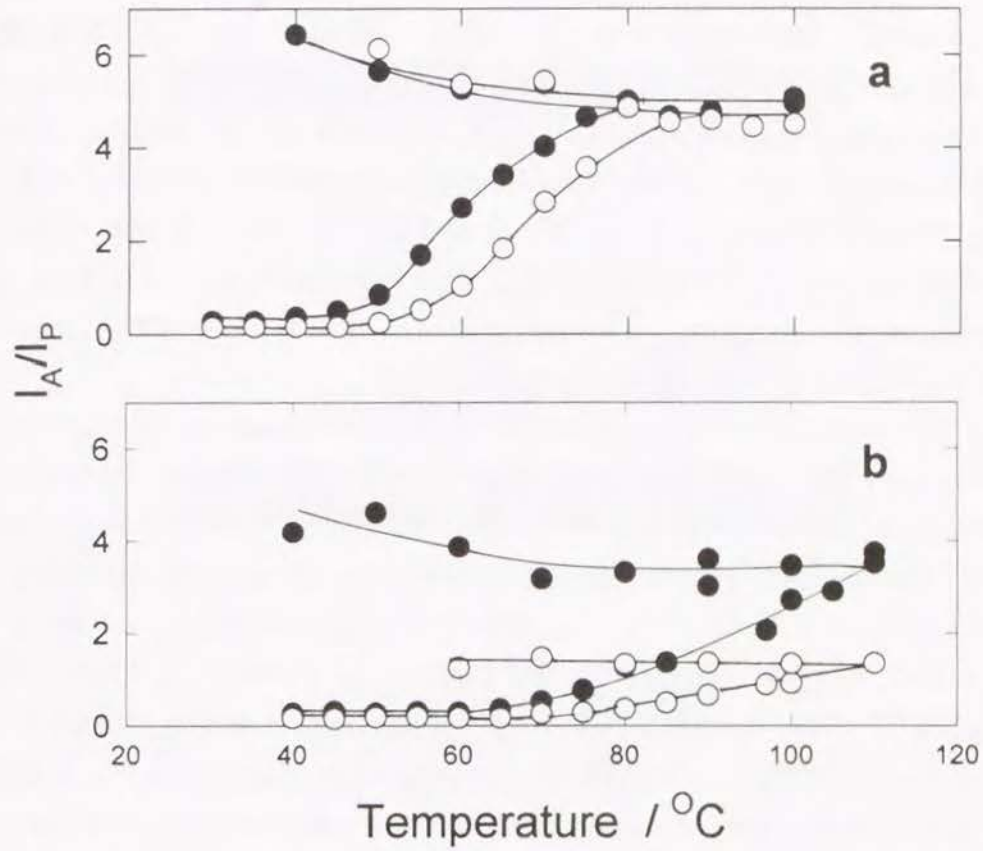

Figure 3-5. Effect of layer number on the relaxation of polymer LB films: (a) PiBMA, (b) PDiPF(H). P4A sample (●), P6A sample (○).

for PDiPF(H)-P4A and that for PDcHF(H)-P4A increased gradually on the heating process up to 120℃, and it may keep on increasing further. However, in this experiment, it was difficult to measure the I_A/I_P value at temperatures above 120℃, where the emission spectra of the fluorescent probes became too broad to obtain accurate values of I_A/I_P. As for the molecular motion of PDiPF in the solid state, Otsu et al. reported that PDiPF does not show a clear Tg below its degradation temperature.[25] Takayanagi et al. observed a small absorption at 97℃ by the measurement of the storage and loss moduli of the PDiPF film.[26] They assigned this absorption to the side chain motion of ester groups. We also detected a small transition signal at 75℃ for the fumarate polymer by the DSC measurement. This temperature is difficult to define as typical Tg owing to the thermal property describes below; it is abbreviated as T_{sub}. This temperature is close to T_C of the sample LB film. Thus, it can be said that very local motions of the fumarate polymer become active at this temperature.

The structural relaxation of the film caused by heating was measured with changing the number of layers (4 or 6). The influence of the layer number of spacer on structural relaxation was studied. The I_A/I_P for PiBMA-PnA (n=4 and 6) and that for PDiPF(H)-PnA (n=4 and 6) were plotted against temperature in Figure 3-5(a) and Figure 3-5(b), respectively. In both samples, T_C was found to be not so different regardless of the thickness of the spacing layers. The I_A/I_P(100℃) value for PiBMA-P6A was almost the same as that for PiBMA-P4A, while, the I_A/I_P(100℃) for PDiPF-P6A was much smaller than that for PDiPF-P4A. The structural relaxation of PiBMA films occurred more drastically with increase of temperature, especially above 53℃: the Tg of PiBMA. This is evidence that the long range motion of polymer segment is induced above its Tg. There, the piled layers penetrated each other three-dimensionally due to the structural relaxation of the multilayer, followed by a rapid aggregation of chromophoric layers. On the other hand, the structural relaxation for PDiPF film occurred very slowly compared with the relaxation of PiBMA film. It took a longer time to induce the structural relaxation and aggregation for P6A film than for P4A film.

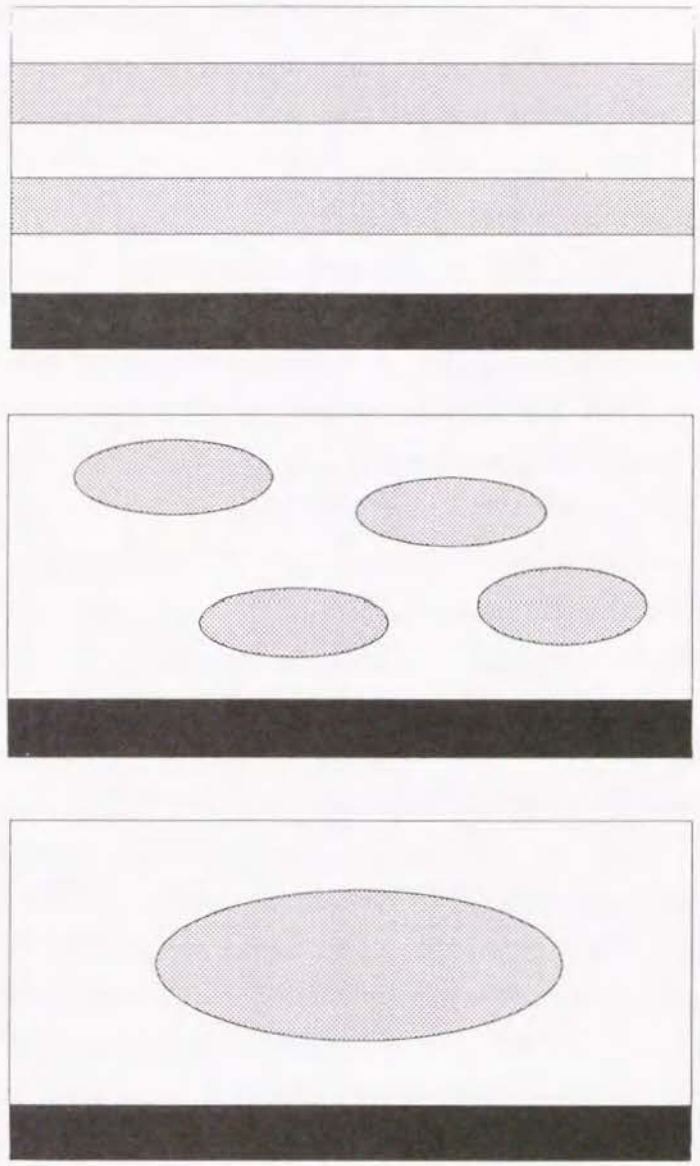

Figure 3-6. The illustration of a phase separation with thermal relaxation of the LB film. The hatched area shows the chromophoric layers. The aggregation proceeds with the increase of temperature.

This slow relaxation speed is probably due to a small scale motion of DiPF polymer. Therefore, the value of I_A/I_P(100℃) for PDiPF-PnA depends on the number of spacing layers. It can be concluded that the different hystereses arise from different mobilities of each polymer.

3-3-4. Phase separation between polymers

Polymer chains begin to move actively above its Tg or T_{sub} and the structural relaxation of the layered structure of LB film proceeds on heating. This process can be monitored by the energy transfer efficiency. The layers interpenetrate each other and as a result, the distance between D and A layers becomes shorter, increasing the energy transfer efficiency I_A/I_P.

In the case of PVO-P4A, the probing layer and the sample layer are composed of the same kind of polymer, PVO. With the increase of temperature, the I_A/I_P value rised to the saturated value of 2.5 - 3.0, which was kept constant during the successive cooling and heating cycles; the system reached a stable disordered state. On the other hand, heterogenious LB film such as PiBMA-P4A, PDiPF-P4A, or PDcHF-P4A shows slight increase in the cooling mode. This increase is due to the phase separation and aggregation of chromophoric layer. The I_A/I_P(100℃) value of PVO films is close to the value predicted by Förster theory under the assumption of the random distribution of chromophores in the whole film. This result means that all the layers are randomly intermingled by structural relaxation. To prove this randomization of chromophores, a PVO cast film was fabricated with the same concentration of chromophores as PVO-PnA film made by the spin-coating method. P and A chromophores can be regarded to take the random distribution in this cast film. The I_A/I_P value of the cast film corresponded to the I_A/I_P(100℃) value of the LB film. This result also indicates the complete disordering of the LB layered structure.

The I_A/I_P(100℃) value for PiBMA LB samples showed higher values than 3.0 as shown in Figure 3-5(a). This behavior can be explained by the phase separation of the probing PVO from a sample polymer, as shown in Figure 3-6.

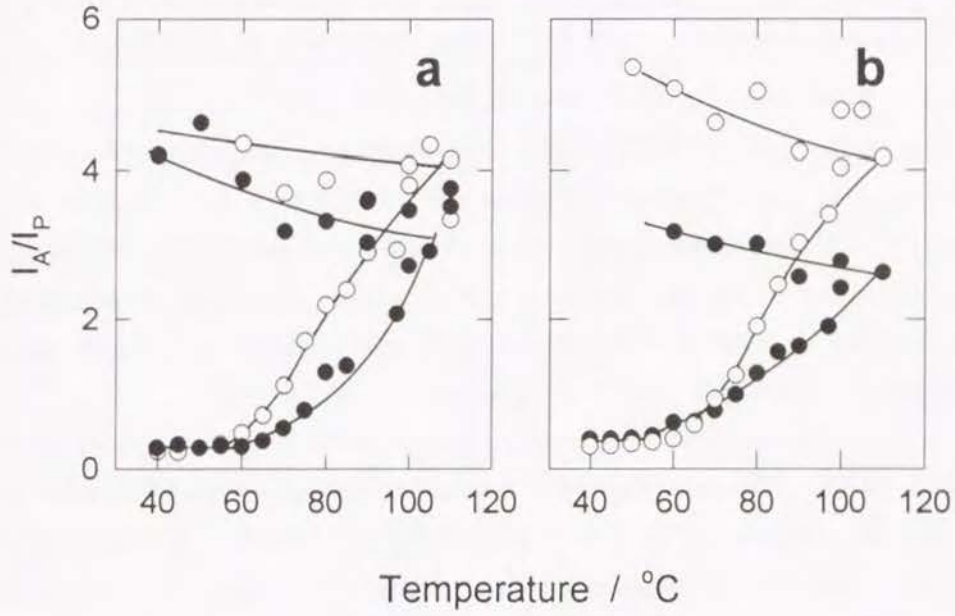

Figure 3-7. Effect of molecular weight on the thermal history of the energy transfer efficiency: (a) PDiPF-P4A, (b) PDcHF-P4A. Higher Mw sample (●), lower Mw sample (○).

The phase separation arises from the structural differences between the chromophoric polymer and a sample polymer. When a polymer chain is allowed to move in the polymer matrix, a planar conformation confined to the two-dimensional layer is relaxed. If the probe polymer is incompatible with the matrix, the polymer is likely to form a droplet in order to decrease the surface energy. A continuous heat treatment will accelerate the growth of the droplet involving the aggregation of both PVO-P and PVO-A polymers. Consequently, P and A chromophores are concentrated in the domain of PVO, resulting in a high energy transfer efficiency compared with that for a homogeneous distribution of chromophores in the matrix. The mobility of polymer chains of PiBMA increases greatly above Tg and a rapid progress of phase separation occurs for PiBMA-PnA (n=4,6) samples (See Figure 3-5(a)). PDiPF(H)-P6A and PDcHF(H)-P6A; however, showed a gradual increase of I_A/I_P and the final value becomes higher than 3.0. In the case of PDiPF(H)-P6A, the small scale segment motion of the sample polymer contributes to the structural relaxation of the LB film. The destruction of film structure is not completed within the observation time and the I_A/I_P is considered to increase further due to the phase separation. The diffusion rate of the spacing layers governs the rate of phase separation and the growth of three-dimensional domain of each component.

To study the influence of diffusion process on the structural relaxation, the molecular weight effect was examined for the fumarate polymers. Figure 3-7(a) and 3-7(b) show the results for PDiPF and PDcHF, respectively. In both polymer LB films, T_C was almost the same despite the difference in the molecular weight. The thermal hysteresis, however, showed different shapes depending on the molecular weight. This difference of hysteresis demonstrated that the chromophoric layers easily aggregate since the spacing layer of PDiPF(S) shows more rapid structural relaxation than that of PDiPF(H).

3-4. Conclusion

Thermal relaxation behavior of several polymer LB films was investigated by observing the change of energy transfer efficiency using PVO-P and PVO-A probes. The structural relaxation of the LB film occurred by heat treatment. A drastic relaxation of the LB film was observed above the Tg of the bulk polymer, where each layer was no longer restricted in a two-dimensional plane. When the probe polymer was incompatible with the sample polymer, a phase separation accompanied the thermal relaxation. The thermal hysteresis of I_A/I_P was characterized by the miscibility of the LB films and also by the diffusion rate of each polymer.

References

(1) Miyashita, T. *Prog. Polym. Sci.* **1993**, *18*, 263.

(2) Breton, M. *J. Macromol. Sci. Rev. Chem.* **1981**,*C21*, 61.

(3) Wegner, G. *Ber. Bunsenges. Phys. Chem.* **1991**, *95*, 1326.

(4) Embs, F.; Funhoff, D.; Laschewsky, A.; Licht, U.; Ohst, H.; Prass, W.; Ringsdorf, H.; Wegner, G.; Wehrmann. R. *Adv. Mater.* **1991**, *3*, 25.

(5) Biddle, M. B.; Lando, J. B.; Ringsdorf, H.; Schmidt, G.; Schneider. J. *Colloid Polym. Sci.* **1988**, *266*, 806.

(6) Erdelen, C.; Laschewsky, A.; Ringsdorf, H.; Schneider, J.; Schuster, A. *Thin Solid Films* **1988**, *180*, 153.

(7) Arndt, T.; Shouten, A. J.; Schmidt, G.; Wegner, G. *Makromol. Chem.* **1991**, *192*, 2215.

(8) Schaub, M.; Mathauer, K.; Schwiegk, S.; Albouy, P. -A.; Wenz, G.; Wegner, G. *Thin Solid Films* **1992**, *210/211*, 397.

(9) Heens, B.; Gregoire, Ch.; Pireaux, J. J.; Cornelio, P. A.; Gardella, J.A. Jr. *Appl. Surface Sci.* **1991**, *47*, 163.

(10) Duda, G.; Schouten, J. J.; Arndt, T.; Lieser, G.; Schmidt, G. F.; Bubeck, C.; Wegner, G. *Thin Solid Films* **1988**, *159*, 221.

(11) Sauer, T.; Arndt, T.; Lieser, G.; Schmidt, G. F.; Bubeck, C.; Wegner, G. *Thin Solid Films* **1990**, *187*, 357.

(12) Penner, T. L.; Schildkraut, J. S.; Ringsdorf, H.; Schuster, A. *Macromolecules* **1991**, *24*, 1024.

(13) (a) Brinkhuis, R. H. G.; Schouten. A. J. *Macromolecules* **1991**, *24*, 1496. (b) Brinkhuis, R. H. G.; Schouten. A. J. *Macromolecules* **1992**, *25*, 2717.

(14) Albrecht, O.; Laschewsky, A.; Ringsdorf, H. *Macromolecules* **1984**, *17*, 937.

(15) Hickel, W.; Duda, G.; Wegner, G.; Knoll, W. *Macromol. Chem. Rapid Commun.* **1989**, *10*, 353.

(16) Hsiung, H.; Beckerbauer, R.; Rodriguez-Parada, J. M. *Langmuir* **1993**, *9*,

1971.

(17) Obrien, K. C.; Lando, J. B. *Langmuir* **1985** *1*, 453.

(18) (a) Ueno, T.; Ito, S.; Ohmori, S.; Onogi, Y.; Yamamoto, M. *Macromolecules* **1992**, *25*, 7150. (b) Ito, S.; Ueno, T.; Yamamoto, M. *Thin Solid Films* **1992**, *210/211*, 614.

(19) Hayashi, T.; Okuyama, T.; Ito, S.; Yamamoto, M. *Macromolecules* **1994**, *27*, 2270.

(20) (a) Shigehara, K.; Hara, M.; Nakahama, H.; Miyata, S.; Murata, Y.; Yamada, A. *J. Am. Chem. Soc.* **1987**, *109*, 1237. (b) Shigehara, K.; Murata, Y.; Amaya, N.; Yamada, A. *Thin Solid Films* **1989**, *179*, 287.

(21) Naito, K. *J. Colloid Int. Sci.* **1989**, *131*, 218.

(22) (a) Oguchi, K.; Yoden, T.; Sanui, K.; Ogata, N. *Polym. J.* **1986**, *18*, 887. (b) Watanabe, M.; Kosaka, Y.; Oguchi, K.; Sanui, K.; Ogata, N. *Macromolecules* **1988**, *21*, 2997.

(23) Ohmori, S.; Ito, S.; Yamamoto, M. *Macromolecules* **1991**, *24*, 2377.

(24) (a) Otsu, T.; Minai, H.; Toyoda, N.; Yasuhara, T. *Makromol. Chem., Suppl.* **1985**, *12*, 133. (b) Ohtsu, T.; Matsumoto, A. *Acta Polymerica* **1988**, *39*, 5. (c) Matsumoto, A.; Tarui, T.; Otsu, T. *Macromolecules* **1990**, *23*, 5102.

(25) Otsu, T.; Yasuhara, T.; Matsumoto, A. *J. Macromol. Sci. Chem.* **1988**, *A25*, 537.

(26) Yamada, K.; Takayanagi, M.; Murata, Y. *Rep. Prog. Polym. Phys. Jpn.* **1984**, *27*, 321.

Chapter 4

Thermal Relaxation Process of Cadmium Stearate Langmuir-Blodgett Film Measured by the Energy Transfer Method and Transmission Electron Microscopy

4-1. Introduction

The LB technique is a useful method to fabricate artificial molecular assemblies. The understanding of the molecularly ordered structure in LB films is essential from the fundamental and application standpoints.[1] Many attempts have been made to determine the mono- and multilayer structures by means of electron diffraction,[2,3] X-ray diffraction,[4-8] Raman scattering,[9] infrared spectroscopy,[10-13] and other methods.[14-18] Transmission electron microscopy (TEM) has also been widely used for the investigation of LB multilayers. The morphology of the fatty acid monolayer was examined by the shadow-casting method at the bright-field imaging mode.[19-21] Matsumoto et al. demonstrated the presence of small scattered cavities in the stearic acid monolayer with a dark-field imaging mode.[22,23]

One important research subject is the stability of LB films against the thermal influence.[24] The conformational relaxation of the fatty acid chains and penetration into the neighboring layers causes structural changes of the whole LB film on the heating process. Detailed studies at elevated temperatures were carried out by Naselli et al.[10] They examined the thermal changes of arachidate LB multilayers by infrared spectroscopy and found a two-step melting process; a pre-transitional disordering of the hydrocarbon tail prior to the melting point of cadmium arachidate.

The energy transfer method was applied as a probing technique for the structural relaxation and the thermal stability of polymer LB films.[25-27] The transfer efficiency is determined by the inverse sixth power of distance between

donating and accepting chromophores. Therefore the energy transfer method is capable of probing a small change in the layer distance, and a sensitive detection is possible even for the weak fluorescence from a monolayer containing only a few percent of fluorescent probes.

In this chapter, the thermal stability of the stearate LB film with chromophoric polymer layers is examined by the energy transfer method. The chromophores are randomly distributed in the polymer layers between which a stearate film is placed. The distance change is monitored by the energy transfer efficiency. Furthermore, a disordered structure at an elevated temperature is observed by TEM. The relaxation processes of the stearate LB film will be discussed.

4-2. Experimental Section

4-2-1. Materials

Poly(vinyl octanal acetal) (PVO) with chromophores was synthesized according to the procedure studied by Ogata et al.[28] Poly(vinyl alcohol) (PVA; dp = 2000, Wako Pure Chemical Industries, Ltd.) was reacted with octanal (Wako Pure Chemical Industries, Ltd.) and chromophoric aldehyde which was phenanthrenecarbaldehyde or anthracenecarbaldehyde (Aldrich Chemical Co. Inc.). The details of the synthesis were reported in chapter 1.[25,26]

From an elementary analysis and UV absorption spectra, the compositions of the chromophoric polymers were determined. PVO with phenanthryl group (PVO-P) contains a phenanthrene moiety of 12%, and PVO with the anthryl group (PVO-A) contains an anthracene moiety of 7%. Stearic acid was purchased from Wako Pure Chemical Industries.

4-2-2. Energy Transfer Efficiency

To probe the structural relaxation of the composite LB films, the energy transfer efficiencies between phenanthrene (P) and anthracene (A) layers were measured. The critical radius of the energy transfer (Förster radius) between P and

A was 2.12 nm, and the donor chromophore P was selectively excited by 298 nm light. The excitation energy on a P unit transfers to the A units over the spacing layers. Here, the energy transfer efficiency depends on the distance between P and A chromophores. Previous studies showed that the chromophores are randomly distributed in the polymer layers. The transfer efficiency was evaluated using the fluorescence intensity ratio, I_A/I_P on the spectrum, where I_A is the intensity of A emission at 438 nm and I_P is that of P emission at 350 nm. The ratio of fluorescence intensities is enough to evaluate the energy transfer efficiency since the emission bands of the chromophores are separated sufficiently. Moreover, this method is convenient to eliminate the errors of intensity measurements among samples and to detect a small change of the distance between P and A chromophores.

4-2-3. Sample Preparation

LB films were prepared as follows. Pure water for the subphase was ion-exchanged, distilled, and then finally passed through a water purification system (Barnstead Nanopure II). For the polymeric monolayer, a benzene-methanol (9:1) solution of the chromophoric polymer (0.01 wt%) was spread onto pure water in a Teflon-coated trough (Kenkosha Model SI-1) at 19℃. The surface pressure-area (π-A) isotherm was recorded by using a Wilhelmy-type film balance (Shimadzu Model ST-1). The surface film was allowed to stand for 10 min to evaporate benzene, compressed at a rate of 10 mm min^{-1}, and then transferred vertically onto a substrate at 17.5 mN m^{-1} for PVO-P, 20 mN m^{-1} for PVO-A. For the stearate monolayer, the subphase was prepared with the mixture of cadmium chloride and sodium hydrogen carbonate (Wako Pure Chemicals). The pH of the subphase was adjusted to be 6.2. The benzene solution of stearic acid (0.1 wt%) was spread onto the subphase at 19℃ and also transferred vertically onto a substrate at 30 mN m^{-1}. This layer is abbreviated as ST. As for the substrate, a clean quartz plate was made hydrophobic by trimethylchlorosilane for LB deposition. Silicon wafers were used for ellipsometry. A thin carbon film

on a cover glass (22x40 mm Matsunami) was prepared as a substrate for the TEM. The carbon was sublimated below 6.7×10^{-5} Pa. The surface film was successfully transferred on a hydrophobic quartz plate and deposited as a Y-type film with a transfer ratio of 0.9 - 1.0. The surface film was transferred onto a silicon wafer only in the up mode for the first dipping because its surface is hydrophilic. The deposition for the following dips took place in both modes and formed a Y-type film.

Protection Layer	ST	6-n (n=0,2,4)
Energy Accepting Layer	PVO-A	2
Spacing Layer	ST	n (n=0,2,4)
Energy Donating Layer	PVO-P	2
Precoating Layer	ST	2
Substrate		

Figure 4-1. Schematic illustration of the multilayer structure of the LB film.

Figure 4-1 illustrates the structure of the LB film for energy transfer measurements. The sample films were fabricated on a quartz plate in the following sequence:

(1) two layers of ST for the precoating layers;
(2) two layers of PVO-P for the energy donating layers;
(3) n layers (n = 0,2,4) of ST for the spacer between the donating layers and the accepting layers;
(4) two layers of PVO-A for the energy accepting layers;
(5) (6-n) layers of ST for the protecting layers

In order to compare the relaxation processes under the same conditions, the total number of layers was kept at 12 layers by adjusting the number of protecting layers. In this way, it was possible to prepare sample films having different spacing layers between the donor and acceptor layers but the same film thickness and the same composition of PVO-P, PVO-A, and ST. These are abbreviated as ST-PnA where n is the number of spacing layers. LB film composed of only polymeric materials was prepared. It contains PVO, PVO-P, PVO-A, where PVO was used as spacing and protecting layers in place of ST. These films were abbreviated as PVO-PnA, where n is the number of spacing layers. The same structure of the LB sample was also prepared on an evaporating thin carbon film for TEM experiments. The deposited carbon film was slowly immersed into pure water at an angle of 10° to peel off from the cover glass and the film was left on the water surface. A 400 mesh copper specimen grid (Oh-ken Trading Ltd.) was placed beneath the film and then lifted up to be covered with the film. This procedure follows the report of Matsumoto et al.[23]

4-2-4. Measurements

The film thickness was measured by an ellipsometer (Mizojiri Kogaku). The content of cadmium in a cadmium stearate monolayer was determined by a flameless atomic absorption spectrometer (AAS; Shimadzu AA-670G). AAS was used for the estimation for the cadmium content in the stearate monolayer. It was

carried out by the standard addition method aiming at an acculate analysis. The reference samples were prepared for making the calibration curve. The fluorescence spectra were recorded by a Hitachi 850 fluorescence spectrophotometer equipped with a thermoregulated sample chamber. Heating and cooling rates were fixed to be 0.5 ° min^{-1} in the range of 30 - 120℃. A transmission electron microscope (TEM: JEM200-CX) was used for the observation of the thermally relaxed LB film. The sample was kept for one night after the thermal treatment and the TEM observation was carried out at room temperature.

4-3. Results and discussion

4-3-1. Surface Pressure-Area Isotherms

Figure 4-2 shows the π-A isotherms of the chromophoric polymers. The surface pressure rose sharply at the area of ca. 1.0 m^2 mg^{-1} and the monolayer collapsed at 25 - 30 mN m^{-1}. The monolayer is transferrable onto various solid substrate, quartz plate, carbon film, silicon wafer, plastic plates and so on, in a wide range of surface pressure. However, the thickness of LB films obtained depends on the pressure of deposition. The film shows the insufficient packing at the lower pressures. Therefore, the deposition was carried out around 20 mN m^{-1} which is 10 - 20% lower than the collapse pressure. The thickness of those polymer LB films was measured by ellipsometry, and the same value (1.02 nm for one layer) was obtained for both PVO-A and PVO-P films.

As for stearic acid, a benzene solution was spread on the subphase which contains cadmium chloride and sodium hydrogen carbonate with various concentrations at 19℃. Figure 4-3 shows the π-A isotherms of the cadmium stearate at various pHs. The pH range was varied from 5.8 to 6.2 by the mixing of cadmium chloride and sodium hydrogen carbonate. Little difference was observed in this pH range. However, without sodium hydrogen carbonate, the pH value of water became rather low, and the stearic acid monolayer was likely to be formed instead of cadmium stearate monolayer. In the high pH range, Hasmony

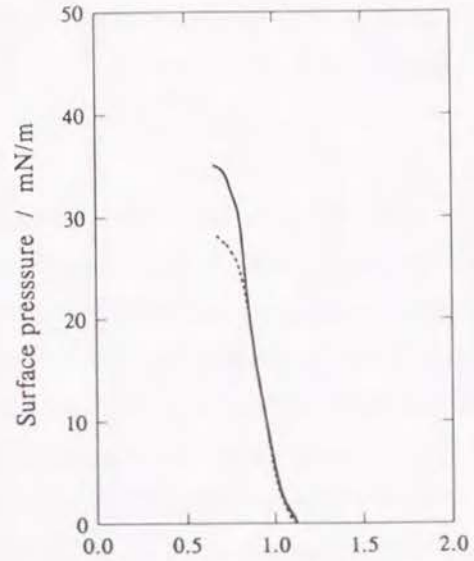

Figure 4-2. Surface-pressure isotherms of a) PVO-P (solid line), and b) PVO-A (dashed line).

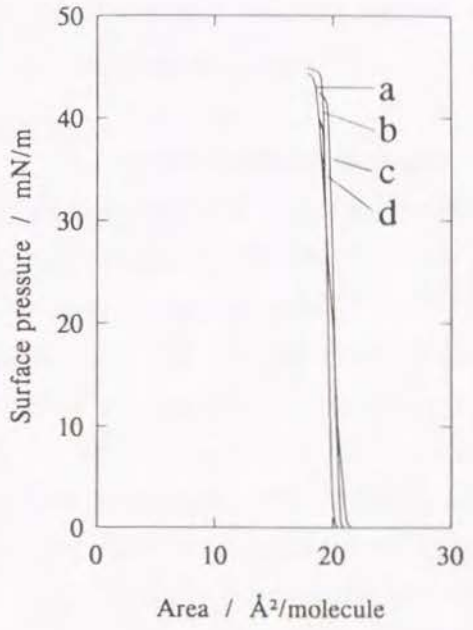

Figure 4-3. Surface-pressure isotherms of cadmium stearate at various pH: a) $CdCl_2$ $3.0x10^{-4}$ mol/*l*, b) $CdCl_2$ $3.0x10^{-4}$ mol/*l*, $NaHCO_3$ $6.0x10^{-5}$ mol/*l*, c) $CdCl_2$ $3.0x10^{-4}$mol/*l*, $NaHCO_3$ $1.5x10^{-4}$ mol/*l*, d) $CdCl_2$ $3.0x10^{-4}$ mol/*l*, $NaHCO_3$ $3.0x10^{-4}$ mol/*l*.

et al. reported that a XY type film was obtained by the vertical dipping.[29] Therefore, to build a stable Y-type multilayer, the deposition of cadmium stearate was carried out at pH 6.2. The thickness of each sample was measured by ellipsometry and it was calculated to be about 2.5 nm from a linear relationship between the number of layers and the film thickness. The value of film thickness was in good agreement with the reported values.[30] The Förster radius between phenanthrene and anthracene is estimated as 2.12 nm, so the energy transfer effectively occurs in the sample with a thickness of a few layers.

4-3-2. Thermal Relaxation Behavior

Figure 4-4 shows the spectral changes of ST-P4A by thermal treatment at 100℃ for 2 hours. At the beginning, the fluorescence from A unit is very little due to the selective excitation of P unit and the long distance of separation between P and A layers. The weak A emission observed prior to heating probably arose from direct excitation of the A unit which has a little spectral overlap of the absorption band at 298 nm. The A emission is also due to energy transfer between P and A; the transfer efficiency at this distance is estimated to be a few percent. The A emission markedly increased with a decrease in the P emission at the elevated temperature. This clearly shows the structural relaxation by heating.

The thermal stability of ST-PnA films was probed by plotting the ratio I_A/I_P as a function of temperature, as shown in Figure 4-5(a). The energy transfer efficiency was measured at every 5° during the heating process and at every 10° during the cooling process. As seen in ST-P2A and ST-P4A, the I_A/I_P rose sharply during the heating process. Chromophores came closer in this disordering process. In the case of ST-P0A which has no spacing layer, the I_A/I_P ratio decreased during the heating process. This result indicates that the average distance between P and A became longer than that of the initial state. This may be caused by segmental diffusion of polymer chain from a two-dimensional form to a three-dimensional one, or by penetration of ST molecules into the polymer domain, which results in dilution of donor density and acceptor density and decreases the number of donors and acceptors participating in energy transfer. In all cases of PnA films, the layers

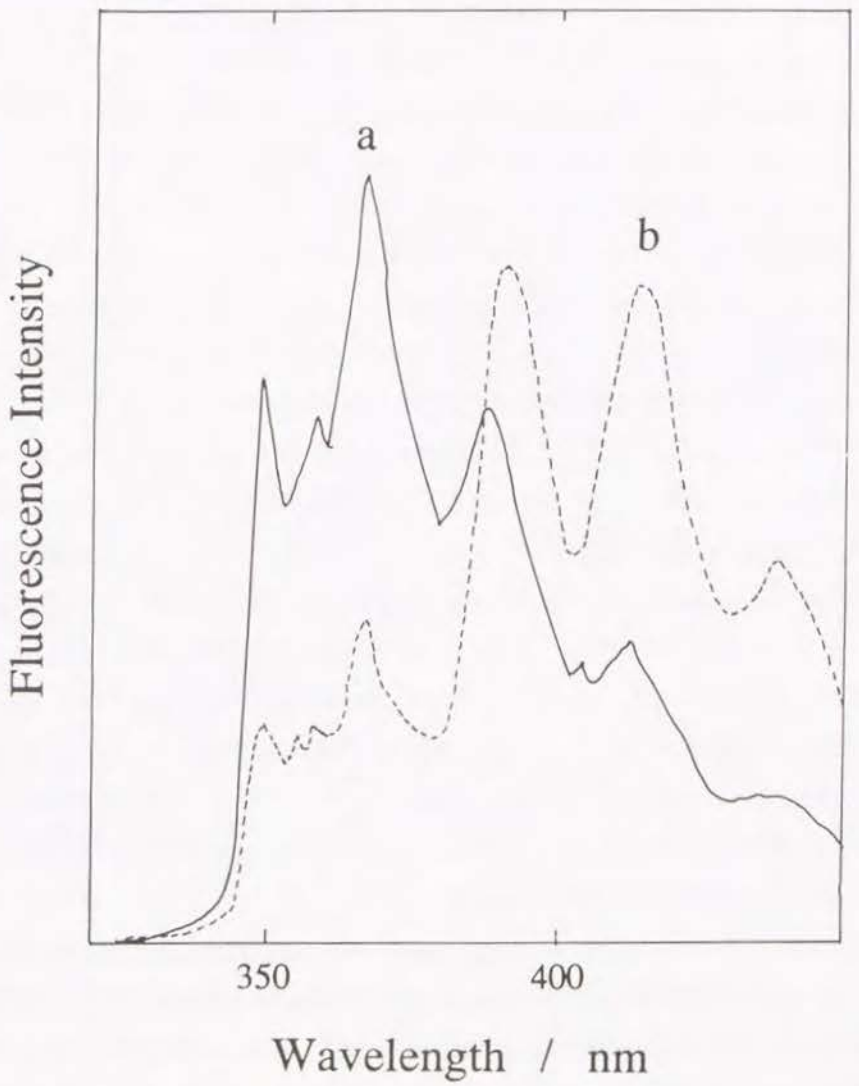

Figure 4-4. Spectral change of ST-P2A by thermal treatment at 100 °C: a) before heating, b) after 2 hours of heating.

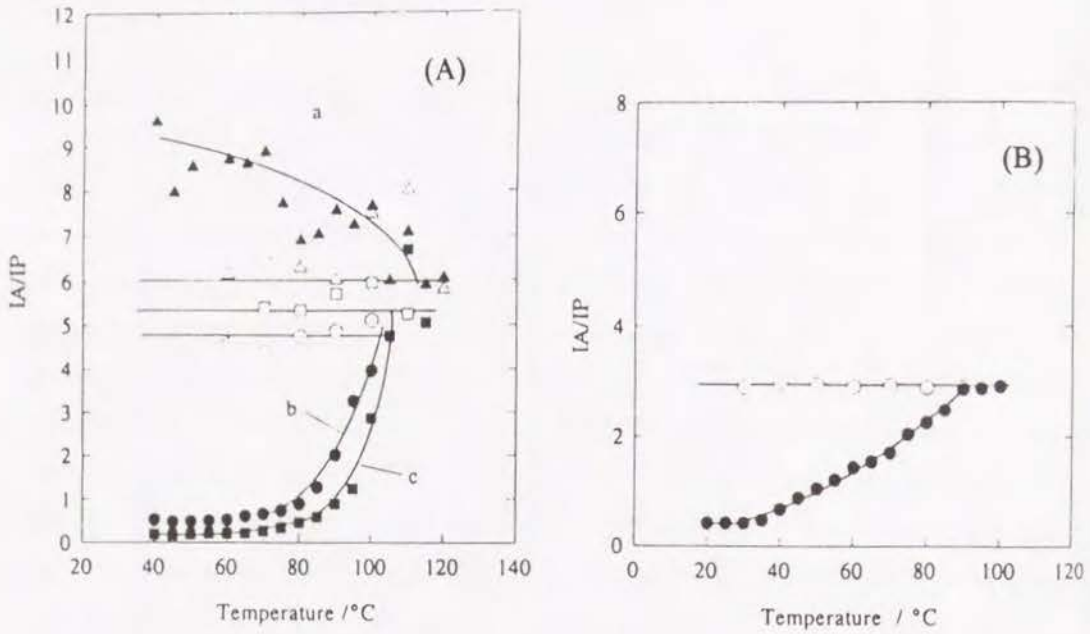

Figure 4-5. (A) Effect of heating on the energy transfer efficiency of ST-PnA LB films: (a) ST-P0A, (b) ST-P2A, (c) ST-P4A, Closed symbols indicate the values for the heating process, and open symbols indicate those for the cooling process. (B) Effect of heating on the energy transfer efficiency of PVO-P4A LB film: Closed symbols indicate the values for the heating process, and open symbols indicate those for the cooling process.

suffered structural relaxation at the elevated temperatures. The composite LB film, ST-PnA composed of chromophoric polymer layers and ST layers with a mixture of stearic acid - cadmium stearate. Compared with the polymeric LB film, PVO-P4A (Figure 4-5(b)), more drastic structural relaxation occurred in ST-PnA around the 80 - 90℃. The spacing layers of ST-PnA consisted of fatty acid and its cadmium salt crystals and melted down at the characteristic temperature. The transition point of ST-PnA depends on the content of cadmium stearate in stearic acid. An atomic absorption spectrometer which is quite effective for the microanalysis of heavy metals was used for measuring the cadmium content in the stearate monolayer. From this measurement, 0.65 ng cm^{-2} of cadmium on average was found to be contained in a ST monolayer, i.e., 62% of stearic acid formed its cadmium salts. The phase transition temperature becomes higher with the increase of cadmium content. Nomaki et. al. reported from DSC measurement[31] that the phase transition of Cd stearate LB films occurs at 80 - 110℃. This DSC result also supports our results of thermal measurement. At temperatures higher than 100℃, the I_A/I_P became constant and did not change even when the temperature decreased. The film was completely disordered and never recovered the initial state. This thermal relaxation process can be regarded as an irreversible process. Regardless of the number of spacing layers, the I_A/I_P for all the samples took a value in the range from 4.5 to 6.0. Whereas, the relevant plateau value of I_A/I_P for the PVO-PnA samples was about 2.5. The layers of the PVO-PnA film can be mixed homogeneously after disordering because all layers are composed of the same kind of polymer chains. Theoretical calculation predicts a similar value of I_A/I_P, i.e., 2.5, when the donor and acceptors are statistically distributed throughout the LB film. The larger value of I_A/I_P for ST-PnA compared with the theoretical prediction suggests that ST and PVO were separated and formed individual domains. In the polymer domain, the distance between the donor and acceptor is much closer than that calculated for a random distribution.

The isothermal measurement of energy transfer efficiency was performed at a constant temperature. I_A/I_P was measured at four different temperatures below

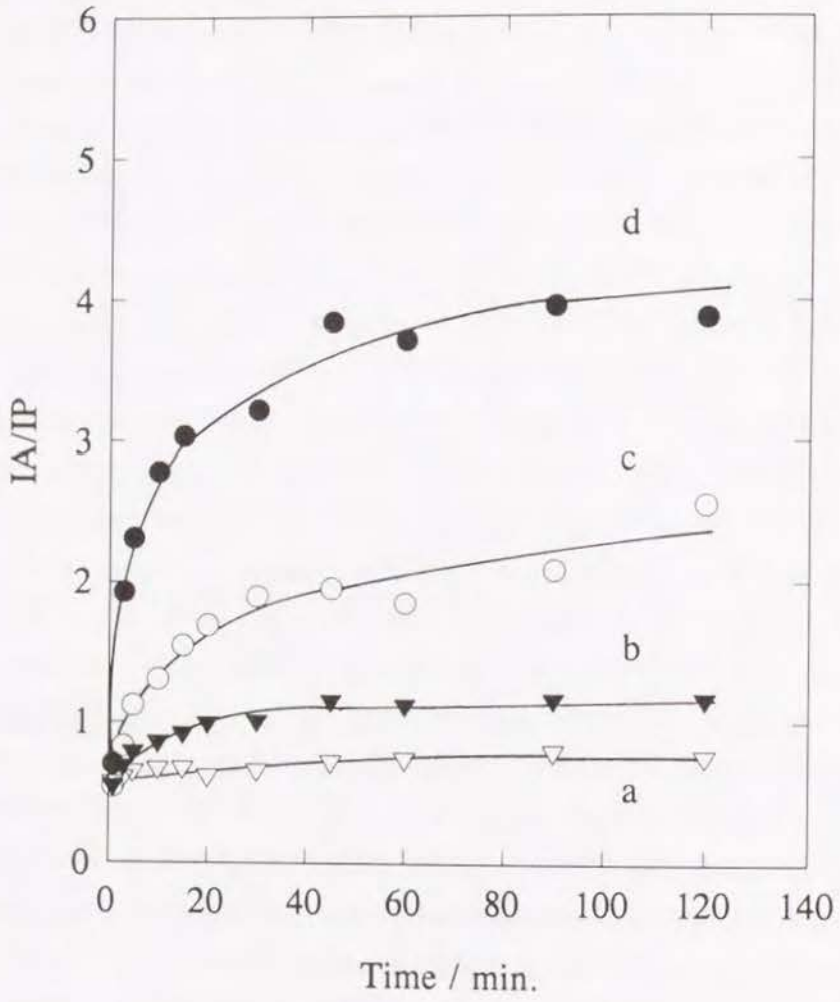

Figure 4-6. Energy transfer efficiencies for ST-P2A as a function of time at different temperatures: (a) 60 °C, (b) 70 °C, (c) 80 °C, (d) 90 °C.

90℃ as shown in Figure 4-6. At 90℃, the I_A/I_P of ST-P2A showed a sharp change related to the melting point of the spacer, and the composite film disordered completely. I_A/I_P at 80℃ changed more slowly than that at 90℃. Under 80℃, the change of I_A/I_P was very slow and the value did not rise to the value 4.5 which is regarded as a completely disordered and separated state. At temperatures lower than 50℃, no obvious change was seen within this experimental time range. These results show that the thermal property of spacing layers predominantly governs the stability of the PnA LB film.

4-3-3. Disordered Structure Observed by TEM

Transmission electron microscopy was used for the observation of disordered structure in the LB film. Figure 4-7 shows a typical dark-field electron micrograph of ST-P2A films: (a) before the heat treatment and (b) after the long-time heat treatment at a high temperature, 120℃. No obvious structure was seen in Figure 4-7(a). However, once it was heated around 120℃ for a sufficiently long time, a structure due to the relaxation of layered film clearly appeared as shown in Figure 4-7(b). As all observations were carried out in a dark-field, the bright portions show the area enriched with cadmium, because of the large scattering power of electron beam. No image could be seen when the sample was prepared without cadmium salt. In the preceding section, the I_A/I_P ratio of ST-P2A was found to reach different values at different temperatures (Figure 4-6). Several temperatures were chosen for the heat treatment to examine the different disordered structures of ST-P2A film by TEM. Figure 4-8 shows the electron micrographs at several temperatures. Unclear striped wrinkle-like patterns appeared at 70℃ (Figure 4-8(a)). This suggests that the relaxation of films occurs partly at 70℃. However the polymer LB film was not separated from the stearate LB films. Judging from the energy transfer efficiency, the layered structure is still kept at this temperature. The sample treated at a high temperature 100℃, at which the I_A/I_P changed markedly, had a different texture in the electron micrograph (Figure 4-8(b)). Many rod-like structures appeared and increased in size as a function of time.

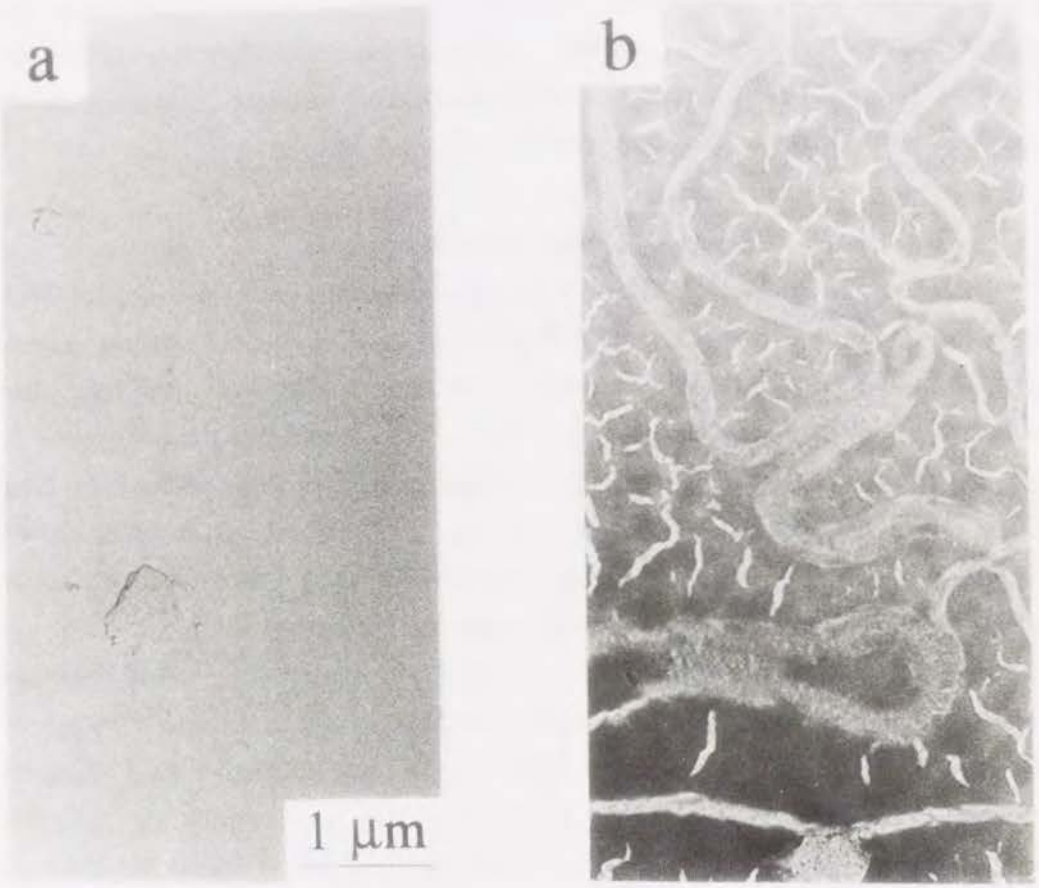

Figure 4-7. Dark-field TEM observation of ST-P2A LB film: (a) before thermal treatment, (b) after thermal treatment at 120 °C for more than 3 hours.

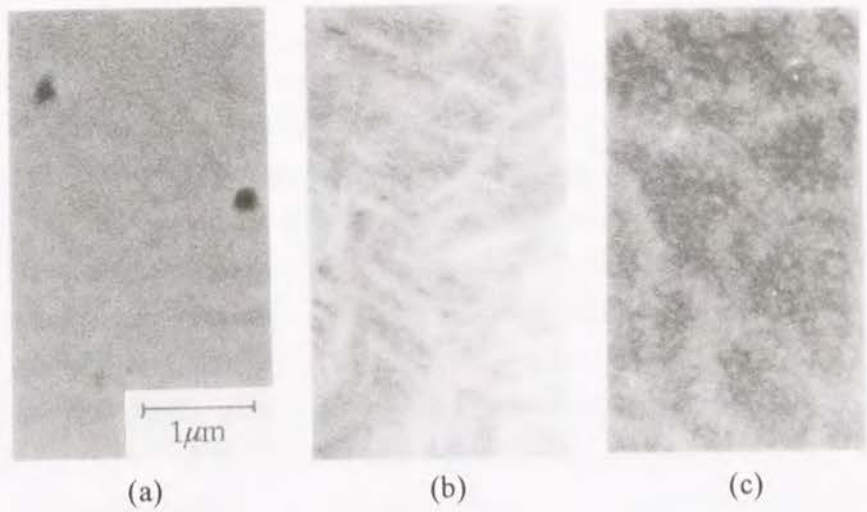

Figure 4-8. Dark-field TEM observation of ST-P2A LB film at different temperatures: (a) thermal treatment at 70 °C for 2 hours, (b) thermal treatment at 100 °C for 3 hours, (c) thermal treatment at 120 °C for 2 hours.

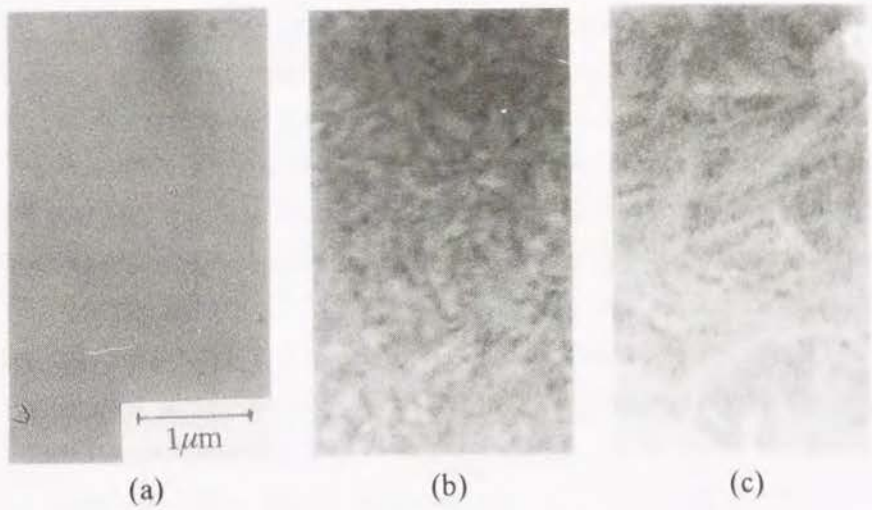

Figure 4-9. Dark-field TEM observation of ST-P2A LB film as a function of time at 100 °C: (a) before heating, (b) after 30 minutes, (c) after 180 minutes.

Figure 4-9 shows the progress of the relaxation process at 100℃ as a function of treating time. At first, no obvious structure was seen before the heat treatment (Figure 4-9(a)). Then, small oval-shaped structures appeared everywhere after 30 min of heating (Figure 4-9(b)). After more than a few hours at 100℃, the structure increased in size and became a rod-like structure of cadmium stearate (Fig.4-9(c)). The results of the energy transfer measurement showed that the relaxation process became saturated within several minutes. In this short time range of minutes, the image of electron micrograph did not show any changes. It took more than 1 h for a major alteration in the TEM image to occur. These stick-like structures seem to correspond to the cadmium stearate crystal. Since this temperature is higher than T_m of stearic acid, the stearic acid in the ST layer cannot hold their layer structures. The T_m of cadmium stearate is known to be 110℃, which is higher than the treatment temperature, 100℃. Cadmium stearate in the ST layer could maintain its structure and became the core of new structure. The layered structures of the ST monolayer were destroyed and rearranged, resulting in the growth of cadmium stearate crystals three-dimensionally. Naselli et al. reported that the disordering of the hydrocarbon tails occurs below the melting point of cadmium arachidate, and concluded that annealing for the LB film at a temperature close to the melting point does not improve the order. The studies by energy transfer method and TEM observation also indicate that ST LB film becomes disordered at 100℃, and that this annealing process accelerates the crystal growth of cadmium stearate.

At 120℃, the lattice of cadmium stearate was completely destroyed and the LB film lost its order as shown in Figure 4-8 (c). Two kinds of structures were observed; one is a thick string-shaped structure and the other is a small spot. Because the string-shaped structure was not seen in the cadmium stearate film without polymer layers, the former structure corresponds to the polymer chain which was stained with cadmium. The latter seems to be cadmium stearate crystals. At this high temperature, polymer chains aggregate and form a large domain separated from the liquid of ST. Thus, the different disordered structures were observed at different temperatures.

4-4. Conclusion

The stearate LB films with the layers of PVO containing fluorescence probes were prepared and the thermal relaxation process of the film was studied by the energy transfer method and a transmission electron microscope. The results of the energy transfer measurement revealed that the irreversible thermal relaxation process of the composite LB film occurs at elevated temperatures. This relaxation hysteresis depends strongly on the thermal property of spacing layers. To obtain direct images during the thermal relaxation process, TEM observation was carried out at three different temperatures which was related to the different relaxation stages observed by ET measurement. As a result, different types of aggregation structures were observed by TEM at several different temperatures. It should be mentioned that the energy transfer measurement is a very sensitive method *in situ* to detect the initial relaxation process of the layered structure, and TEM measurement helps visualize clearly the image of the macroscopic disordering process and phase separation, successively occurring after the relaxation of the layered structure.

References

(1) Ulman, A., *An Introduction to Ultrathin Organic Films from Langmuir-Blodgett to Self-Assembly*; Academic Press: San Diego, 1991.

(2) Bohm, C.; Steitz, R.; Riegler, H. *Thin Solid Films* **1989**, *178*, 511.

(3) Riegler, J. E. *J. Phys. Chem.* **1989**, *93*, 6475.

(4) Fukui, T.; Sugi, M.; Iizima, S. *Phys. Rev. B* **1980**, *22*, 4898.

(5) (a) Sasanuma, Y.; Kitano, Y.; Ishitani, A. *Thin Solid Films* **1990**, *190*, 317. (b) Sasanuma, Y.; Kitano, Y.; Ishitani, A.; Nakahara, H.; Fukuda, K. *Thin Solid Films* **1990**, *190*, 325. (c) Sasanuma, Y.; Kitano, Y.; Ishitani, A.; Nakahara, H.; Fukuda, K. *Thin Solid Films* **1991**, *199*, 359.

(6) Tippmann-Krayer, P.; Kenn, R. M.; Mohwald, H. *Thin Solid Films* **1992**, *210/211*, 577.

(7) Mizushima, K.; Egusa, S.; Azuma, M. *Jpn. J. Appl. Phys., Part 1* **1988**, *27*, 715.

(8) Fromhelz, P.; Oelschlägel, U. *Thin Solid Films* **1988**, *159*, 421.

(9) Rabe, J. P.; Novotny, V.; Swalen, J. D.; Rabolt, J. F. *Thin Solid Films* **1988**, *159*, 359.

(10) (a) Naselli, C.; Rabolt, J. F.; Swalen, J. D. *J. Chem. Phys.* **1985**, *82*, 2136. (b) Naselli, C.; Rabe, J. P.; Rabolt, J. F.; Swalen, J. D. *Thin Solid Films* **1985**, *134*, 173.

(11) Saperstein, D. *J. Phys. Chem.* **1987**, *91*, 2922.

(12) Rothberg, L.; Higashi, G. S.; Allera, D. L.; Garoff, S. *Chem. Phys. Lett.* **1987**, *133*, 67.

(13) Hasegawa, T.; Kamata, T.; Umemura, J.; Takenaka, T. *Chem. Lett.* **1990**, 1543.

(14) Ushikausa, T. *Jpn. J. Appl. Phys. Part 1* **1990**, *29*, 2460.

(15) Rothberg, L.; Higashi, G. S.; Allara, D. L.; Garoff, S. *Chem. Phys. Lett.* **1987**, *133*, 67.

(16) (a) LeGrange, J. D.; Riegler, H. E.; Zurawsky, W. P.; Scarlata, S. F., *J. Chem. Phys.* **1989**, *90*, 3838. (b) LeGrange, J. D.; Riegler, H. E.; Zurawsky, W. P.; Scarlata, S. F. *Thin Solid Films* **1988**, *159*, 101.

(17) Hönig, D.; Möbius, D. *Chem. Phys. Lett.* **1992**, *195*, 50.

(18) Murakata, T.; Miyashita, T.; Matsuda, M. *Langmuir* **1986**, *2*, 786.

(19) (a) Ries Jr., H. E.; Kimball, W. A. *Nature* **1958**, *181*, 901. (b) Ries Jr., H. E.; Kimball, W. A. *J. Colloid Sci.* **1961**, *16*, 361.

(20) (a) Iriyama, K.; Araki, T. *Chem. Lett.* **1990**, 1189. (b) Iriyama, K.; Araki, T.; Iwasaki, T. *Chem. Lett.* **1990**, 1365. (c) Iriyama, K.; Araki, T.; Shimada, N.; Iwamoto, M.; Sasaki, T,; Atsuzawa, M. *Thin Solid Films* **1991**, *201*, 175.

(21) (a) Kajiyama, T.; Oishi, Y.; Uchida, M.; Morotomi, M.; Ishikawa, J.; Tanimoto, Y. *Bull. Chem. Soc. Jpn.* **1992**, *65*, 864. (b) Kajiyama, T.; Oishi, Y.; Uchida, M.; Tanimoto, Y.; Kozuru, H. *Langmuir* **1992**, *8*, 1563. (c) Kajiyama, T.; Zhang, L.; Uchida, M.; Oishi, Y.; Takahara, A. *Langmuir* **1993**, *9*, 760.

(22) Uyeda, N.; Takenaka, T.; Aoyama, K.; Matsumoto, M.; Fujiyoshi, Y. *Nature* **1987**, *327*, 319.

(23) Matsumoto, M.; Uyeda, N.; Fujiyoshi, Y.; Aoyama, K. *Thin Solid Films* **1993**, *223*, 358.

(24) Richardson, W.; Blasie, J. K. *Phys. Rev. B* **1989**, *22*, 39.

(25) Ohmori, S.; Ito, S.; Yamamoto, M. *Macromolecules* **1991**, *24*, 2377.

(26) Ueno, T.; Ito, S.; Ohmori, S.; Onogi, Y.; Yamamoto, M. *Macromolecules* **1992**, *24*, 2377.

(27) Ito, S.; Ueno, T.; Yamamoto, M. *Thin Solid Films* **1992**, *210/211*, 614.

(28) Watanabe, M.; Kosaka, Y.; Oguchi, K.; Sanui, K.; Ogata, N. *Macromolecules* **1988**, *21*, 2997.

(29) Hasmony, H.; Vincent, M.; Dupeyrat, M. *Thin Solid Films* **1980**, *68*, 21.

(30) Naito, K. *J. Colloid Int. Sci.* **1989**, *131*, 218.

(31) Nomaki, T.; Yamanaka, A.; Sasaki, H.; Naito, K. *Nippon Kagaku Kaishi*

1993, 1349.

Chapter 5

Photochemical Stabilization of Polymeric Langmuir-Blodgett Films

5-1. Introduction

The ultrathin polymer film prepared by Langmuir-Blodgett (LB) technique is an attractive candidate in the field of microelectronics.[1,2] Besides the thinness of each layer, the designed structure in a molecular dimension enables one to give various functions to the polymer film. For application of the LB films, the mechanical and thermal stability of the layered structure is crucial.[3-13] Polymer LB films are expected to be more stable than the films made of conventional long-chain fatty acids.[14,15] Furthermore, they have many advantages as LB materials, e.g., variety of chemical structure,[14,16] easy introduction of functional groups,[17] fewer pin-holes and so on.[18] Introduction of reactive groups to a polymer LB film gives rise to a further possibility to realize highly thermal and mechanical stability, keeping such advantages arising from the intrinsic character of amorphous materials.

Poly(vinyl octanal acetal) (PVO) is known to form a stable monolayer on water[19], and is easily transferred onto solid substrates with a good transfer ratio around unity under a wide range of transfer conditions. Therefore, this polymer is useful for application as an insulating thin layer and as a base polymer modified with various functional groups.[20] However, the layered structure deposited on a substrate was found to be disordered at elevated temperatures.[21,22] To overcome this drawback, one effective method is the crosslinking of polymer chains. Ito et al. have already reported that the formalization reaction markedly improves the thermal stability[23]. However, there is a possibility of decomposition of the fluorescent probes during the chemical treatment. Another way to improve the thermal stability is to utilize the photochemical reaction after the LB deposition. Cinnamate ester is one of the well-known photoreactive moieties for this

purpose.[24-27]

Recently, the author has applied the energy transfer method as a probing technique for the structural relaxation and the thermal stability of polymer LB films.[21,28] The energy transfer efficiency is determined by the inverse sixth power of distance between energy donating and energy accepting chromophores. Therefore the energy transfer method is capable of probing a small change in the layer distance, and a sensitive detection is possible even for the weak fluorescence from a monolayer containing only a few percent of fluorescent probes.[29]

In this chapter, the author demonstrate the photo-control of thermal and chemical durability of ultrathin polymer films made by the LB method. This technique is of great importance in the field of coatings, adhesives, and interfacial materials.

5-2. Experimental Sections

5-2-1. Materials

Poly(vinyl octanal acetal) (PVO) was synthesized from commercial poly(vinyl alcohol) (PVA; dp=2000, Wako Pure Chemical Industries, Ltd.) according to the report by Ogata et al.[19] For the energy transfer measurement, PVO with a phenanthrene group (PVO-P) and PVO with an anthracene group (PVO-A) were also prepared with the same procedure.

Cinnamoyl groups were introduced in PVO as a photoreactive side chain by esterification of cinnamoyl chloride. The structure of poly(vinyl octanal acetal-*co*-vinyl cinnamate) (P(VO-VC)) obtained is shown in Scheme 5-1. The extinction coefficient of cinnamoyl units was determined to be 17,230 L mol^{-1} cm^{-1} at 278 nm in dichloromethane using ethyl cinnamate which is regarded as a model compound of the cinnamoyl unit. The fractions of octanal units and cinnamoyl units in the obtained polymers were calculated from the UV absorbance of cinnamoyl groups and the carbon fraction in elementary analysis. The glass transition temperature (T_g) of this polymer was determined by differential scanning

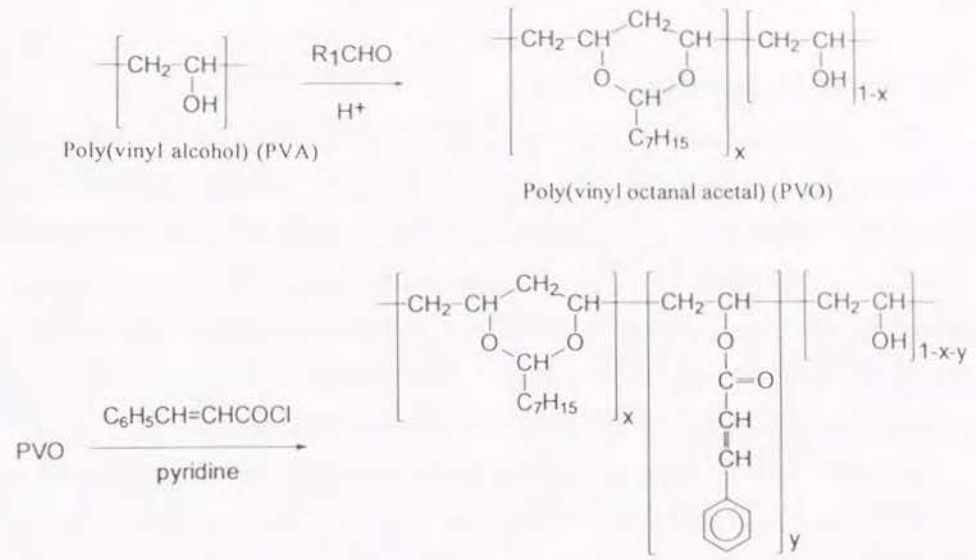

Scheme 5-1.

Table 5-1. Compositions of Synthesized Polymers and Glass Transition Temperatures

samples	octanal unit (%)	chromophore unit (%)	cinnamate unit (%)	hydroxyl unit (%)	Tg (°C)
P(VO-VC)	60.4	-	34.9	4.7	32
PVO-P	57.0	12.0	-	31.0	50
PVO-A	55.0	7.1	-	38.0	48

calorimetry (DSC). Table 5-1 shows these data together with the data for PVO, PVO-P and PVO-A.

5-2-2. Sample Preparations

The LB films were prepared as follows. Pure water for the subphase was ion-exchanged, distilled, and finally passed through a water purification system (Barnstead Nanopure II). A benzene solution of each polymer (0.01 wt%) was spread on pure water at 19 ℃ in a Teflon-coated trough (Kenkosha model SI-1). The surface film was allowed to stand for 15 min to evaporate the solvent, and compressed at a rate of 15 mm/min. The surface pressure of the film was measured by a Wilhelmy-type film balance (Shimadzu Model ST-1).

A clean non-fluorescent quartz plate (10 mm x 40 mm) was made hydrophobic by trimethylchlorosilane, and was used as a substrate for the UV irradiation and the fluorescence measurements. A silicon wafer was used for ellipsometry. The surface film on water was successfully transferred onto a substrate by the vertical dipping method at 17.5 mN m^{-1} for PVO-P, 21.0 mN m^{-1} for PVO-A, 22.0 mN m^{-1} for PVO, and 12.5 mN m^{-1} for P(VO-VC). These films were all deposited as Y-type films with good transfer ratios around unity.

5-2-3. Measurements

Surface Plasmon Spectroscopy

The use of evanescent waves has proved to be greatly helpful for the characterization of thin organic films.[30,31] Surface plasmon (SP) is one of the effective measurements which uses the evanescent waves. Figure 5-1 shows a schematic view of optics. The nearly free electron gas in the thin silver film evaporated onto the base of a prism acts as an oscillator that can be driven by the electromagnetic wave impinging on that interface. The sharp resonant excitation of a coupled state between the plasma oscillations and photons occurs at a particular angle in the range of total internal reflection. A thin dielectric coating on the bottom of the prism causes a shift of the resonance to a higher angle. From this shift and Fresnel's equations, one can evaluate the optical thickness of the

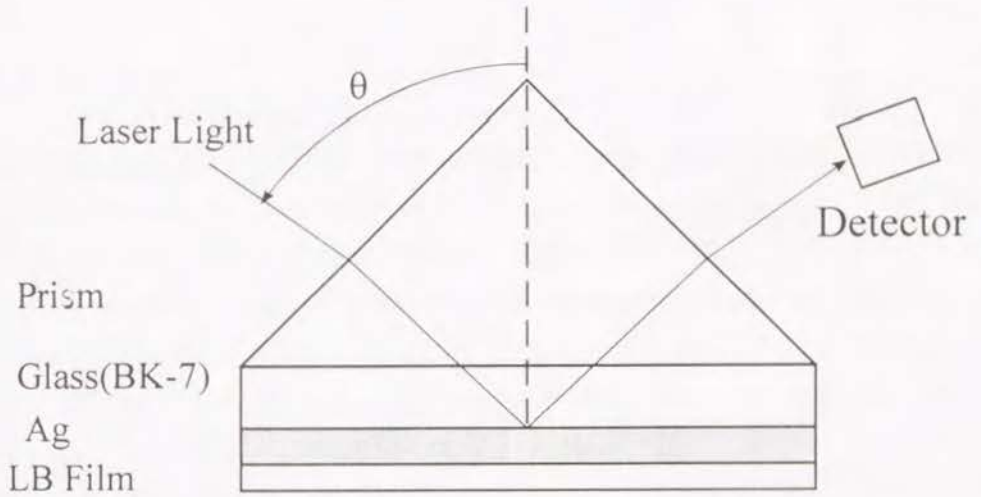

Figure 5-1. Attenuated total reflection (ATR) setup for the excitation of surface plasmon in Kretchmann geometry. A thin silver film is evapolated onto the base of the prism and acts as a resonator driven by the photon field.

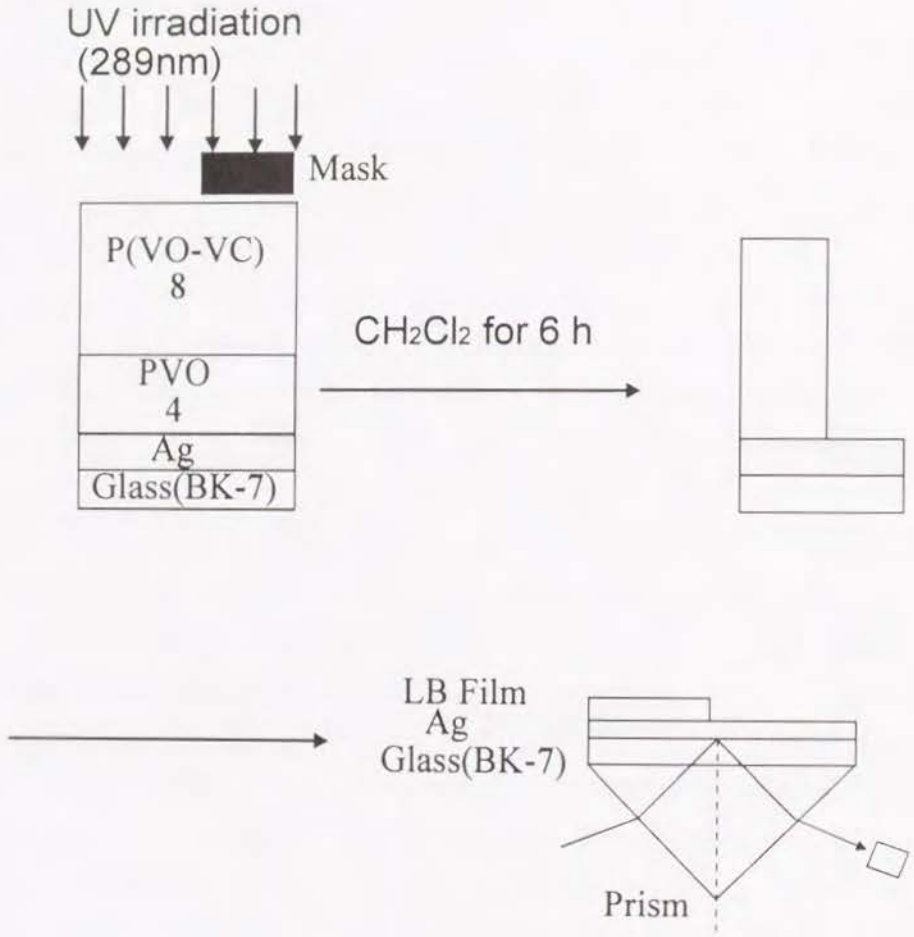

Figure 5-2. Schematic illustration of the multilayer structure of the LB film for surface plasmon measurements.

coating.

Figure 5-2 shows the layer structure of the sample for the surface plasmon experiment. The sample was fabricated on the silver coated glass plate, and UV light at 289 nm was irradiated with or without masking. Then, both portions were immersed into dichloromethane to develop the image by the difference of solubility. For the SP measurement, the glass plate was placed on the bottom of the prism, both the glass plate and the prism being optically coupled with an index matching oil. The sample was mounted on a θ-2θ goniometer, and a linearly polarized beam from a He-Ne laser, 5 mW at 632.8 nm was focussed on the prism with a beam diameter less than 0.1 mm. The p-component of the reflected light was detected by a photodiode.

Energy Transfer Method

Figure 5-3 illustrates the fabrication of LB films for the energy transfer measurements. The sample films were prepared on a quartz plate in the following sequence; At first, (1) four layers of PVO for the precoating layers, (2) two layers of PVO-P for the energy donating layers, (3) n layers (n=0, 2, 4, 6) of P(VO-VC) which act as a photoreactive spacer between the donating layers and the accepting layers were deposited. Then half of the sample was irradiated at 289 nm light for 5 min and the other half was kept under a mask. After this treatment, (4) two layers of PVO-A for the energy accepting layers, (5) (8-n) layers of PVO for the protecting layers were deposited. In order to fix the composition of the film, the total number of layers was kept to be 16 layers by adjusting the number of protecting layers; i.e., the total thickness was ca. 16 nm. Thus, the sample film having irradiated or non-irradiated spacing layers was obtained. Irradiated samples (Figure 5-3 (a)) are abbreviated as PnC'A and non-irradiated samples (Figure 5-3 (b)) are abbreviated as PnCA, where n is the number of spacing layers.

To probe the structural relaxation of the LB films, the energy transfer efficiencies between phenanthrene (P) and anthracene (A) labeled layers were measured. The critical radius of energy transfer (Förster radius) between P and A is 2.12 nm, and the donor chromophore P is selectively excited by 298 nm light.

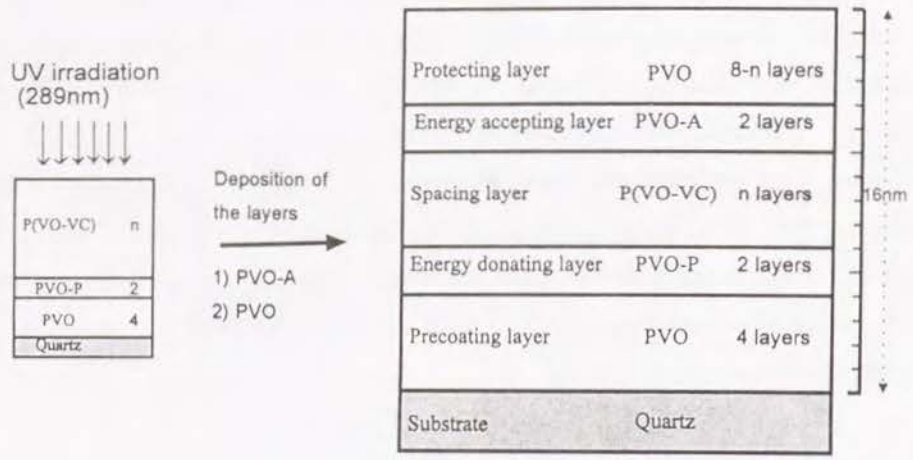

Figure 5-3. Schematic illustration of the multilayer structure of the LB film for the energy transfer measurement; (a) sample with UV irradiation (PVO-PnC'A), (b) sample without irradiation (PVO-PnCA).

The excitation energy on a P unit transfers to the A unit over the spacing layers. Here, energy transfer efficiency is determined by the distance between P and A chromophores. In the previous chapters the author showed that the chromophores are randomly distributed in the polymer layers. The transfer efficiency was evaluated using the fluorescence intensity ratio I_A/I_P on the spectrum, where I_A is the intensity of the A emission at 438 nm and I_P is that of the P emission at 350 nm. This method is convenient for eliminating the errors of intensity measurements among samples and for detecting a small change of the distance between P and A chromophores.

Other Measurements

The thickness of the LB films was measured by ellipsometry (Mizojiri Kogaku) to be 1.02 nm for a monolayer of PVO, PVO-P, and PVO-A, 0.95 nm for P(VO-VC). The glass transition temperature (T_g) for the bulk polymers was obtained by Rigaku Thermoflex DSC-8320. The samples having a cinnamoyl group were irradiated with 289 nm light from a high pressure mercury lamp (Ushio USH-102D: 100 W) for the photocrosslinking reaction. UV absorption spectra were measured by a Hitachi U-3210 spectrophotometer. The fluorescence spectra for the energy transfer measurement were recorded by a Hitachi 850 fluorescence spectrophotometer equipped with a thermo-regulated sample chamber. Heating and cooling rates were fixed to be 0.5 deg/min in the range of 20-100°C.

5-3. Results and Discussion

5-3-1. Photoreaction of P(VO-VC) LB films

Figure 5-4 shows UV absorption spectra of P(VO-VC) LB films before and after irradiation with 289 nm light. The sample consists of 4 layers of precoating PVO, 20 layers of photoreactive P(VO-VC), and 2 layers of protecting PVO on a clean quartz plate in this order. The absorption band of cinnamoyl group at 280 nm decreases with a few minutes of irradiation. IR studies have shown that the photodimerization mainly occurs by the UV irradiation.[24-27] The decrease at the

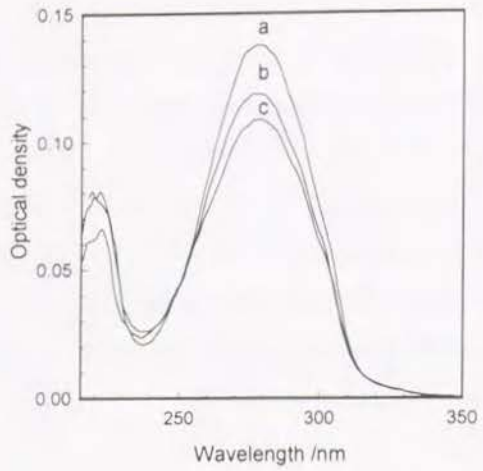

Figure 5-4. Spectral change of P(VO-VC) 20-layer film by UV irradiation: (a) before irradiation, (b) after 0.5 min irradiation, (c) after 1 min irradiation.

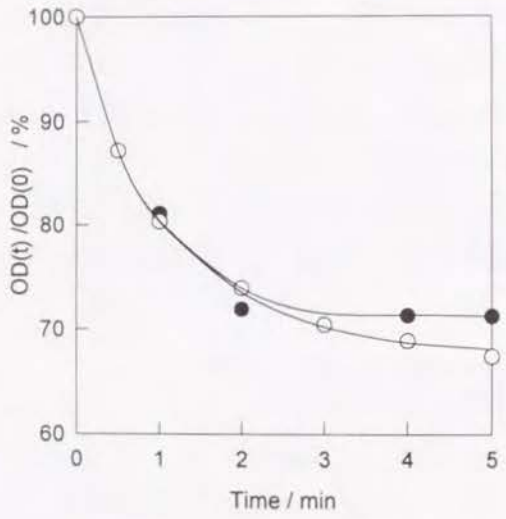

Figure 5-5. The residual cinnamoyl groups of P(VO-VC) with 289 nm irradiation as a function of time: (○) P(VO-VC) 20-layer film (ca. 26 nm in thickness), (●) P(VO-VC) cast film (ca. 40 nm in thickness).

280 nm absorption band suggests that the irradiation effectively causes photodimerization between double bonds of cinnamoyl groups which happen to be located at a position adjacent to each other in the LB film.

Figure 5-5 shows the fraction of cinnamoyl groups remaining in P(VO-VC) layers as a function of irradiation time. Within 5 min, about 35% of cinnamoyl groups reacted with each other and the photo-reaction was saturated. Although the number of cinnamoyl layers were varied from 16 to 48, the feature of the reaction curve was the same for all samples. This shows that the LB films are thin enough to be excited homogeneously across the film thickness. In order to compare the reactivity with the 3D-random system, a cast film of P(VO-VC) was prepared from the benzene solution, and then irradiated it under the same condition. The saturated values of the photoreaction curve were similar in both cases of the LB and the cast films. This indicates that there is no specific aggregation of the cinnamoyl groups, being randomly dispersed in the layer plane.

After the exposure to UV light with various irradiation periods, the LB film was dipped into dichloromethane in order to measure the solubility in the good solvent of PVO. Figure 5-6 shows the residual fractions of cinnamoyl units in P(VO-VC) 20-layer film as a function of dipping time. The non-irradiated film dissolved in dichloromethane within a few minutes of dipping, but the film became completely insoluble when it was irradiated by 289 nm light for more than 30 s. Only 1% of the film dissolved in the solvent after 1 minute irradiation. Judging from this solubility data, one can say that the film structure was completely fixed by the photoirradiation.

The author examined whether the reaction in the photocrosslinking of P(VO-VC) LB film proceeds in the inter- or intra-layer process. An alternating structure of PVO and P(VO-VC) layers (PVO-alt-P(VO-VC)) was prepared and compared with 4 layers of P(VO-VC) LB film covered with PVO layers. These two samples have different layer structures but the same number of layers and the same compositions of PVO and P(VO-VC). Both samples were irradiated with 289 nm light and the absorbance due to the remaining cinnamoyl groups was plotted as a function of irradiation time (Figure 5-7). No obvious differences in the reaction

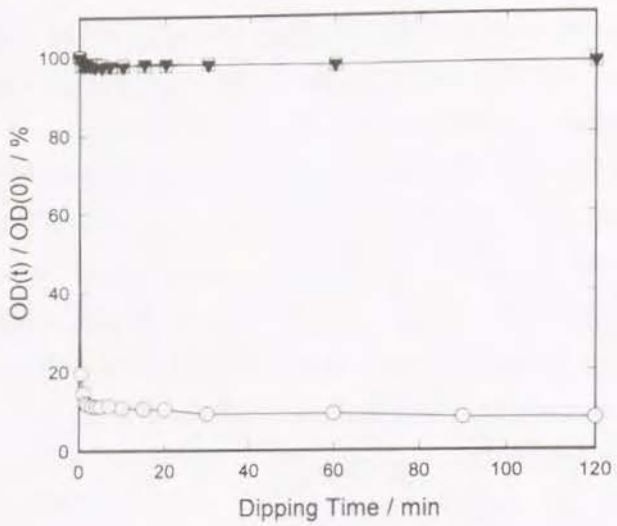

Figure 5-6. The solubility of UV irradiated P(VO-VC) 20-layer film vs. dipping time in dichloromethane; irradiation for (○) 0 min, (▼) 0.5 min, (□) 1 min.

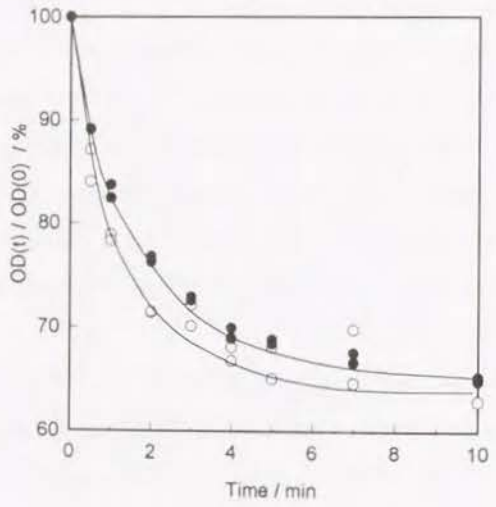

Figure 5-7. The comparison of the reactivity of P(VO-VC) LB film having different layered structures: (○) alternative LB layers of PVO and P(VO-VC), (●) P(VO-VC) LB film protected with PVO layer.

curve could be seen between these two samples. This result suggests that the intralayer photocrosslinking is predominant in the reaction of LB films.

5-3-2. Solvent Durability of Crosslinked LB Films Measured by Surface Plasmon Method

The stabilization of layered structure has been studied by the surface plasmon microscopy (SPM). Figure 5-8 shows the reflectivity of the laser light from the sample film (see Figure 5-2) as a function of the angle of incidence. The solid lines were calculated by Fresnel's formula with parameters listed in Table 5-2.

From this experiment, the thickness of the bare silver was obtained as 56 nm. Deposition of the LB film on the silver layer made the resonance curve shift to the larger angles. With the Abbe refractometer, the refractive indices of PVO and P(VO-VC) were measured to be 1.480 and 1.491, respectively. Using these values, the thicknesses of 4 layers of PVO and 8 layers of P(VO-VC) were determined as 4.1 nm and 7.6 nm, respectively. Then, the sample was irradiated with 289 nm light for 1h to complete the photoreaction; photocrosslinking was not sufficient with 5 min irradiation owing to the effect of silver coating. The contrast of the irradiated portion and nonirradiated portion in the film became clear by the treatment with dichloromethane for 6h. After this treatment, the thickness of the nonirradiated part of the film was obtained as 0 nm, i.e., the bare silver, and that of the irradiated part became 7.6 nm by the shift of resonance curve. This indicates that the masked portion dissolved completely in dichloromethane, while the irradiated portion dissolved partially. The decrease of layer thickness for the irradiated part is probably due to the dissolution of the precoating PVO layers; the underlying layers were selectively lost by the treatment. Further investigation is required for this problem.

The example presented in Figure 5-9 concerns the application of the surface plasmon. This method can be used for the microscopic characterization of the lateral thickness homogeneities of a polymeric planar waveguide structure prepared by the LB technique. This figure shows the surface plasmon microscope (SPM)

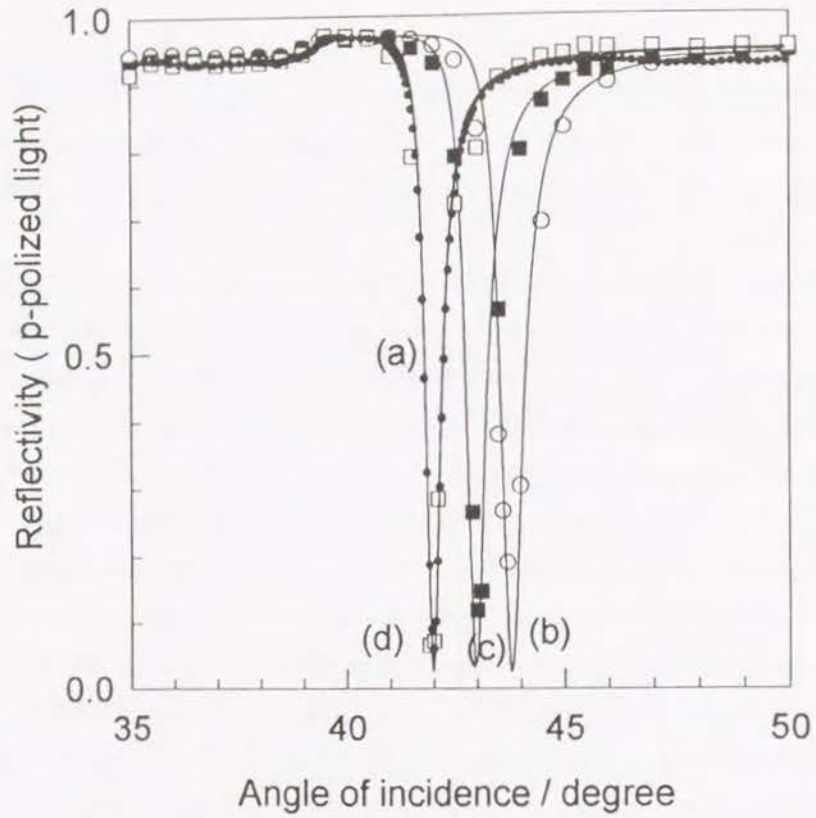

Figure 5-8. Reflected intensity vs. angle of incidence for the LB film.; resonance curve of (a) bare silver, (b) no treatment film covered with 4 layers of PVO and 8 layers of P(VO-VC), (c) the film irradiated for 1 hour and immersed in CH_2Cl_2 for 6 hours, (d) the non-irradiated film immersed in CH_2Cl_2 for 6 hours. Solid lines are Fresnel calculation.

Table 5-2. Fitting Parameters of Surface Plasmon Measurement

sample	ϵ_r [1]	ϵ_i [2]	d [3]	θ_{min} [4]
bare silver	-16.2	0.68	56.0	42.0
PVO(4)+P(VO-VC)(8) [5]	2.19	0	4.1	43.8
	2.26	0	7.6	
irradiated part	2.22	0	7.6	43.0
nonirradiated part	-	-	0	42.0

1) Real part of dielectric constant. 2) Imaginary part of dielectric constant. 3) Film thickness (nm). 4) Angle of incidence at the minimum (deg). 5) The LB film consists of 4 layers of PVO and 8 layers of P(VO-VC).

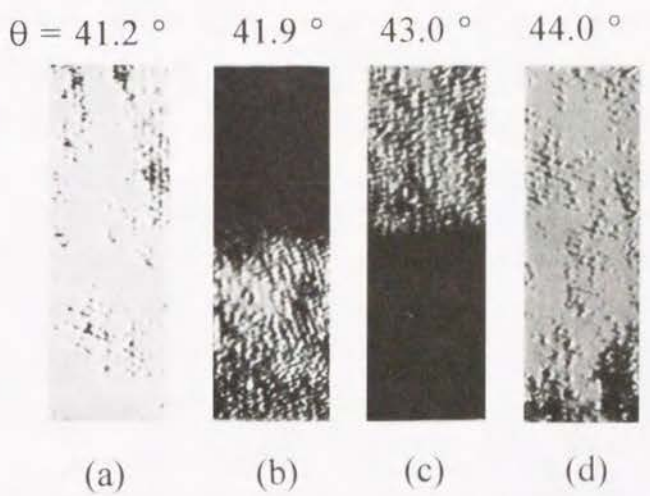

Figure 5-9. Surface plasmon microscopic image of 4 layers of PVO and 8 layers of P(VO-VC) LB film: (a) θ= 41.2° (b) θ= 41.9° (c) θ= 43.0° (d) θ= 44.0°

picture taken with p-polarized light of 632.8 nm reflected from the LB sample. Irradiation of 289 nm light with masking (the upper side of the picture) or without masking (the lower side) was done for 1h prior to the observation. When the angle of incidence was varied from 41.2° to 44.0° , one can see a clear contrast between the two parts. The dark portion of Figure 5-9 (b) (41.9°) corresponds to the sharp dip in Figure 5-8 (d), and the dark portion of Figure 5-9 (c) (43.0°) corresponds to the sharp dip in Figure 5-8 (c). Optical waveguide microscopic pictures clearly demonstrated the flatness of the LB film. Furthermore the SPM has a possibility of an optical storage with an ultrathin film in the future.

5-3-3. Thermal Stability of the Layered Structure

In the previous reports[21,23,28], the energy transfer method were successfully applied to study the thermal stability of polymeric LB films consisting of poly(vinyl alkylal acetal)s. In these cases, there were no photosensitive moieties in the sample except for energy donor and acceptor chromophores. In the present case, however, spacing layers also have photosensitive moiety and one should examine the interaction between chromphores and photocrosslinkable cinnamoyl unit before applying the energy transfer method. The following three points were checked.

1) The durability of phenanthrene probe against the 289 nm irradiation for the crosslinking of cinnamoyl unit: the PVO-P LB film was irradiated for 5 minutes by 289 nm light of a high-pressure Hg lamp, but no decrease of fluorescence intensity of phenanthrene probe was observed with this treatment. Consequently, 289 nm irradiation for the crosslinking of the cinnamoyl unit does not destroy the phenanthrene probe under this experimental condition.

2) The effect of phenanthrene probe on the photoreaction of the cinnamoyl group: The decrease of cinnamoyl groups by the UV irradiation was compared between the samples containing PVO-P layers (See Figure 5-3) and the samples without PVO-P layers. No obvious difference was seen in the reaction curve, i.e., the photoreaction is not affected by the presence of phenanthrene units.

3) Quenching of donor fluorescence by the cinnamoyl group: Various numbers

(n=0-20) of P(VO-VC) layers were deposited over the 2 layers of PVO-P, and the fluorescence intensity of phenanthrene probes (I_P) was measured. A slight decrease of I_P intensity with the increase of P(VO-VC) layers was observed. There was a linearity between log I_P and n according to the Lambert-Beer law. This result indicates that the decrease of I_P results from the absorption of the excitation light by the cinnamoyl group which has a large extinction coefficient in the wavelength range of P excitation. Thus, it can be concluded that the excitation energy on P does not transfer to cinnamoyl units.

These three experiments strongly indicate that the thermal relaxation process can be measured by the energy transfer method without interfering with cinnamoyl units.

Figure 5-10 shows the thermal stability of P6CA film and P6C'A film by plotting the ratio I_A/I_P as a function of temperature. The heating rate was fixed to 0.5℃ min^{-1}. The energy transfer efficiency was measured at every 5° in both in the heating and cooling processes. The energy transfer efficiency became higher with the approach of P and A chromophores by thermal relaxation. As seen in P6CA film which was nonirradiated, a steep rise of the ratio I_A/I_P was observed on the heating process. The film was completely disordered when the temperature rose to 100℃. After heating the film up to 100℃, the energy transfer efficiency reached a plateau region and maintained its value even when the temperature decreased, indicating that this thermal relaxation process is an irreversible process. Moreover, the energy transfer efficiencies of all samples after the complete relaxation gave a similar value around 2.5, regardless of the number of spacing layers at the initial stage. The theoretical value of I_A/I_P calculated on the basis of a random distribution of P and A chromophores showed a good agreement with the observed value: 2.5. On the other hand, I_A/I_P of P6C'A film gave a rather low value on the heating process compared with that of the P6CA film. This means that the spacing layer was fixed by the photocrosslinking, and the thermal relaxation of the film was suppressed. However, a slight increase of I_A/I_P was still observed. This is explained by the relaxation mechanism that the donor and

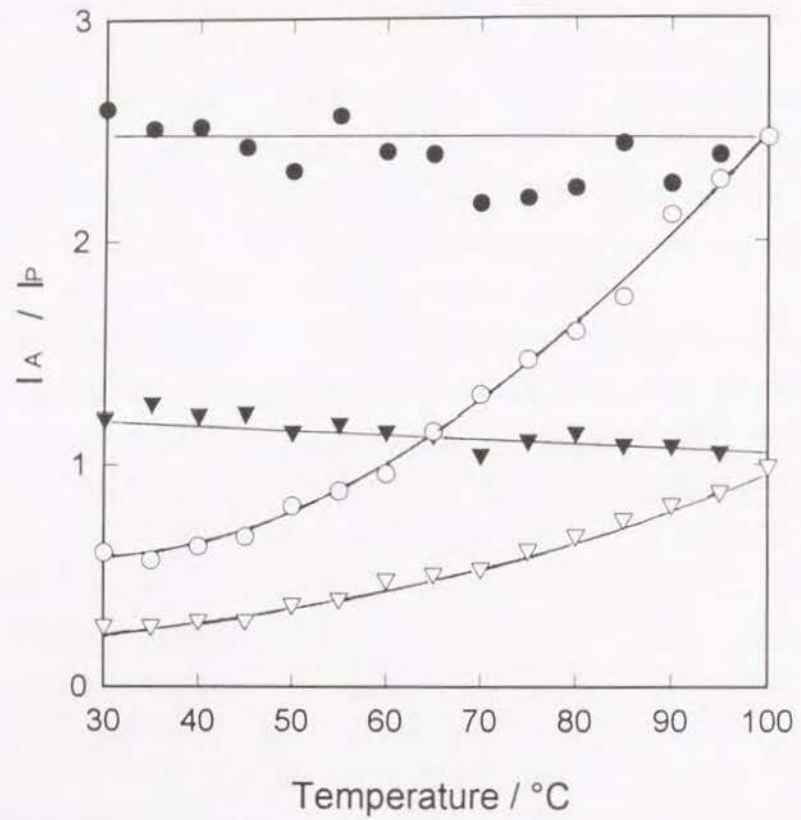

Figure 5-10. Relationship between energy transfer efficiency and temperature. Heating and cooling rates were 0.5℃ min^{-1}; energy transfer efficiency was measured at every 5 deg both in heating mode (open symbol) and cooling mode (closed symbol). Triangle represents P6C'A (5 min irradiation) and circle represents P6CA (without irradiation).

acceptor polymers penetrate into the network of fixed spacing layers. To suppress the relaxation of the LB film completely, all the layers must be fixed, including the chromophoric layers.

5-4. Conclusion

LB films containing fluorescence probes and photoreactive groups were prepared from PVO. Photochemical crosslinking after the deposition makes the LB film highly durable to the good solvent of PVO. Using energy transfer measurements, it was demonstrated that the thermal stability of layered structure is greatly improved without any serious disordering of the layers. It should be noted that photochemical crosslinking is an effective method to fix the layered structure of thin films.

References

(1) Ulman, A. An Introduction to Ultrathin Organic Films from Langmuir-Blodgett to Self-Assembly; Academic Press: San Diego, **1991**.

(2) Roberts, G. G. *Adv. Phys.* **1985**, *34*, 475.

(3) Richardson, W.; Blasie, J. K. *Phys. Rev. B* **1989**, *22*, 39.

(4) Rabe, J. P.; Rabolt, J. F. *Thin Solid Films* **1988**, *159*, 359.

(5) (a) Naselli, C.; Rabolt, J. F.; Swalen, J. D. *J. Chem. Phys.* **1985**, *82*, 2136. (b) Naselli, C.; Rabe, J. P.; Rabolt, J. F.; Swalen, J. D. *Thin Solid Films* **1985**, *134*, 173.

(6) Hasegawa, T.; Kamata, T.; Umemura, J.; Takenaka, T. *Chem. Lett.* **1990**, 1543.

(7) Saperstein, D. D. *J. Phys. Chem.* **1986**, *90*, 1408.

(8) Fukui, T.; Sugi, M.; Iizima, S. *Phys. Rev. B* **1980**, *22*, 4898

(9) Tippman-Krayer, P.; Kenn, R. M.; Möhwald, H. *Thin Solid Films* **1992**, *210/211*, 577.

(10) Sasanuma, Y.; Kitano, Y.; Ishitani, A.; Nakahara, H.; Fukuda, K. *Thin Solid Films* **1991**, *199*, 359.

(11) Böhm, C.; Steitz, R.; Riegler, H. *Thin Solid Films* **1989**, *178*, 511.

(12) Riegler, J. E. *J. Phys. Chem.* **1989**, *93*, 6475.

(13) Rothberg, L.; Higashi, G. S.; Allara, D. L.; Garoff, S. *Chem. Phys. Lett.* **1987**, *133*, 67.

(14) (a) Laschewsky, A.; Ringsdorf, H.; Schmidt, G.; Schneider, *J. Am. Chem. Soc.* **1987**, *109*, 788. (b) Ringsdorf, H.; Schmidt, G.; Schneider, J. *Thin Solid Films* **1987**, *152*, 207.

(15) Schneider, J.; Ringsdorf, H.; Rabolt, J. F. *Macromolecules* **1989**, *22*, 205.

(16) Embs, F.; Funhoff, D.; Laschewsky, A.; Licht, U.; Ohst, H.; Prass, W.; Ringsdorf, H.; Wegner, G.; Wehrmann, R. *Adv. Mater.* **1991**, *3*, 25.

(17) Ohmori, S.; Ito, S.; Yamamoto, M.; Yonezawa, Y.; Hada, H. *J. Chem. Soc. Chem. Commun.* **1989**, 1293.

(18) Matsuda,H.; Kawada, H.; Takimoto, K.; Morikawa, Y.; Eguchi, K.; Nakagiri, T. *Thin Solid Films* **1989**, *178*, 505.

(19) (a) Oguchi, K.; Yoden, T.; Sanui, K.; Ogata, N. *Polym. J.* **1986**, *18*, 887. (b) Watanabe, M.; Kosaka, Y.; Sanui, K.; Ogata, N.; Oguchi, K.; Yoden, T. *Macromolecules* **1987**, *20*, 452. (c) Watanabe, M.; Kosaka, Y.; Oguchi, K.; Sanui, K.; Ogata, N. *Macromolecules* **1988**, *21*, 2997.

(20) Ito, S.; Okubo, H.; Ohmori, S.; Yamamoto, M. *Thin Solid Films* **1989**, *179*, 445.

(21) Ueno, T.; Ito, S.; Ohmori, S.; Onogi, Y.; Yamamoto, M. *Macromolecules* **1992**, *25*, 7150.

(22) (a) Erden, C.; Laschewsky, A.; Ringsdorf, H.; Schneider, J.; Schuster, A. *Thin Solid Films* **1989**, *180*, 153. (b) Schneider, J.; Erdelen, C.; Ringsdorf, H.; Rabolt, J. F. *Macromolecules* **1989**, *22*, 3475.

(23) Ito, S.; Ueno, T.; Yamamoto, M. *Thin Solid Films* **1992**, *210/211*, 614.

(24) (a) Minsk, L. M.; Smith, J. G.; Van, Deuen, W. P.; Wright, J. F. *J. Appl. Polym. Sci.* **1959**, *2*, 302. (b) Robertson, E. M.; Deusen, W. P. V.; Minsk, L. M. *J. Appl. Polym. Sci.* **1959**, *2*, 308.

(25) Tsuda, M. *J. Polym. Sci., Part A* **1964**, *2*, 2907.

(26) Reiser, A.; Egerton, P. L. *Photograph. Sci. Eng.* **1979**, *23*, 144.

(27) Oikawa, S.; Tsuda, M.; Ueno, N.; Sugita, K. *Chem. Phys. Lett.* **1980**, *74*, 379.

(28) (a) Ohmori, S.; Ito, S.; Yamamoto, M. *Macromolecules* **1991**, *24*, 2377. (b) Hayashi, T.; Okuyama, T.; Ito, S.; Yamamoto, M. *Macromolecules* **1994**, *27*, 2270.

(29) Ito, S.; Kanno, K.; Ohmori, S.; Onogi, Y.; Yamamoto, M. *Macromolecules* **1991**, *24*, 659.

(30) Knoll, W. *Mater. Research Soc.* **1991**, *16*, 29.

(31) Knoll, W. *Makromol. Chem.* **1991**, *192*, 2827.

Chapter 6

Fluorescence Spectroscopy for a Polymer Monolayer at the Air/Water Interface

6-1. Introduction

A variety of polymers can be spread in a monolayer form at the air/water interface.[1,2] The fine structure and properties at the interface are critical to fabricate high quality polymer LB films. Electron microscopy[3] and various optical microscopies[4-8] provide direct information on the morphology of surface films, but it is difficult by microscopy to obtain molecular level information, e.g., conformation and dynamic properties of the polymer at the interface. Fluorescence spectroscopy provides another approach for the study of monolayers. Recent instrumental developments, especially the use of optical fibers and the fluorescence microscope[9] have made in situ measurements of surface films possible. The extremely high sensitivity of light detection enables one to obtain sufficient signals, even if the specimen is a monolayer containing only a few percent of fluorescent probes. Itoh et al. applied fluorescence spectroscopy for in situ study of the surface film, and some preliminary results for cellulose derivatives, which form a relatively hard and condensed type monolayer was reported in the previous study.[10]

In this chapter, flexible amphiphilic polymers, poly(vinyl alkanal acetal)s are employed as samples, and fluorescent probes, pyrene chromophores are introduced to the side chains.[10] The fluorescence behavior at the interface is carefully observed with respect to excimer formation and oxygen quenching, as a function of surface pressure.

6-2. Experimental Section

6-2-1. Materials

Poly(vinyl alkanal acetals)s were synthesized by acetalization of commercial poly(vinyl alcohol) (WakoPure Chemical Industries, DP=2000). Details have been described in the previous report of our laboratory.[11] The polymer was labeled with pyrene chromophores by a reaction of pyrenecarbaldehyde (Aldrich Chemical). Table 6-1 shows the fraction of pyrene unit and of the alkyl unit in the acetalized polymer, where octanal and dodecanal were employed as the alkyl group. These fractions were determined by UV absorption of the pyrene unit and from the carbon fraction measured by elementary analysis.

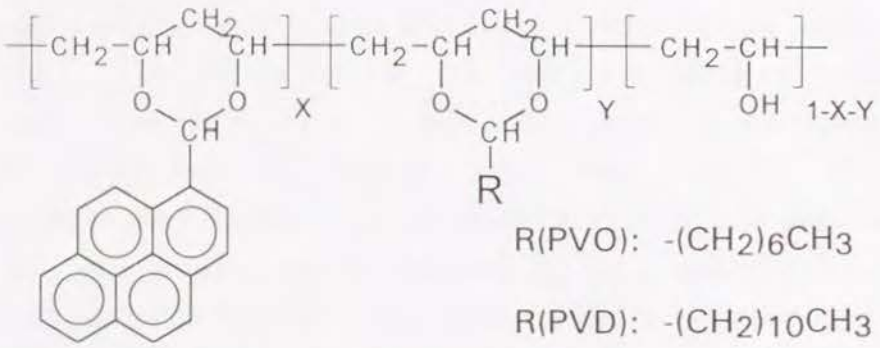

Table 6-1. Composition of Poly(vinyl alkanal acetal) and the Glass Transition Temperatures (Tg)

Sample	Alkanal	X[a] (%)	Y[b] (%)	Tg (℃)
PVO-0	Octanal	0.00	70.0	25
PVO-1	Octanal	2.91	60.3	35
PVO-2	Octanal	9.07	63.6	50
PVD-0	Dodecanal	0.00	43.9	3
PVD-1	Dodecanal	3.53	70.3	18
PVD-2	Dodecanal	11.6	64.3	38

6-2-2. Preparation of monolayer

A dilute solution of the acetalized polymer (0.01 wt%) in benzene (Dojin, spectrograde) was spread onto the surface of pure water in a Teflon-coated rectangular trough (Kenkosha Model SI-2, 15 cm x 60 cm) equipped with a Wilhelmy-type film balance. The water was purified by deionization, distillation, and then passing through a water purification system (Barnstead Nanopure II). The monolayer, which was allowed to stand for 5 min after spreading, was compressed at a rate of 10 mm min^{-1}. For comparison, a built-up film (LB film) consisting of a chromophoric monolayer was prepared on a quartz plate.

6-2-3. Measurements

Figure 6-1 shows a schematic illustration of the apparatus used in the present work. A pair of quartz optical fibers 3 mm in diameter was placed in the middle of the trough, at a distance of 5 mm above the water surface. One was used as the excitation light from a xenon flash lamp (Hamamatsu L2359 and C2190, 5W) was introduced into the entrance end of the fiber. The wavelength between 250 - 340 nm was chosen by a suitable combination of optical filters: Toshiba UVD33S and $NiSO_4$ solution filter. The other optical fiber, used for the observation of emission from the surface film, was set normal to the water surface. The exit end of the emission fiber was connected to a fluorescence spectrophotometer (Hitachi model 850). To make quantitative measurements, nitrogen gas was gently flowed over the water surface at a flow rate of 2 L min^{-1}.

Time-resolved fluorescence measurements were performed with the same apparatus, but the picosecond pulsed light (wavelength 315 nm, pulse width 20 ps, and repetition frequency 400 kHz) from a mode-locked argon and synchronously pumped dye laser system (Spectra Physics) was focused at the entrance end of the excitation light guide. The emission fiber was connected to a time-correlated single photon counting system, where a photon through a monochrometer was detected with a photomultiplier (Hamamatsu R3234) and by conventional Ortec photon counting electronics. The full width at half-maximum of the excitation pulse was observed to be 600 ps, including the total response function of the

instrument.

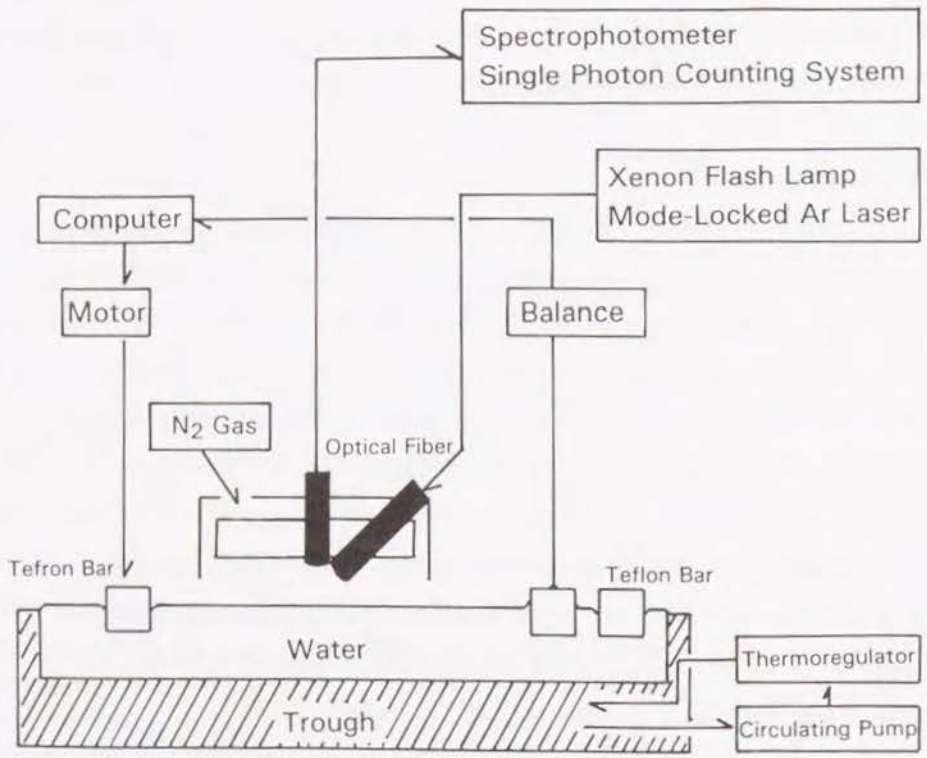

Figure 6-1. Schematic illustration of the apparatus for measuring fluorescence spectra and decay curves of monolayers at the air-water interface.

6-3. Results and discussion

6-3-1. Fluorescence intensity

Poly(vinyl alkanal acetal) is known to form a stable monolayer on the water surface and is transferable onto a solid substrate with a good transfer ratio of around unity under a wide range of transfer conditions. Therefore this polymer is useful for application to an insulating thin layer and as a base polymer containing various functional groups.[12] Figure 6-2 shows the surface pressure-area isotherms of the pyrene labeled acetalized polymers. The cohesive force between alkyl chains gives rise to a so-called condensed-type monolayer. Since the area is plotted in units of $m^2\ mg^{-1}$, a steep increase in the surface pressure is observed at different positions depending on the length of the alkyl chain and on the pyrene content. However, on the assumption that the area of a vinyl alcohol unit is 0.12 nm^2, the limiting area of acetalized unit can be evaluated to be in the range of 0.35-0.36 nm^2 for each polymer. Although the collapse pressure tends to decrease with increase in pyrene content, the monolayer is still stable and easily transfered onto a quartz substrate. This indicates that the introduction of pyrene units up to 12% does not alter the monolayer characteristics.

The emission with sufficient sensitivity could be obtained even for the monolayer containing only a few percent of chromophores. Since PVD-1 and PVO-1 provide the monomer emission of pyrene chromophores, the deactivation process of the excited state can be expected to be simple, i.e., additional interchromophore interaction such as excimer formation between chromophores need not be considered. Figure 6-3 shows the fluorescence intensity at 396 nm (monomer emission) vs. surface concentration. The broken lines in this figure show the surface pressure plotted against the surface concentration. The diagram is devided into three parts.

a) *Low concentration range below the critical concentration c*, at which the surface pressure begins to rise steeply*. In this region, the fluorescence intensity was seriously scattered, depending on the position of observation. When the emission is detected, the intensity is comparable with that observed at around c*. This means that the surface film forms a so-called island structure; a large domain

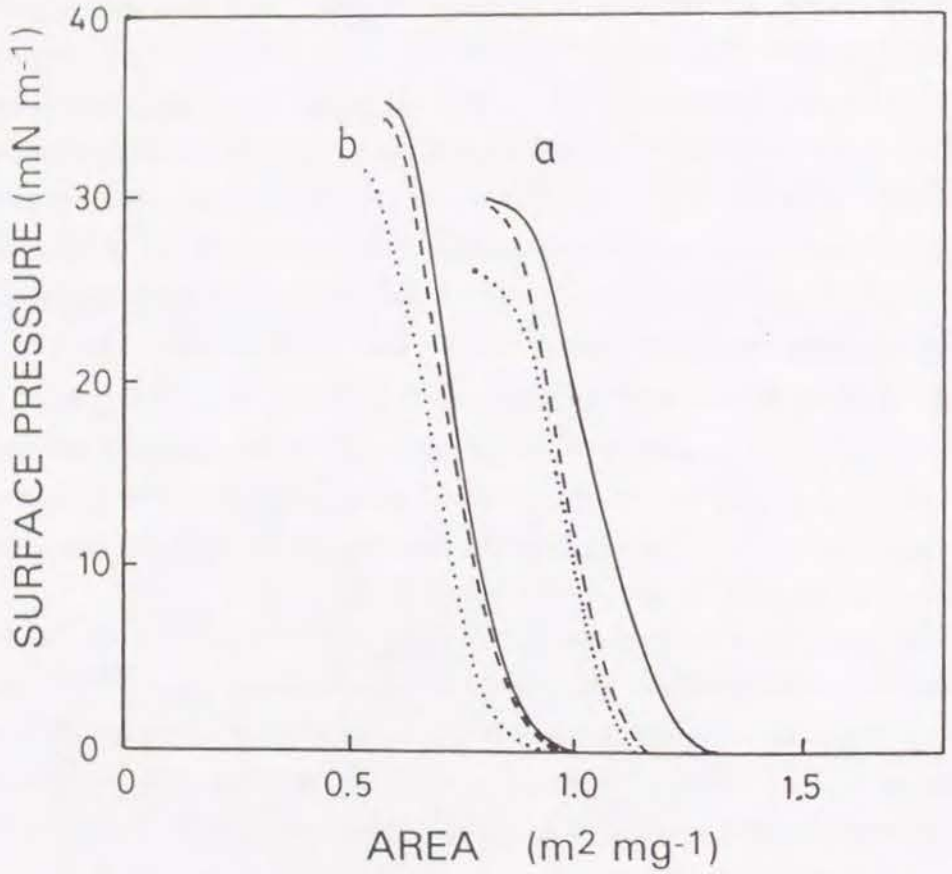

Figure 6-2. Surface pressure-area isotherms of poly(vinyl alkanal acetal)s containing pyrene chromophores at 18℃: curves a, PVO-0 (solid line), PVO-1 (dashed line), and PVO-2 (dotted line); curves b, PVD-0 (solid line), PVD-1 (dashed line), and PVD-2 (dotted line).

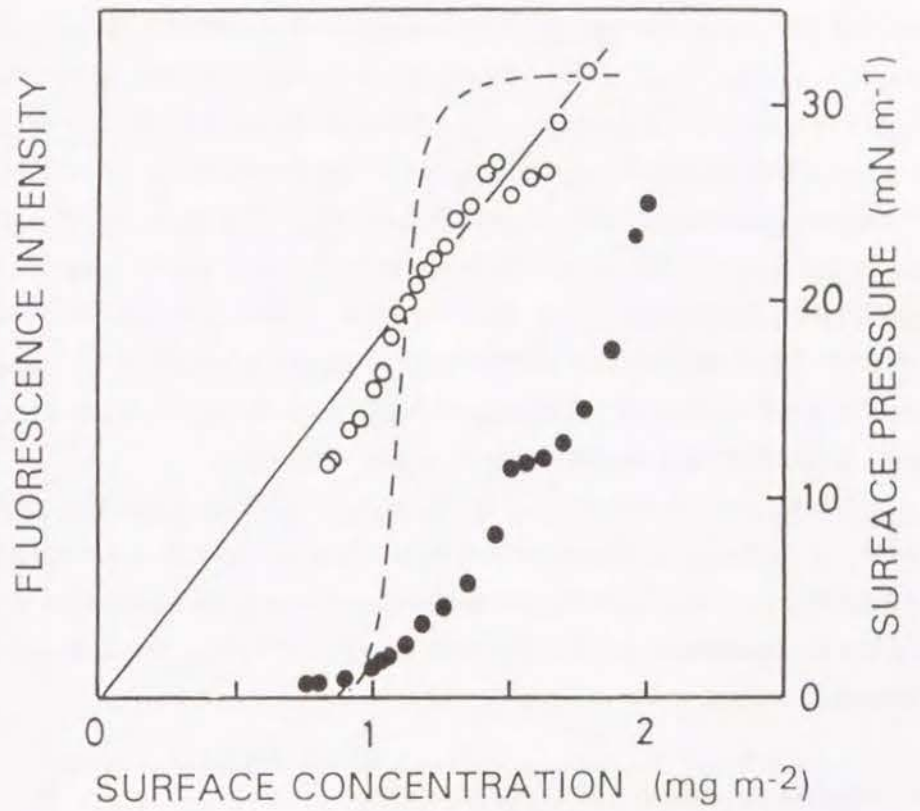

Figure 6-3. Intensity of pyrene monomer emission at 396 nm and surface pressure (dashed line) as a functions of surface concentration of PVO-1: ○, in a nitrogen atmosphere; ●,in air.

of the monolayer is floating on the water surface, but all of it is not covered yet. This situation was directly observed by a Brewster angle microscope. The image moves rapidly on the water surface, so the intensity of fluorescence also changes with time.

b) *Intermediate range between c* and the collapse concentration*. Reliable data could be obtained in this range. The fluorescence intensity is constant regardless of the position and the elapse of time. The intensity under a nitrogen atmosphere is propotional to the surface concentration, as shown by the solid line in Figure 6-3, i.e., the intensity is simply given by the total number of fluorescent molecules present within the detection area of the optical fiber. A striking effect on the intensity appeared when the atmosphere was changed to air. The intensity in air is very weak and does not show such a linear relationship to surface concentration. Quenching of the excited pyrenes by oxygen drastically weakens the intensity to about one tenth of that in the nitrogen atmosphere. The degree of quenching is affected by the shielding of the pyrenes due to the surrounding alkyl chains. This effect will be discussed in a later section.

c) *High concentration range*. In the area of collapse, a marked increase in the intensity was seen in the air atmosphere. This indicates that the pyrene units are effectively screened from oxygen molecules owing to the folded film structure.

The fluorescence behavior was well interpreted by the island model for the monolayer structure.

6-3-2. Oxygen quenching

The fluorescence response to oxygen is particularly sensitive, which may afford new means to study the packing state of the monolayer. The behavior was further investigated using time-resolved measurements. Figure 6-4 shows the decay curves of the pyrene monomer emission for a PVD-1 monolayer observed under air and nitrogen atmosphere. It is obvious that very rapid quenching occurs in air. Although the decay profile could not be fitted with a single exponential function, the main decay components at 20 mN m^{-1} were 7.4 ns in air, but 360 ns in the nitrogen atmosphere. The large discrepancy between these two values is

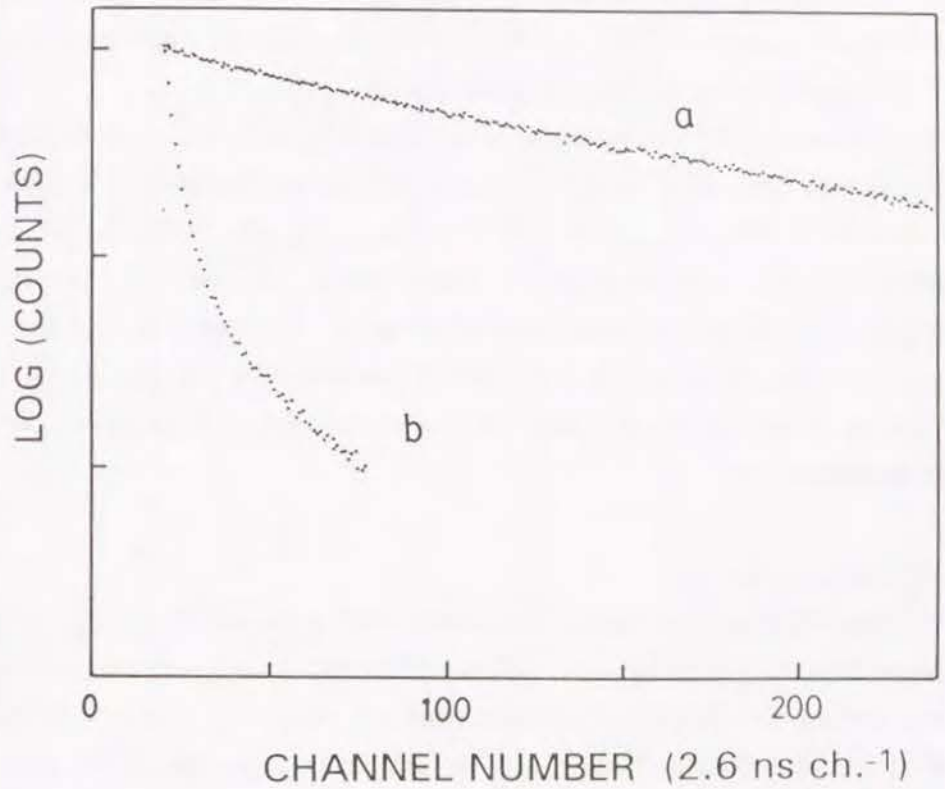

Figure 6-4. Fluorescence decay curves of PVD-1 monolayer at 20 mN m^{-1} and 18°C: points a, in a nitrogen atmosphere; points b, in air.

decreases with the increase in the surface pressure. The higher the pressure applied, the lower the quenching rate observed. This indicates that the shielding effect due to the surrounding alkyl chains becomes more effective with the compression. More important is that the quenching proceeds with a dynamic process. If the quenching takes place with a static process, e.g., complex formation between oxygen molecules and pyrenes in the ground state, there would be no change in the decay profile. The steep decay in Figure 6-4 indicates an efficient encounter of oxygen to the excited pyrenes. In order to interpret this phenomenon, it is necessary to take into account the fact that the monolayer is still flexible and mobile even in the condensed phase.

This is confirmed by comparison of the quenching efficiency with deposited monolayers (LB film) on a substrate. Figure 6-5 shows fluorescence intensities under alternation of the atmosphere. LB films are hardly affected by the presence of oxygen, but the monolayer on the water surface is markedly quenched. Considering that both consist of the same monolayer, it may safely be said that the monolayer on water is so mobile that it can be penetrated by oxygen, but the LB monolayer is closely packed with alkyl chains, which screen off the pyrenes from the oxygen quenching.

6-3-3. Excimer formation

Excimer formation provides more information on the dynamics of the monolayer, because it is formed by a collision of two pyrenes during the excitation lifetime. Indeed, the surface film showed high efficiency of excimer formation compared with the deposited films, and the efficiency depended on the applied surface pressure. Figure 6-6 shows the fluorescence spectra of the monolayer containing pyrene probes. The emission at around 380 - 400 nm is of the excited pyrene monomer, and the excimer emission appears at around 480 nm. The spectra were normalized at the maximum intensity of the monomer emission. With an increase in the surface pressure, the excimer formation was suppressed, although the probe density on the surface increased by compression. When the monolayer was deposited onto a solid substrate, the spectra changed to almost

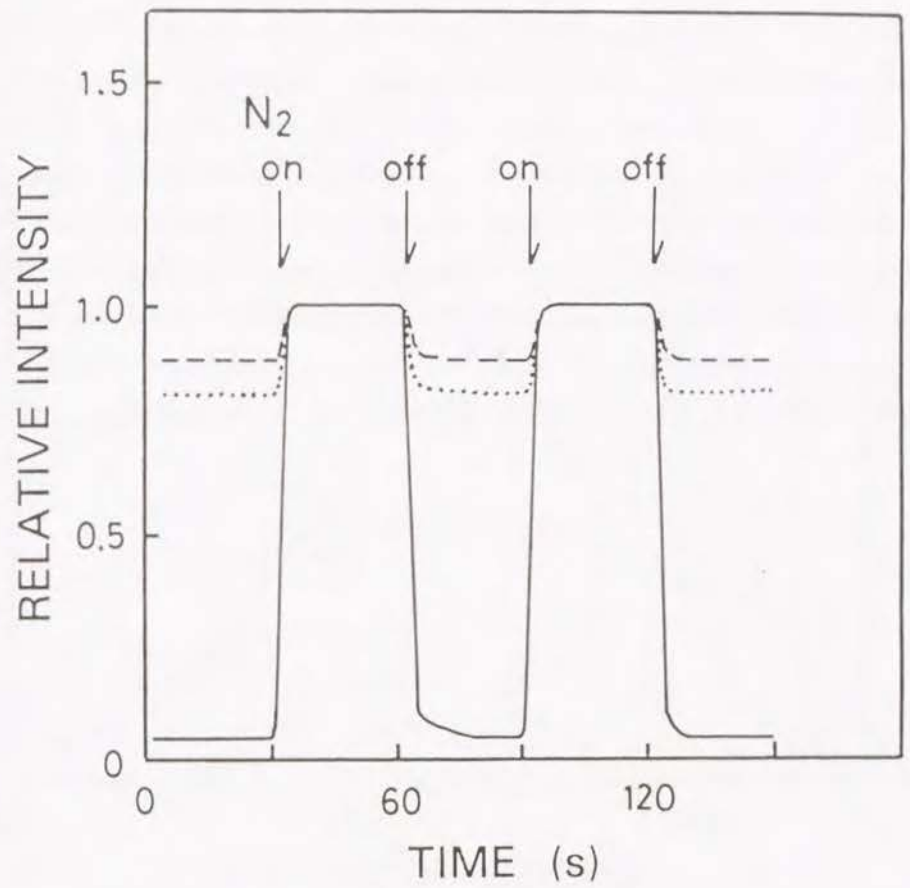

Figure 6-5. Fluorescence intensity of PVD-1 monolayer at 20 mN m^{-1} (solid line), a deposited monolayer on a quartz plate (broken line), and a deposited monolayer but covered with two layers of PVO-0 film (dashed line).

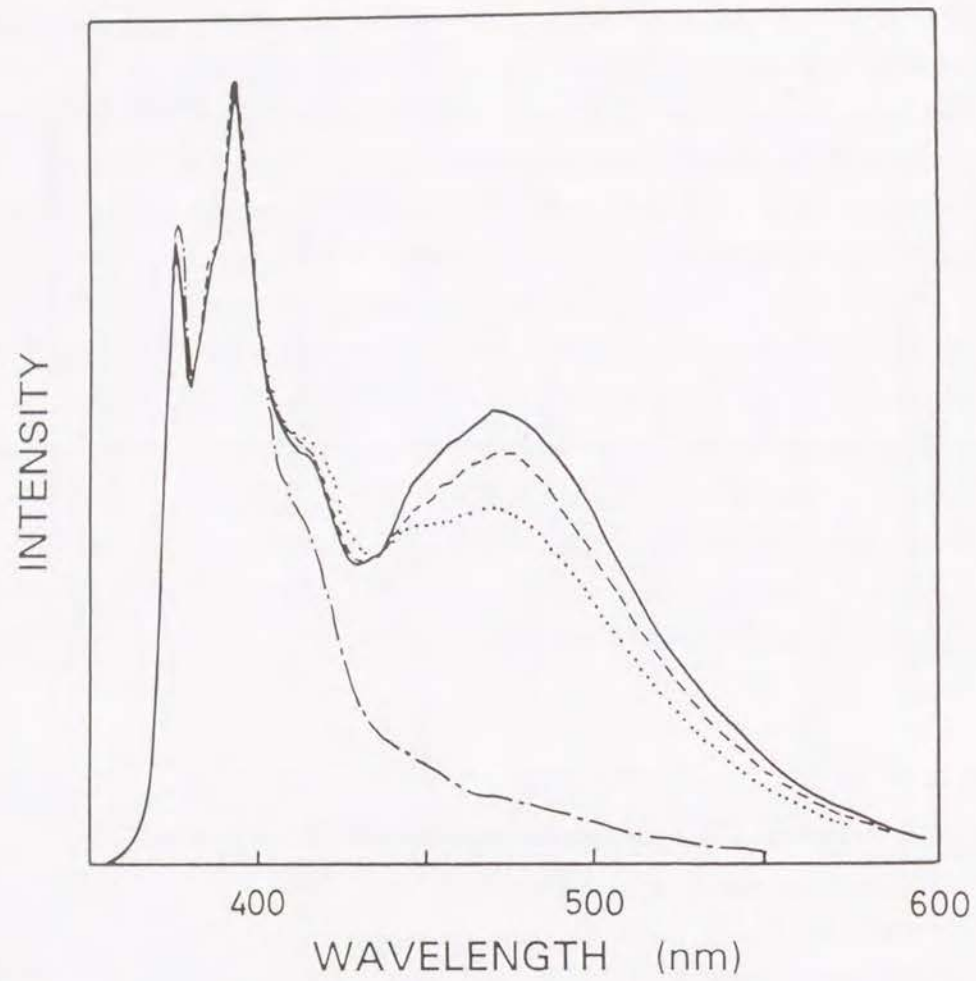

Figure 6-6. Fluorescence spectra of a PVO-2 monolayer in a nitrogen atmosphere at 18°C; 0.1 mN m^{-1} (solid line), 10 mN m^{-1} (dashed line), 25 mN m^{-1} (dotted line), deposited monolayer on a quartz plate (mixed line).

monomer emission. These results indicate that the excimer is formed mainly by a dynamic process due to microscopic diffusion of polymer segments. This is in contrast with the previous data obtained in a monolayer of cellulose derivatives, which consist of hard chain molecules.[10]

Figure 6-7 shows the rise and decay curves of excimer emission observed for the PVD-2 monolayer on water and on a solid substrate. As for the deposited film, the excimer intensity is weak and there is no rising component in the decay curve. This indicates the way of static excimer formation at a site where two pyrene units happen to take a parallel arrangement in the monolayer. On the other hand, the clear rise component for the monolayer on water means that the excimer is formed by a dynamic process during the excitation lifetime. These results show that the monolayer from poly(vinyl alkanal acetal) maintains mobility even in the compressed state. This is probably due to the flexible molecular structure of the acetalized polymer chain. Furthermore, the acetal head group has a larger area

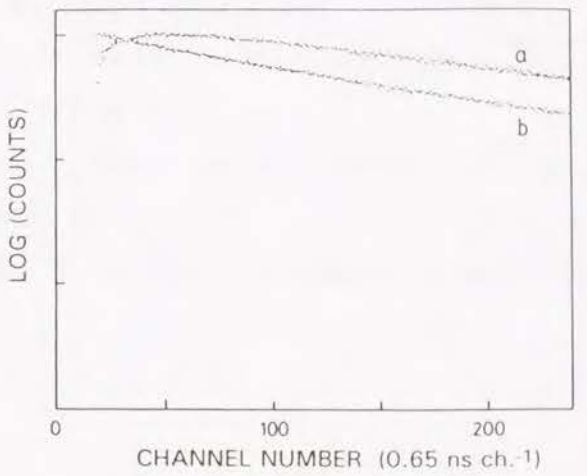

Figure 6-7. Rise and decay curves of excimer emission (500 nm) of a PVD-2 monolayer: points a, at the nitrogen-water interface; points b, deposited monolayer on a quartz plate.

than a single alkyl chain and the alkyl chain is too short to crystallize. This polymer is known to be easily transferred onto a substrate and gives rise to uniform LB films with few pin-holes. The dynamic properties at the interface must be a critical factor determining the quality of the relevant LB films. Fluorescence spectroscopy provides a unique and valuable technique for studying monolayers in situ from the molecular side.

6-4. Conclusion

Poly(vinyl alkanal acetal)s were synthesized and part of the side chains were labeled with pyrene chromophores. The packing state of the monolayer on water surface or on solid substrate was examined by the measurement of fluorescence intensity and lifetime of pyrenes. The intensity of monolayer was greatly influenced by the surroundings. Time-resolved measurement of the excimer formation of pyrenes revealed the dynamic behavior of the monolayer. Thus, *in situ* fluorescence spectroscopy provides molecular information on monolayers at the air / water interface.

References

(1) Crisp, D. J. *Surface Phenomena in Chemistry and Biology*, D. J. Danielli, K. G. A. Pankhurst and A. C. Riddiford Eds., Pergamon, Oxford, **1958**, p. 23.

(2) Tredgold, R. H.; Winter, C. S. *Thin Solid Films* **1983**, *99*, 81.

(3) Kato, T.; Iriyama, K.; Araki, T. *Thin Solid Films* **1992**, *210*, 79.

(4) Takoshima, T.; Masuda, A.; Mukasa, K. *Thin Solid Films* **1992**, *210*, 51.

(5) Overbeck, G. A.; Hönig, D.; Möbius, D. *Langmuir* **1993**, *9*, 555.

(6) Mann, E. K.; Henon, S.; Langevin, D.; Meunier, J. *J. Phys. II, Paris*, **1992**, *2*, 1683.

(7) Putman, C. A. J.; Hansma, H. G.; Gaub, H. E.; Hansma, P. K. *Langmuir* **1992**, *8*, 3014.

(8) Vaidyanathan, S.; Patterson, L. K.; Möbius, D.; Gruniger, H. R. *J. Phys. Chem.*, **1985**, *89*, 491.

(9) Meller, P. *J. Microsc.*, **1989**, *156*, 241.

(10) Itoh, T.; Tsujii, Y.; Fukuda, T.; Miyamoto, T.; Ito, S.; Asada, T.; Yamamoto, M. *Langmuir* **1991**, *7*, 2803.

(11) Ohmori, S.; Ito, S.; Yamamoto, M.; Yonezawa, Y.; Hada, H. *J. Chem. Soc., Chem. Commun.* **1990**, *23*, 4047.

(12) Ohmori, S.; Ito, S.; Yamamoto, M. *Macromolecules* **1990**, *23*, 4047.

Part II

Photocontrol of Liquid Crystal Formation

Chapter 7

Phase Transition Behavior Induced by Photoisomerization for the Mixture of Liquid Crystal - Photochromic Compound

7-1. Introduction

Liquid crystalline molecules can accommodate guest molecules in the liquid crystalline state.[1-3] If the structure of the guest molecule is greatly different from that of the host molecule, a small amount of guest molecule distorts the liquid crystalline structure and inhibits the formation of the liquid crystal in the system. Therefore, the structural change of the guest molecules determines the capability of liquid crystal formation. Recently many researchers have shown great interests in the switching behavior of liquid crystal and are examining the applications for photo-recording materials.[4-10] Ikeda et al. extensively studied photochemically induced isothermal phase transition in polymer liquid crystals (PLC).[10-15] They prepared PLC with azobenzene and examined the chain length effect and molecular weight effect on the photo-induced phase transition behavior.

One of the research projects is to understand the characters of photofunctional liquid crystalline polymers. In this chapter, the following points are examined. Firstly, the author examine the condition to control the phase transition by photoisomerization. Secondly, the author examine the polymer effect on liquid crystal formation. Two types of mixed systems are examined. One is the mixture of a low molecular weight liquid crystal with a low molecular weight photosensitive azo compound, and the other is the mixture of a low molecular weight liquid crystal with a photosensitive azo-containing polymer.

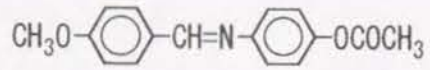

APAPA

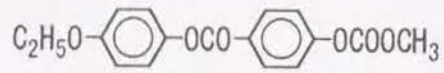

MEPC

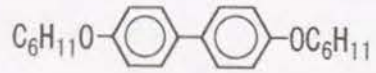

HOD

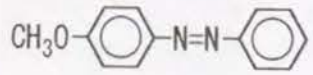

MAZO

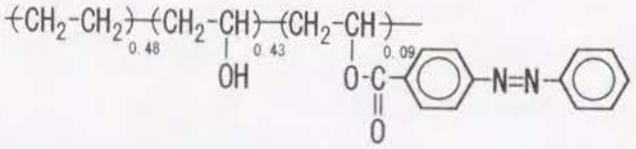

Eval-Azo

7-2. Experimental Section

7-2-1. Materials

(4-Methoxybenzylidene)-4-acetoxyaniline (APAPA), methyl-4-(4'-ethoxyphenoxycarbonyl) phenylcarbonate (MEPC), and 4,4'-di-n-hexyloxydiphenyl (HOD) were purchased from Tokyo Kasei as the samples of low molecular weight liquid crystal. Trans-*p*-methoxyazobenzene (MAZO) (Tokyo Kasei) was used for the low molecular weight photosensitive molecule.

A photosensitive polymer was synthesized starting from Eval (EP-G110A: Kuraray, ethylene content 48mol%) by esterification with *p*-phenylazobenzoylchloride (Tokyo Kasei). The product was purified by the precipitation method from dimethylformamide (DMF) solution into diethylether three times. This photosensitive polymer is abbreviated as Eval-Azo.

7-2-2. Measurement

DSC (Mettler FP-85) measurements were carried out to analyze the thermotropic properties of liquid crystalline mixtures with various content. Phase transition behavior was observed by a polarization microscope (Nihon Kogaku, OPTIPHOTO-POL) attached with a hot stage. A photodetector (Nihon Kogaku, P1) was used for the measurement of transmission light intensity. For photoisomerization of azobenzene moieties, the samples were irradiated with 365 nm or 436 nm light from a high pressure mercury lamp (Ushio USH-102D: 100W) until it reached a photostationary state, e.g., more than 30 min. UV absorption spectra were measured by a spectrophotometer (Shimadzu, UV-200S).

7-3. Results and Discussion

7-3-1. Doping effect of azobenzene unit into liquid crystal

Trans-*p*-methoxyazobenzene (MAZO) is a rodlike molecule. Its inclusion does not disturb the liquid crystal formation because of the rodlike structure of MAZO. MAZO was mixed in the low molecular weight liquid crystal with various contents, and then the temperature range of its liquid crystalline state

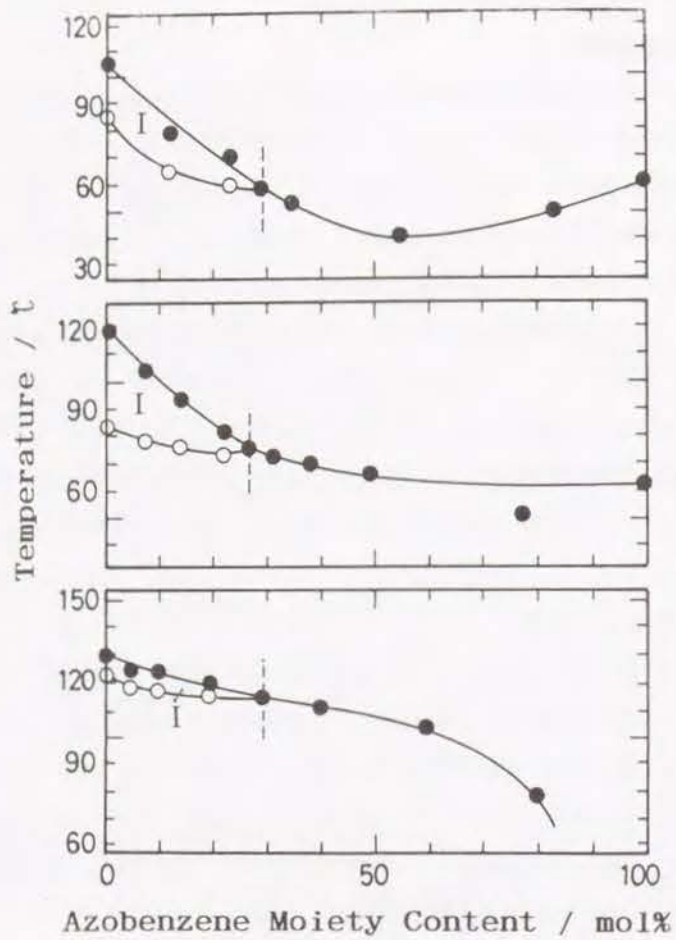

Figure 7-1. Phase diagrams of the mixtures of a low molecular weight liquid crystal and a low molecular weight photosensitive azo compound; (a) mixture of APAPA and MAZO, (b) mixture of MEPC and MAZO, (c) mixture of HOD and MAZO. (○) the transition temperature from glassy state to liquid crystalline state, (T_{LC}), (●) transition temperature from a liquid crystal state or a glassy state to the isotropic liquid (T_{ISO}).

was measured. Three different types of low molecular weight liquid crystals were chosen for the measurement. Figure 7-1 (a), (b) and (c) show the phase diagrams for the mixture of MAZO with azomethine liquid crystal (APAPA), carbonate liquid crystal (MEPC), and biphenyl liquid crystal (HOD), respectively. Transition temperatures were measured by DSC. Open circles represent the transition temperature from a glassy state to nematic liquid crystal (T_{LC}), and closed circles represent the transition temperature from nematic liquid crystal or glassy state to isotropic liquid phase (T_{ISO}). A polarized microscope was also used for the observation of these transition temperatures. These transition temperatures observed by a polarized microscopy agreed with DSC data within the experimental error. The temperature range of liquid crystal formation became narrower with increasing the guest molecule content of MAZO. All three mixed samples lost their ability to form the liquid crystal by the addition of 25-30 mol% MAZO. The azobenzene unit showed the same effect as the guest molecule in these three kinds of low molecular weight liquid crystals.

7-3-2. Photo- and thermal isomerization of azobenzene unit

The photo- and thermal isomerization of MAZO was investigated. First, the photo-isomerization of MAZO in chloroform solution was studied. Figure 7-2 (a) and (b) shows the UV spectral changes by 365 nm or 436 nm irradiation as a function of the irradiation time. By the irradiation of 365 nm light, MAZO easily turned from trans form to cis form. On the other hand, the irradiation of 436 nm light to cis-MAZO changed its form to trans-MAZO. The photoisomerization products reached an equilibrium state within 90 min irradiation either with 365 nm light or 436 nm light.

Secondly, the thermal effect for the isomerization was studied. MAZO was mixed with MEPC and was irradiated by 365 nm light at various temperatures. The influence of environment to the photoisomerization of MAZO was shown in Figure 7-3. The cis fraction of MAZO mixed with MEPC and that of MAZO alone in DMF solvent are plotted as a function of temperature. The latter was used as the reference. The concentrations of MAZO in MEPC were

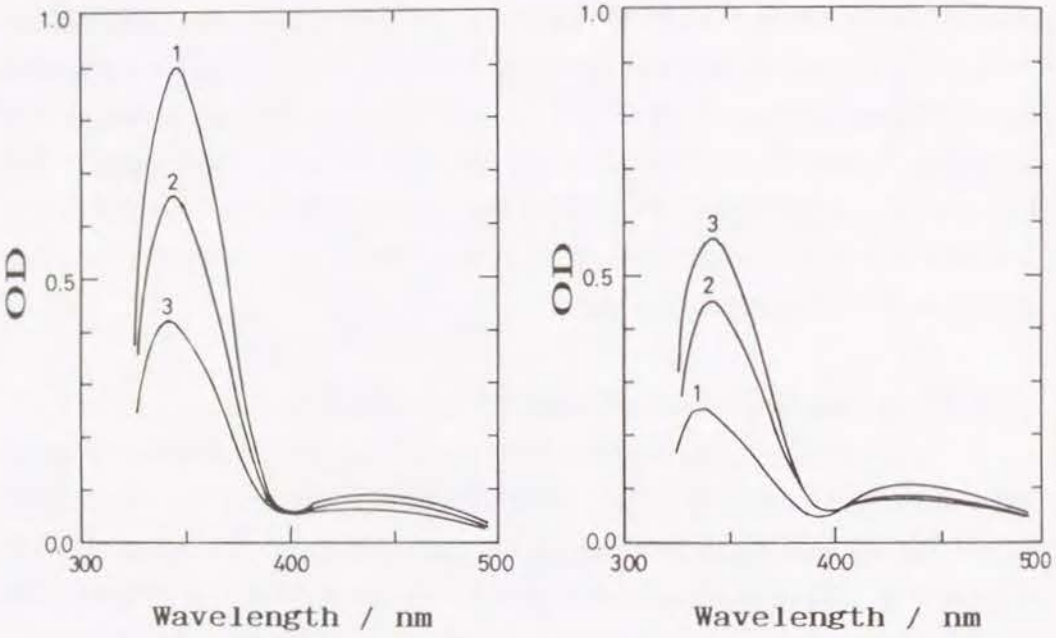

Figure 7-2. Absorption spectra of MAZO in chloroform; (left) spectral changes from trans to cis with 365 nm light irradiation for (1) 0 min, (2) 5 min, and (3) 10 min. (right) spectral changes from cis to trans with 436 nm light irradiation for (1) 0 min, (2) 5 min. (3) 10 min.

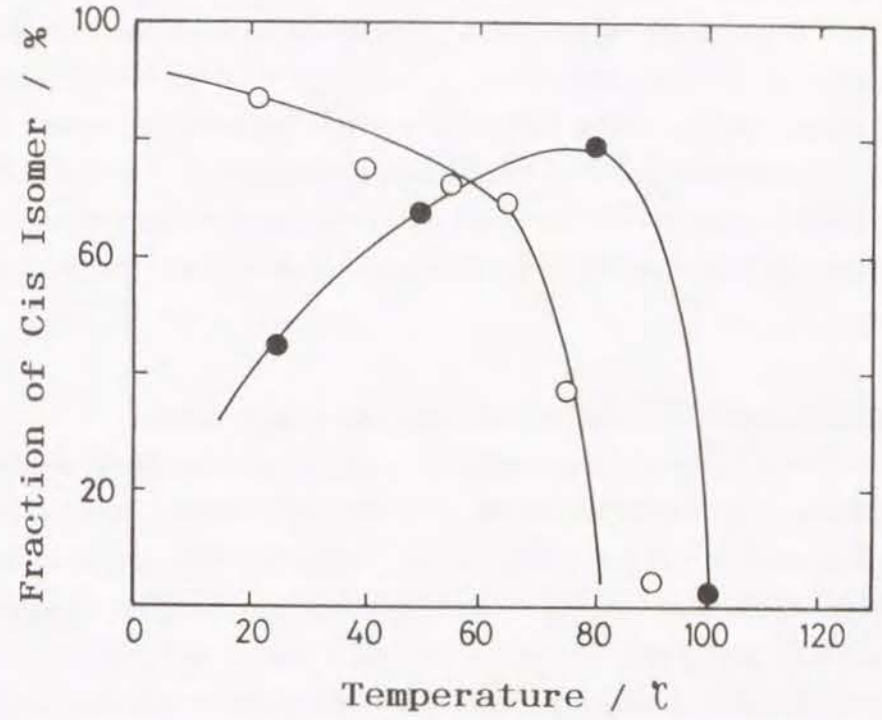

Figure 7-3. Temperature dependence of trans to cis photo-isomerization with 365 nm light irradiation for 90 min; (○) MAZO in DMF solvent, (●) MAZO with MEPC.

varied from 13.8 mol% to 27.4 mol%, however, no obvious difference in the result was seen, therefore only the result for 27.4 mol% MAZO in MEPC (MAZO27) is plotted in this figure. The liquid crystalline mixture such as MAZO27 decreased its T_{LC} from 80℃ to 70℃. In a low temperature range, MAZO27 is in a solid phase and MAZO is difficult to isomerize owing to the ambient restriction. When the temperature becomes 60℃, much free volume around MAZO is obtained and it makes the isomerization much easier. With further increase of temperature, the thermal back reaction from cis to trans form becomes predominant and the cis content of MAZO at 100℃ becomes very small. As a result, the cis content of MAZO in MEPC showed a maximum at around 70℃ to 80℃. In DMF solvent, MAZO has no special restriction to the isomerization, the effect of thermal back reaction is predominantly observed with the increase of temperature.

7-3-3. Photoirradiation effect of the low molecular weight mixture

The influence of photoirradiation on the liquid crystal formation ability for the mixture of a low molecular weight liquid crystal with a low molecular weight photosensitive azo compound was investigated. The carbonate liquid crystal MEPC-MAZO mixture was selected for this study. The phase diagram of the mixture before and after 365 nm irradiation is shown in Figure 7-4. This diagram was plotted by measuring transmission light intensity with the change of temperature. As already mentioned in Figure 7-1 (b), unirradiated samples showed the liquid crystalline state up to 28 mol% of azobenzene unit. On the other hand, the irradiated samples with 18 mol% of azobenzene unit no longer showed the liquid crystalline state. The region II in the diagram represents a photocontrolled area, that is, the liquid crystalline state before irradiation and the isotropic state after irradiation. However, for the low molecular weight mixture, the photo-recording ability decreased drastically with repeating cycles because the phase separation of the mixture easily occurred by the crystalization.

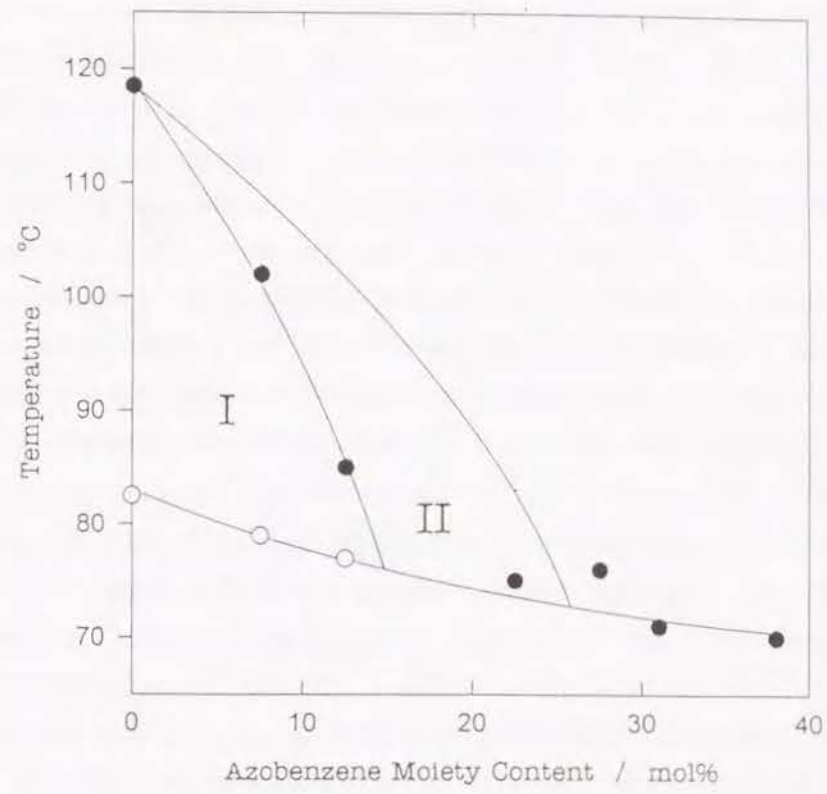

Figure 7-4. Phase diagram of mixtures of MEPC and MAZO after 365 nm irradiation; (○) the transition temperature from the glassy state to liquid crystalline state, (T_{LC}), (●) transition temperature from the liquid crystalline or from the solid state to the isotropic state (T_{ISO}). Area I is liquid crystalline regardless of the irradiation. Area II is liquid crystalline before irradiation and isotropic after irradiation. Photo-induced phase transition occurred in the area II.

7-3-4. The photoirradiation effect of the polymer mixture

In order to distribute photo-functional groups randomly in a low molecular weight liquid crystal, azobenzene group was attached as the polymer side chain and this polymer is called Eval-Azo. The azomethine liquid crystal (APAPA) was mixed with the photosensitive polymer of Eval-Azo (polymer mixture) and the effect of azobenzene content on the ability of liquid crystal formation was investigated. The phase diagram of the polymer mixture is shown in Figure 7-5. The abscissa in Figure 7-5 represents the mol% of azobenzene unit in the mixture; azobenzene units in the total of APAPA and azobenzene residue are counted. Since the polymer main chain is excluded from the liquid crystalline part, the volume of polymer chain was not taken into account in this value. The reason is described later. The liquid crystalline state was formed until the dopant concentration reached to 8 mol%. Compared with the diagram of the low molecular weight mixtures (Figure 7-1), the decrease of T_{LC} with the increase of the photosensitive polymer content was not observed in Figure 7-5. This is because azobenzene unit is covalently bonded to the polymer chain, and is not incorporated into the liquid crystal domain. However, the temperature range of liquid crystalline state became narrower with increasing Eval-Azo content. This indicates the photosensitive molecules effectively disperse in the mixture. Though it is difficult to estimate the disturbing effect of polymer, it can be said that the polymer distributed randomly in the system without getting into the liquid crystal domain.[16-18] Namely, polymer main chain exists outside the domains and only the photosensitive side chains are incorporated in the domain.

The polymer mixture was irradiated by 365 nm light for 90 min at 80℃. Figure 7-6 shows the diagram of the irradiated and unirradiated samples. In this system, the limiting concentration of azobenzene unit reduced to ca. 2.8 mol%. The T_{LC} in the irradiated system agreed with that of unirradiated system within experimental error. This result also supports the fact that polymer itself is not incorporated into the liquid crystal domain.

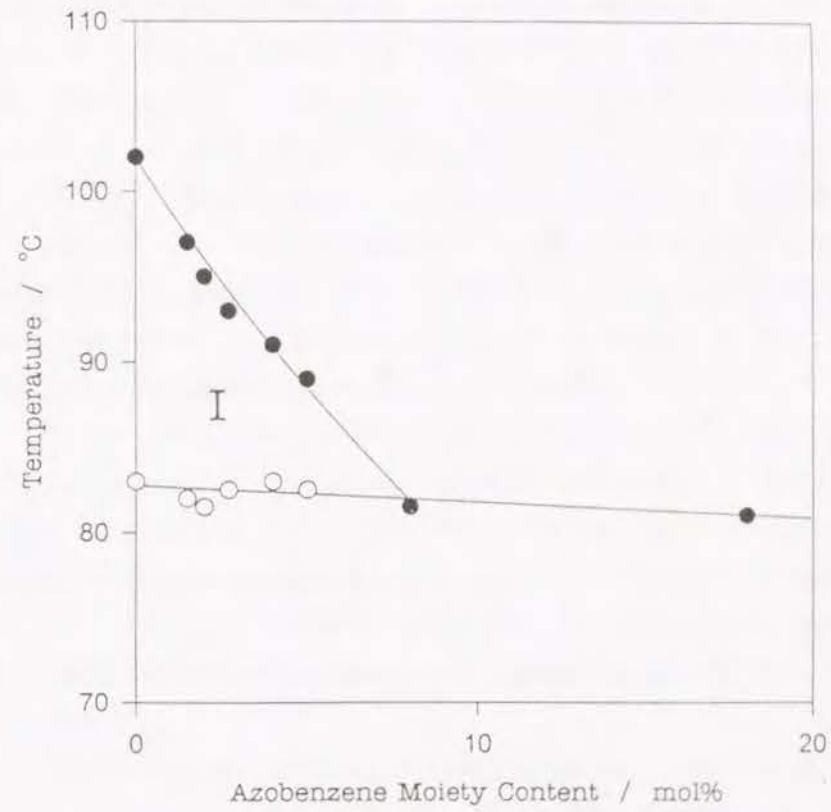

Figure 7-5. Phase diagram of mixtures of APAPA and Eval-Azo; (○) T_{LC}, (●) T_{ISO}. Area I denotes the liquid crystalline state.

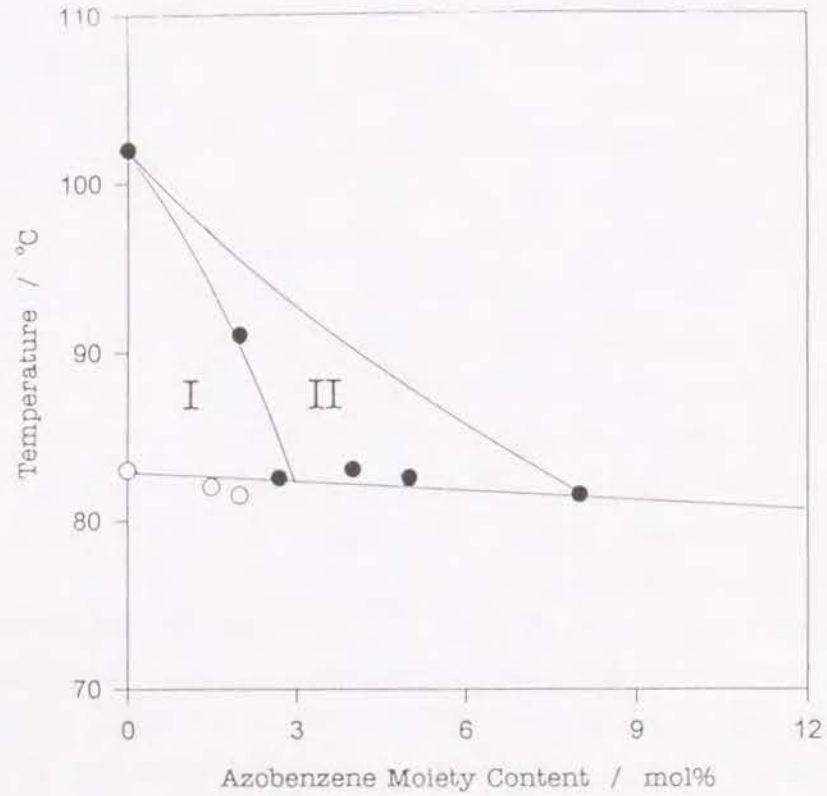

Figure 7-6. Phase diagram of mixtures of APAPA and Eval-Azo after 365 nm irradiation; (○) T_{LC}, (●) T_{ISO}. Area I is liquid crystalline regardless of the irradiation. Area II is liquid crystalline before irradiation and isotropic after irradiation. Photo-induced phase transition occurred in the area II.

7-3-5. Photo-recording of a liquid crystal film mixed with a photosensitive molecule

A liquid crystal mixture containing the low molecular weight photochromic compound (low molecular weight system) and a liquid crystal mixture containing photochromic polymer (polymer system) were prepared. For the low molecular weight system, MAZO 13.8 mol% was doped in MEPC and for the polymer system, Eval-Azo having 4 mol% of azobenzene unit was doped in APAPA . The samples were fabricated on a glass slide and sandwiched with two cover glasses. A half of the film was masked and irradiated with 365 nm light for 30 min at 80℃. The observation by polarized microscope showed that the irradiated part of both samples became isotropic, and the unirradiated part remained in a liquid crystal state. When these samples were cooled down to room temperature, all part of the films became anisotropic because the low molecular weight liquid crystal crystallized at a room temperature.

In the case of the low molecular weight system, the reheating of the system made an anisotropic domains appear in the irradiated part. This is because of the phase separation of MEPC from MAZO in the process of crystallization. MEPC aggregated and separated out, then made a liquid crystal domain in the irradiated part. Furthermore, the boundary between the irradiated part and the unirradiated part became vague because the system became fluid in the liquid crystalline state.

In the polymer mixture, however, reheating of the system made an isotropic phase appear in the irradiated part and an anisotropic phase in the unirradiated part again. The repeated cycles of the phase changes with changing the temperature gradually induced the appearance of anisotropic phase in the irradiated part, since the thermal back reaction of cis to trans isomerization took place gradually.

7-4. Conclusion

The behavior of the liquid crystal formation by adding

photoisomerizable azo compound was studied in this chapter. Three different types of nematic liquid crystal were used for this experiment and a similar behavior was observed among those liquid crystals. The cis form of azobenzene greatly disturbed the formation of liquid crystal. It was confirmed that the liquid crystal formation is controlled by photoisomerization of azobenzene from trans to cis or from cis to trans. For the low molecular weight mixture, the phase separation occurred and decreased the durability of photo-recording. The photo-recorded image for the liquid crystalline mixture with a photosensitive polymer is more stable than that for the low molecular weight system.

References

(1) Heilmeir, G. H.; Zanoni, L. H. *Appl. Phys. Lett.* **1968** *13*, 91.

(2) Steinstrasser, R.; Pohl, L. *Angew. Chem.* **1973**, *85*, 706.

(3) Finkelmann, H. *Angew. Chem. Int. Ed. Engl.* **1987**, *26*, 816.

(4) Ringsdorf, H.; Urban, C. *Makromol. Chem.* **1992**, *193*, 1235.

(5) Cabrera, I.; Krongauz, V.; Ringsdorf, H. *Angew. Chem. Int. Ed. Engl.* **1987**, *26*, 1178.

(6) Eich, M.; Wendorff, J. H. *Makromol. Chem., Rapid Commun.* **1987**, *8*, 67.

(7) Ichimura, K.; Suzuki, Y.; Seki, T.; Hosoki, A.; Aoki, K. *Langmuir* **1988**, *4*, 1214.

(8) Seki, T.; Ichimura, K. *Thin Solid Films* **1989**, *179*, 77.

(9) Aoki, K.; Tamaki, T.; Seki, T.; Ichimura, K. *Langmuir* **1992**, *8*, 1014.

(10) Yamaguchi, H.; Ikeda, T.; Tazuke, S. *Chem. Lett.* **1988**, 539.

(11) Ikeda, T.; Horiuchi, S.; Karanjit, D.B.; Kurihara, S.; Tazuke, S. *Macromolecules* **1990**, *23*, 36.

(12) Ikeda, T.; Horiuchi, S.; Karanjit, D. B.; Kurihara, S.; Tazuke, S. *Macromolecules* **1990**, *23*, 42.

(13) Ikeda, T.; Kurihara, S.; Karanjit, D. B.; Tazuke, S. *Macromolecules* **1900**, *23*, 3938.

(14) Kurihara, S.; Ikeda, T.; Tazuke, S. *Macromolecules* **1990**, *24*, 627.

(15) Kurihara, S.; Ikeda, T.; Sasaki, T.; Kim, H. -B.; Tazuke, S. *Mol. Cryst. Liq. Cryst.* **1991**, *195*, 251.

(16) Kajiyama, T.; Nagata, Y.; Washizu, S.; Takayanagi, M. *J. Membrane Sci.* **1982**, *11*, 39.

(17) Kajiyama, T.; Washizu, S.; Takayanagi, M. *J. Appl. Polym. Sci.* **1984**, *29*, 3955.

(18) Kajiyama, T.; Kikuchi, H.; Shinkai, S. *J. Membrane Sci.* **1988**, *36*, 243.

Chapter 8

Phase Transition Behavior Induced by Photoisomerization for the Side Chain Liquid Crystalline Copolymers with Photochromic Group

8-1. Introduction

Many liquid crystalline polymers have been prepared and their behavior has been studied in detail.[1-5] Thermotropic liquid crystalline polymers are divided into two types; the main chain type and the side chain type.[6,7] The latter shows a liquid crystalline state at lower temperatures than the former. Because of the long chain, the polymer molecule usually has a longer relaxation time of molecular motions and the polymer liquid crystal seems to be far from practical use. However, polymer liquid crystals have an advantage to reserve the chain orientation of liquid crystalline state for a fairly long time. Taking this advantage into consideration, polymer liquid crystals can be used as a recording or memory material.[8-11] Recently, many attempts have been made to develop liquid crystalline side chain polymers for this purpose.

Liquid crystalline molecules accommodate guest molecules in the liquid crystalline state if the structure of the guest molecule is not so different from that of the liquid crystalline host molecule,[5,12,13] However, once the conformation of a guest molecule is photochemically changed from a rodlike form to a sterically obstructing form, e.g., from trans to cis form of azobenzene, it disturbs the liquid crystal structure of the system. Hence, the phase transition between liquid crystalline phase and isotropic phase is controlled photochemically and this phenomenon can be used as a photo-recording system.

Ikeda et al. studied extensively about photochemically induced isothermal phase transition in polymer liquid crystals (PLC).[14] They prepared PLC with azobenzene and examined the chain length effect and molecular weight effect on the photo-induced phase transition behavior.

There are varieties of organic compounds which have potential to improve the phase transition behavior. One of the research projects concerns exploration of new PLC which may provide novel characteristics and give insight into photo-responsive transition behavior. In this chapter, the author studied at the following points. First, the author paid attention to the structure of the copolymer, and chose the chain length of 11 for both mesogenic groups and photochromic groups. This is because the good mobility of the side chain and the effective obstruction by placing the functional groups adjacent to the mesogens are expected. Here, there is no substituent at the para-position of azobenzene group to suppress mesogenic ability of azobenzene group and this is expected to amplify the effect of photoisomerization. Second, the author examined the concentration effect for the phase transition. Furthermore, to simplify the mechanism of photoinduced phase transition, a liquid crystalline homopolymer of azobenzene group was prepared and its phase transition behavior was examined.

8-2. Experimental Section

8-2-1. Materials

Liquid crystalline copolymers were synthesized by the method reported by Shibaev et al.[15] Preparation methods are described below.

Monomer Synthesis

4'-Cyanobiphenyl-4-oxyundecylacrylate (CBO-11-A) was synthesized starting from 4-hydroxy-4'-cyanobiphenyl (Tokyo Kasei) by etherification with ω -bromoundecyl alcohol (Tokyo Kasei). Then this was added dropwise to a methanol solution (10wt%) of 4-hydroxy-4'-cyanobiphenyl and potassium hydroxide. The mixture was refluxed for 8h. After this reaction, this product was recrystallized from benzene twice (yield 45%). After recrystallization, it was treated with acryloyl chloride and triethylamine to yield a mesogenic monomer. After being stirred for 7h at room temperature, this monomer (CBO-11-A) was purified by column chromatography on silica gel using dichloromethane, and finally recrystallized from methanol twice (yield 28%). This is shown in Scheme

8-1.

Phenylazophenyloxyundecylacrylate (ABO-11-A) was synthesized by a similar method as for CBO-11-A. Instead of 4-hydroxy-4'-cyanobiphenyl, 4-hydroxyazobenzene was used as the starting substance. The reaction yield for the etherification with ω-bromoundecyl alcohol is about 30%. The yield of esterification for photosensitive monomer ABO-11-A was 31%. This reaction scheme is shown in Scheme 8-2.

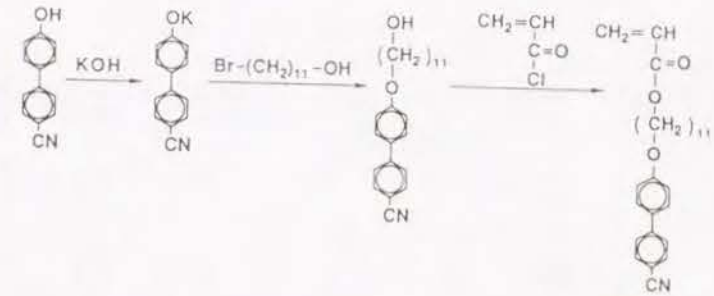

Scheme 8-1

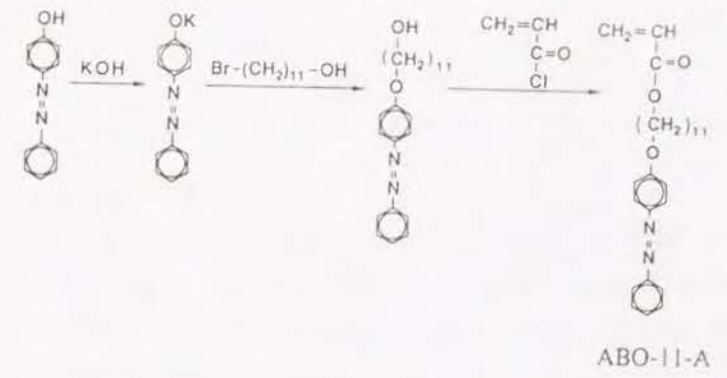

Scheme 8-2

Polymerization.

Monomers were dissolved in benzene with an initiator, azobisisobutyronitrile (AIBN). The reaction vessel was sealed in a degassed condition, then kept at 60℃ for 30 h for polymerization. Here, polymer AZO-X denotes a copolymer of ABO-11-A and CBO-11-A whose ABO-11-A content is X%. Namely, AZO-100 means a homopolymer of ABO-11-A. After polymerization, all the polymers except homopolymer of CBO-11-A were purified twice by the ordinary precipitation method from chloroform solution into hexane. In the case of CBO-11-A, methanol was used as the precipitant. The structures of the copolymers are shown in the following Formula.

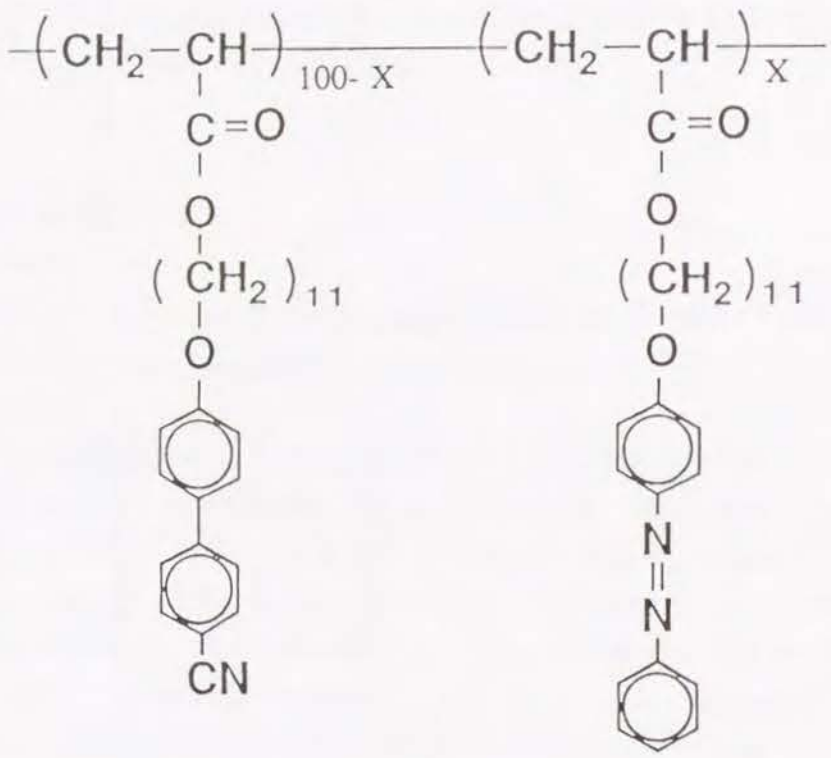

AZO-X

8-2-2. Measurements

The azobenzene unit content of the copolymers was determined by using the elementary analysis, and molecular weight of the copolymers was determined by GPC (Toyo Soda HLC-802UR) calibrated with standard polystyrene. Table 8-1 shows the azobenzene fraction of the copolymers and their molecular weights.

Table 8-1. Characterization of Samples

Sample	Fraction of Azobenzene Group Content mol%	M_w x 100
AZO-0	0.00	98
AZO-9	8.61	120
AZO-20	19.5	98
AZO-24	24.6	150
AZO-49	49.8	150
AZO-67	67.8	130
AZO-87	86.8	98
AZO-100	100.0	77

DSC (Rigaku Thermoflex DSC-8230) measurements were carried out to analyze the thermotropic properties of these polymers. Phase transition behavior was observed by a polarization microscope (Nikon Optiphoto) with an attachment (Ohkura EC5500B) of heating-cooling stage.

For photoisomerization of the azobenzene moieties, the samples were irradiated with 365 nm light from a high pressure mercury lamp (Ushio USH-

102D: 100W) until it reached a photostationary state, e.g., 30 min. Quantitative analysis of photoisomerization of azobenzene in the liquid crystal could not be made since the liquid crystal was turbid. An excimer pulse laser (Lambda Physik EMG 101 MSC: 351nm, 20 ns) was also used to analyze the photoisomerization and the subsequent phase transition. An optical setup, schematically illustrated in Figure 8-1 was used to follow the phase transition behavior of the liquid crystalline system. The sample on the hot stage was irradiated by the excimer laser at various temperatures and the intensity of the transmission light from the He-Ne laser through the crossed polarizer was detected by a photomultiplier.

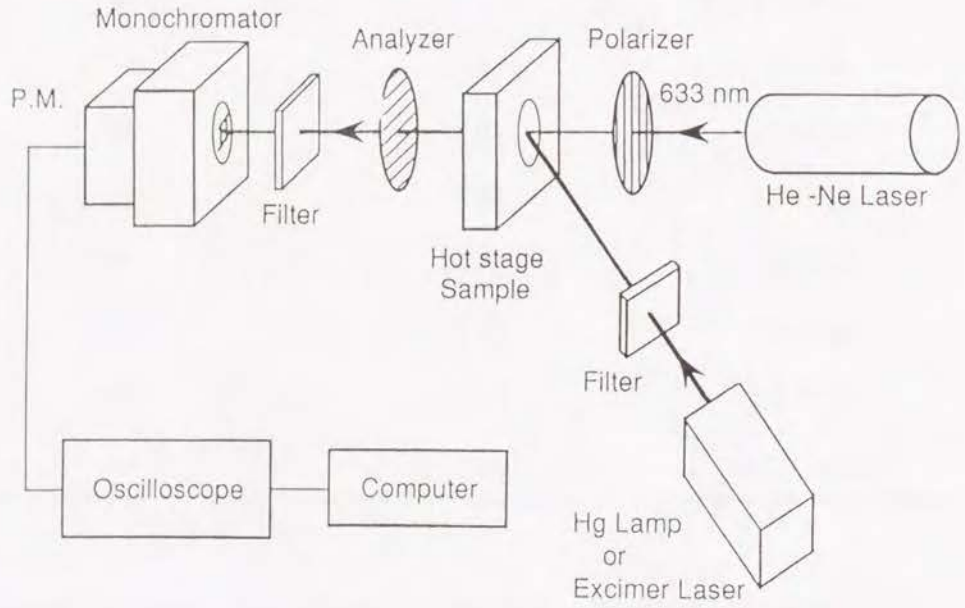

Figure 8-1. Schematic illustration of the optical setup for the response time measurement of phase transition caused by photoisomerization of azobenzene group.

8-3. Results and discussions

8-3-1. Phase diagram of copolymers

Figure 8-2 shows the typical DSC thermogram of AZO-25 on the heating mode. There were two endothermic peaks. The lower and upper peaks were assigned to the glass-liquid crystal transition of the polymer (Tg) and the phase transition from nematic phase to isotropic phase. Similar peaks were also observed in the DSC thermogram on the cooling mode.

The DSC peaks of polymer liquid crystals were summarized in a phase diagram as a function of azobenzene content in Figure 8-3. The temperature range of the liquid crystalline state of this copolymer decreased with increase of the concentration of azobenzene moiety. However, the temperature range of liquid crystal formation remained wide even at the concentration of 50 mol% azobenzene moiety. This is due to the fact that the azobenzene moiety is rigid and acts as a mesogen even though it has no para-substituent such as methoxy group, i. e., homopolymer AZO-100 showed a liquid crystalline state from 69.0℃ to 82.7℃. Samples having a higher content of azobenzene moiety such as AZO-75 and AZO-90 showed three peaks on the DSC thermogram. The highest peak represents T_{ISO} of the sample, and the lowest peak represents the transition from glassy state to liquid crystalline state. However, no change was observed under the polarization microscope at the temperature corresponding to the middle peak of the DSC thermogram. The middle peak increased with the increase of azobenzene moiety and the temperature at the peak maximum approximated the Tg of AZO-100. This suggests that these copolymers have two microscopically discrete regions in which the azobenzene moiety is rich or poor; the microscopic phase separation was occurred though it probably could not be observed under optical microscopy. Namely, two types of liquid crystalline domain exist in the system; one is mainly composed of a cyanobiphenyl group and the other is mainly composed of an azobenzene group. In this copolymer system, there still remains a possibility of a phase transition such as a smectic to nematic transition. Further studies are required.

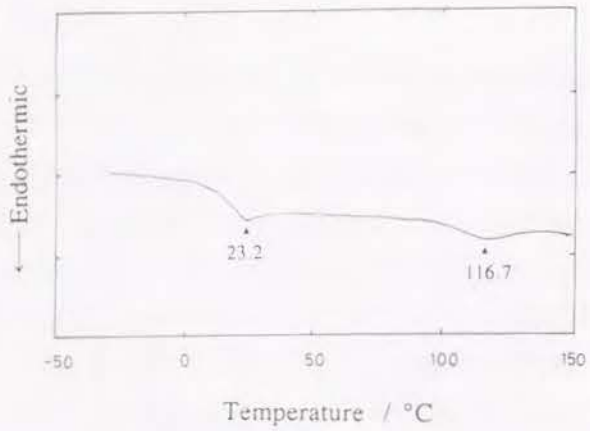

Figure 8-2. DSC diagram of AZO-25 with increasing temperature at a rate of 10 °C/*min*.

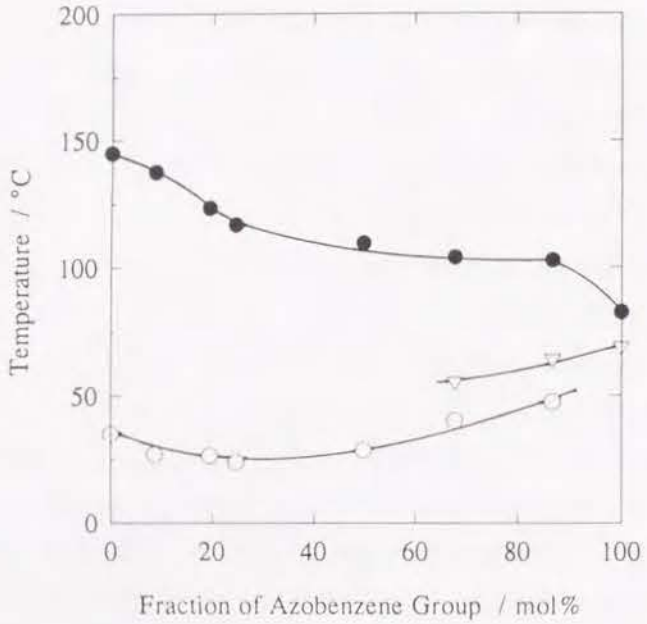

Figure 8-3. Phase diagram of AZO-X based on DSC heating measurements: Open circles represent the transition temperature from glassy state to liquid crystalline state, and closed circles represent the transition temperature to isotropic liquid state.

8-3-3. Phase Transition Induced by UV Irradiation

The phase transition from liquid crystalline to isotropic state was observed using a polarization microscope under crossed polarizers after irradiation of 365 nm from a high pressure Hg lamp. Photoirradiation was carried out until it reached a photostationary state. Owing to the polydispersity of molecular weight of copolymers and moreover polydomain structure of the polymer liquid crystal, this phase transition occurred in a somewhat wider temperature range. T_{ISO} was measured as the temperature in which the transmitted light intensity decreases to 50% of the value in the liquid crystalline state. Copolymers with an azobenzene content lower than 50% did not show the obvious decrease of T_{ISO} by the 365 nm irradiation. However, in copolymers with an azobenzene content higher than 50%, T_{ISO} decreased after the irradiation. The decrease of T_{ISO} after the irradiation became larger with the increase of azobenzene content as shown in Figure 8-4 The cis-formed azobenzene photoisomerized from the trans form obstructed the liquid crystal formation of the copolymers. In a previous chapter, the author studied several mixtures composed of mesogenic group and photosensitive group as photo-induced phase transition systems. One of the mixtures was a low molecular weight azomethine liquid crystal (4'-methoxybenzylidene-4-acetoxyaniline, APAPA) and a photo-sensitive polymer (Eval-Azo) which is a copolymer of ethylene (48 mol%) and vinyl alcohol (52 mol%) (Kurarey, Co. Eval, EP-G 110A), and azobenzene is attached to the hydroxy group.[15] In the Eval-Azo system, irradiation of 365 nm light caused a drastic phase change, in which T_{ISO} decreased from 90℃ to 80℃. The content for the perfect obstruction after irradiation of 365 nm light was only 2.3 mol%. Without irradiation, the content of azobenzene group for the perfect obstruction was more than 7 mol%. Unlike this mixture, the mesogenic group and photochromic group were attached to a polymer main chain in AZO-X copolymers. The photochemically induced phase transition occurred reversibly between liquid crystal phase and isotropic phase by UV irradiation. However, these copolymers required a larger content of azobenzene group to induce the phase transition. Two possible explanations for the large difference between the two systems follow. 1) In the mixed system of

Eval-Azo and APAPA, Eval-Azo does not form a liquid crystalline state. Therefore, it disturbs the formation of the azomethine liquid crystal. On the other hand, AZO-X is a liquid crystalline itself and the azobenzene group assists the mesogenic groups to form a stable liquid crystal. Therefore, a large effect is needed to cause a phase transition from isotropic to anisotropic in this AZO-X copolymer system.

2) T_{ISO} of the AZO-X system is located at a rather high temperature, e.g., 100℃ for X = 67 -87. Consequently, backward thermal isomerization (from cis to trans-form) occurred with a considerably higher rate.

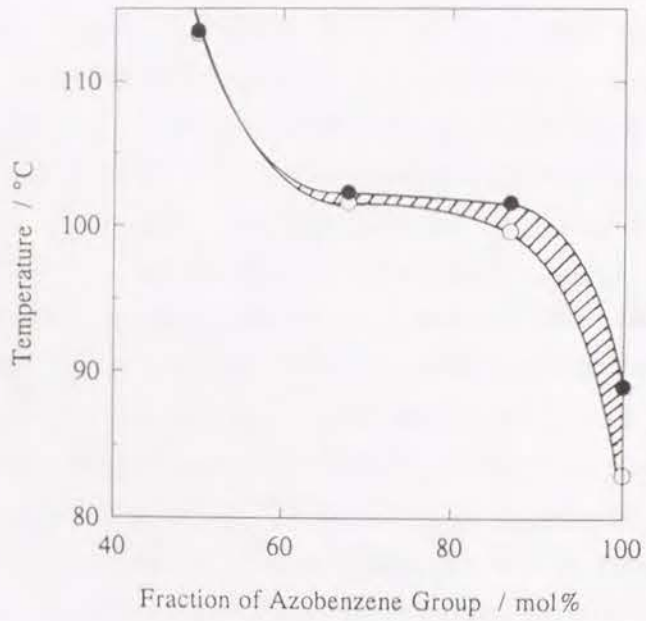

Figure 8-4. Phase diagram of AZO-X before (●) and after (○) 365 nm irradiation at 70℃. It was made by the transmission intensity measurement with polarization microscope: The shaded portion represents the range in which isothermal phase transition was induced by the photo-isomerization of azobenzene group.

For the reasons mentioned above, the liquid crystalline state for the photo-controlled system should have an appropriate temperature range of liquid crystal formation: not too high, not too low. On irradiation below Tg, it was difficult to obtain a high resolution of photo-recording. In the previous chapter, a clear image was obtained in the temperature range which corresponded to the shaded portion of Figure 8-4. Therefore, the T_{ISO} of the liquid crystalline polymer must be low enough to suppress backward thermal isomerization to obtain an effective photo-recording system.

Note that the liquid crystalline polymer is able to keep its memory below Tg, which indicates that the imaged liquid crystal with a liquid crystalline area and isotropic one can be frozen and stored in a glassy state below Tg. On the other hand, a low molecular weight liquid crystal destroys its memory once it is cooled down below Tg because it is crystallized in the whole part.

8-3-4. Response Time of the Phase transition

As mentioned in the introduction, AZO-100 polymer was prepared for measuring response time of the phase transition. The system can be regarded as homogeneous because the sample is homopolymer of azobenzene unit. The side chain provides both photochromic and liquid crystalline characters when most azobenzene groups are in the trans form. One can escape from the trivial effect resulting from to the microstructure of copolymers. This system will demonstrate a photoinduced phase transition simply by the isomerization of azobenzene groups.

Nano-second pulse of 351 nm from the excimer laser was used in order to measure the response time of the phase transition after the irradiation. Phase transition behavior of this liquid crystalline system was followed by the transmission of polarized light. Figure 8-5 shows the decrease of transmission intensity after pulse irradiation for AZO-100 polymer at 80℃. The rate of photoisomerization of azobenzene in solution is known to be in the nano-second range,[18] so this intensity change shows the rate of the phase transition of the samples from anisotropic to isotropic phase caused by the photo-isomerization.

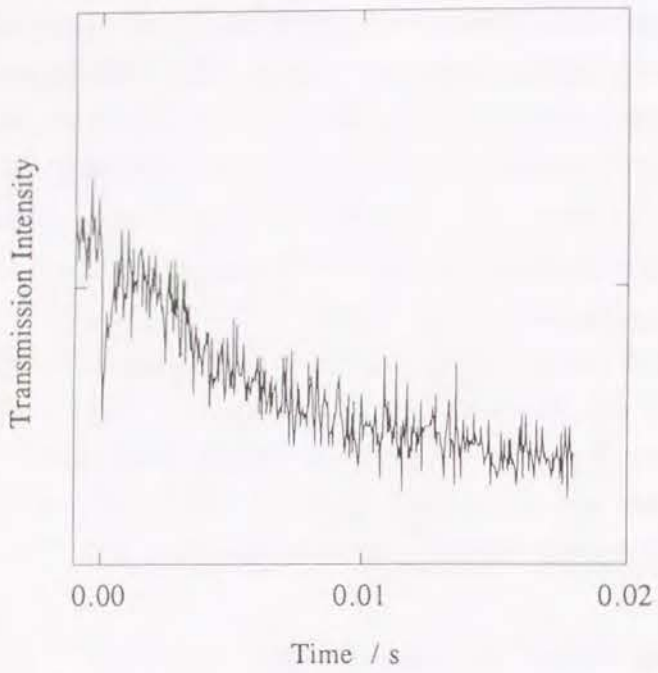

Figure 8-5. Transient transmission intensity after 351 nm pulse excitation; AZO-100 at 80℃

Table 8-2. Response Time for Phase Transition of AZO-100

Temperature	Response Time
℃	*ms*
70	600
80	10

The response time was determined by measuring the decrease of light intensity through crossed polarizer from 90% to 10% of its initial intensity. Table 8-2 shows the response times for phase transition at 70℃ and 80℃. The AZO-100 polymer forms liquid crystals at both temperatures and their reduced temperatures (T / T_{ISO}) are 0.85 and 0.97, respectively. The higher the reduced temperature, the faster the phase transition occurred in the liquid crystalline state. The phase transition of liquid crystal took place in the range from a few *ms* to several hundreds *ms* for these copolymer systems. The response time at 80℃ was measured to be 10 *ms*. For low molecular weight liquid crystals under an electric field, the same order of response time can be obtained though the process of the response system is rather different from this case. The polymer liquid crystal usually requires a long response time of phase transition compared to the response time of low molecular weight liquid crystals. Then this fast response can be ascribed to high mobility of a long alkyl spacer at a high temperature. The increase of temperature decreases the response time of phase transition from anisotropic to isotropic phase very steeply.

The backward thermal-isomerization takes place inevitably with increase of temperature. This thermal effect is not so large for AZO-100 because the irradiation temperatures can be kept below 80℃, while it affects significantly AZO-X (X = 0 - 87) copolymers owing to the high irradiation temperature such as 100℃. Thus, it was difficult to determine quantitatively the response times of phase transition for these copolymers. However, the tendency of temperature dependence of response time for these copolymers was the same as that of AZO-100. Further investigation of the liquid crystal domain structure will be required to understand the mechanism of isothermal phase transition.

8-4. Conclusion

Copolymers having various contents of CBO-11-A and ABO-11-A were prepared. All samples showed a liquid crystalline state, but the increasing of azobenzene content narrowed the temperature range of liquid crystalline state.

Isothermal phase transition occurred by the irradiation of 365 nm light for the samples with an azobenzene content of more than 50 mol%. The response time for AZO-100 varied from a few *ms* to several hundred *ms* by changing the temperature from 80 ℃ to 70℃.

References

(1) Ringsdorf, H.; Schmidt, H. -W. Baur, G.; Kiefer, R. *Recent Advances in Liquid Crystalline Polymer* chap. 16, Chapoy, L.L., Ed., Elsevier Appl. Sci., Pub., London, 1985.

(2) Gray, G. W. *Thermotropic Liquid Crystals* Gray, G. W. Ed., John Wiley, New York, 1987.

(3) *Polymeric Liquid Crystals* Blumstein, A. Ed., Plenum Press, New York, 1985.

(4) Ciferri, A.; Krigbaum, W. R.; Meyer, R. B. *Polymer Liquid Crystals* Academic Press, New York, 1982.

(5) Finkelmann, H. *Angew. Chem. Int. Ed. Engl.*, **1987**, *26*, 816.

(6) Sagane, T.; Lenz, R. W. *Macromolecules*, **1989**, *22*, 3763.

(7) Imrie, C. T.; Karasz, F. E. *Macromolecules*, **1992**, *25*, 1278.

(8) Ringsdorf, H.; Urban, C. *Makromol. Chem.*, **1992**, *193*, 1235.

(9) Cabrera, I.; Krongauz, V.; Ringsdorf, H. *Angew. Chem. Int. Ed. Engl.*, **1987**, *26*, 1178.

(10) Eich, M.; Wendorff, J. H. *Makromol. Chem., Rapid Commun.*, **1987**, *8*, 67.

(11) (a) Ichimura, K.; Suzuki, Y.; Seki, T.; Hosoki, A.; Aoki, K. *Langmuir*, **1988**, *4*, 1214. (b) Seki, T.; Ichimura, K. *Thin Solid Films*, **1989**, *179*, 77. (c) Aoki, K.; Tamaki, T.; Seki, T.; Ichimura, K. *Langmuir*, **1992**, *8*, 1014.

(12) Heilmeir, G. H.; Zanoni, L. A. *Appl. Phys. Lett.*, **1968**, *13*, 91.

(13) Steinstrasser, R.; Pohl, L. *Angew. Chem.*, **1973**, *85*, 706.

(14) (a) Ikeda, T.; Horiuchi, S.; Karanjit, D. B.; Kurihara, S.; Tazuke, S. *Macromolecules*, **1990**, *23*, 36. (b) Ikeda, T.; Horiuchi, S.; Karanjit, D. B.; S. Kurihara, S.; Tazuke, S. *Macromolecules*, **1990**, *23*, 42. (c) Ikeda, T.; Kurihara, S.; Karanjit D. B.; Tazuke, S. *Macromolecules*, **1990**, *23*, 3938. (d) Kurihara, S.; Ikeda, T.; Tazuke, S. *Macromolecules*, **1990**, *24*, 627. (e) Kurihara, S.; Ikeda, T.; Sasaki, T.; Kim, H. -B.; Tazuke, S. *Mol. Cryst. Liq. Cryst.*, **1991**, *195*, 251.

(15) Shibaev, V.; Kostromin, S. G.; Plate, N. A. *Makromol. Chem. Rapid Commun.*, **1981**, *2*, 651.

(16) Irie, M.; Schnabel, W. *Macromolecules*, **1985**, *18*, 394.

Summary

In Chapter 1, the structural relaxation of Langmuir-Blodgett (LB) films of poly(vinyl pentanal acetal) (PVPe) was examined by the interlayer energy transfer from energy donor to acceptor moieties labeled to the polymer chain. The polymer monolayer on a water surface was successively deposited on a solid substrate as a two-dimensional form, but after the deposition, thermal relaxation of the layered structure occurred at elevated temperatures. The spatial order of multilayers was irreversibly disordered and mixed by the thermal treatment. The structural relaxation clearly proceeded at temperatures higher than the glass transition temperature. Theoretical calculations based on Förster kinetics were applied to this phenomenon, which was well simulated by assuming a Gaussian distribution of chromophores in the direction normal to the layer plane. The fitting with the experimental data allowed the evaluation of the diffusion constant of polymer segments in the order of 10^{-16} - 10^{-18} cm^2 s^{-1} and the apparent activation energy of 150 kJ mol^{-1}. The diffusion process of polymer segments in the ultrathin LB films could be examined by the energy transfer method.

In Chapter 2, several polymer LB films of poly(vinyl alkanal acetal) which have different hydrophobic chain lengths were made with a thickness of only 1 nm per layer. The structural change in the nanometer dimension could be sensitively and quantitatively examined by the use of energy transfer between fluorescent chromophores incorporated into each layer. The diffusion constants observed as a function of temperature were in the order of 10^{-18} - 10^{-15} cm^2 s^{-1}. The thermal properties of the LB films were well characterized by the glass transitions of bulk polymers.

In Chapter 3, the thermal stability of Langmuir-Blodgett (LB) films of various polymers, poly(vinyl octanal acetal) (PVO), poly(diisopropyl fumarate) (PDiPF), poly(dicyclohexyl fumarate) (PDcHF), and poly(isobutyl methacrylate) (PiBMA), were examined. The energy transfer method was employed for studying the structural relaxation of these films in which a pair of energy donating and

accepting PVO layers were incorporated as the probes for the observation of the relaxation of the layered structure. In the temperature range between 30℃ and 120℃, all these polymer LB films showed structural relaxation. A close relationship between the structural relaxation of polymer LB films and the glass transition temperature, Tg, of the corresponding polymer bulk, was observed. Although the fumarate polymers did not show clear Tg in the temperature range observed, the structural relaxation of LB films was observed and this was attributed to the short-range motions of the polymer chain; the DSC also showed a transition as a small signal. After the thermal treatment, the miscible LB films composed of PVO's provided an energy transfer efficiency expected for a random distribution of the chromophores, whereas the other polymer LB films showed phase separation between the probing layers and the examined layers. For PiBMA-LB film, the rapid progress of phase separation was observed owing to the long-range motions of the polymer segment at temperatures higher than Tg. For PDiPF-LB film and PDcHF-LB film, the phase separation proceeded gradually because only a short-range motion of the polymer was involved in the process. The effects of molecular weight and the initial spatial arrangement of each layer indicated that the relaxation process is governed by the rate of diffusion of each polymer.

In Chapter 4, the structural relaxation of the Langmuir-Blodgett (LB) films composed of cadmium stearate and poly(vinyl octanal acetal) was examined by the interlayer energy transfer method and transmission electron microscopy (TEM). The energy transfer method is very sensitive to the alteration of layer distance, i. e., to the microscopic structural relaxation of the layered structure. The layered structure in the LB film was lost at the melting temperature (T_m) of the stearate layers. The disordering process proceeded irreversibly and the heat treatment above the melting temperature (T_m) completely destroyed the structure within a few minutes. Different types of disordered structures were observed by TEM in three temperature ranges. Heating at temperatures lower than T_m yielded wrinkles of the film, but no aggregation of cadmium salt was observed. At a temperature near T_m, the crystalline structure of cadmium stearate grew gradually.

At a temperature higher than T_m, cadmium stearate completely dissolved and two distinct phases were observed in the TEM image; one corresponding to the polymer chain stained with cadmium and the other corresponding to cadmium stearate. Several hours were required for the occurrence of the structural change in the scale observed by TEM. The structural relaxation process of cadmium stearate LB films could be determined clearly by the energy transfer method and TEM observation .

In Chapter 5, photoreactive Langmuir-Blodgett films were made of poly(vinyl octanal acetal-*co*-vinyl cinnamate) (P(VO-VC)), and the effect of photocrosslinking on the stability of a layered structure against thermal and chemical treatments was demonstrated by the energy transfer and the surface plasmon spectroscopy. Photochemical crosslinking in P(VO-VC) layers easily occurred by UV irradiation for a few minutes, and consequently the polymer became insoluble in a good solvent, dichloromethane. The durability against the solvent was measured by both UV absorption and surface plasmon resonance. A clear contrast between the irradiated part and non-irradiated part was seen in the picture taken by a surface plasmon microscope. The curing effect on the thermal relaxation of the layered structure was studied by the energy transfer method, which is very sensitive to changes in the layer distance. These findings indicated that photochemical crosslinking of the LB film greatly improved the thermal stability without any serious disordering of the layered structure.

In Chapter 6, fluorescence spectroscopy was introduced for in situ studies of the structure and properties of monolayer films, especially of preformed polymer films at the air/water interface. Poly(vinyl alkanal acetal)s were synthesized and a part of the side chains were labeled with pyrene chromophores. The fluorescence intensity and lifetime of pyrenes were strongly quenched by oxygen in the air. The surface film sensitively responded to the surrounding changes. This behavior could be used as a probing technique for the packing state of the monolayer. The excimer formation of pyrenes revealed the dynamic behavior of the monolayer. Time-resolved measurements showed a clear rise of excimer emission, i.e., the excimer was formed by microscopic diffusion of polymer

segments. These findings indicated that the monolayer maintained the mobility even in the condensed phase. Fluorescence spectroscopy provides molecular information and is a valuable technique for the studies of the monolayers in situ.

In Chapter 7, the photoisomerization of azobenzene moiety was utilized for the control of liquid crystal formation. A polymer having an azobenzene moiety as a side chain was synthesized by esterification of the OH groups of the polymer. Liquid crystal formation was examined with the mixture of azobenzene moiety (photo-sensitive molecule) and a liquid crystalline compound. Two types of mixture were examined by DSC and polarizing optical microscope; one was the mixture of low molecular weight photosensitive molecules with low molecular weight liquid crystals, and the other was the mixture of a photosensitive polymer with low molecular weight liquid crystals. The temperature range of liquid crystal formation of this mixture decreased linearly with the increase of the concentration of azobenzene moiety in both systems. The liquid crystal formation was confirmed to be controlled by photoisomerization of azobenzene (trans to cis structural change). The liquid crystalline mixture of photo-sensitive polymer showed better resistability in the recording image than that of *p*-methoxy-azobenzene.

In Chapter 8, liquid crystalline copolymers containing 4'-cyanobiphenyl-4-oxyundecylacrylate (CBO-11-A) groups and phenylazophenyloxy-undecylacrylate (ABO-11-A) groups with various proportions were synthesized. The copolymers took a highly liquid crystalline state but the temperature range of the liquid crystalline state was narrowed with increasing azobenzene content. Isothermal phase transition of the copolymers was induced by the photoisomerization of the azobenzene moiety with irradiation of 365 nm light. The response time of this phase transition was measured using an excimer pulse laser (351 nm). It took from a few ms to several hundred ms at 70 - 80℃ to cause a phase transition in these liquid crystalline systems.

List of Publications

Chapter 1

(1) **Polymer Diffusion in a Layered Structure of Poly(vinyl pentanal acetal) Langmuir-Blodgett Films Studied by the Energy Transfer Method**
Hayashi, T.; Okuyama, T.; Ito, S.; Yamamoto, M. *Macromolecules* **1994**, *27*, 2270.

Chapter 2

(2) **Diffusion of Polymer Segments in Ultra-thin Polymer Films Prepared by the Langmuir-Blodgett Technique**
Yamamoto, M.; Kawano, K.; Okuyama, T.; Hayashi, T.; Ito, S. *Proc. Japan Acad.* **1994**, *70(B)*, 121.

Chapter 3

(3) **Thermal Stability in Nanometer Level of Polymeric Langmuir-Blodgett Films Studied by the Energy Transfer Method**
Hayashi, T.; Ito, S.; Yamamoto, M.; Matsumoto, A. *Polymer, Submitted*

Chapter 4

(4) **Thermal Relaxation Process of Stearate LB Film Sandwiched by Chromophoric Polymer LB Layers Studied by the Energy Transfer Method and Transmission Electron Microscopy**
Hayashi, T.; Ito, S.; Yamamoto, M.; Tsujii, Y.; Matsumoto, M.; Miyamoto, T. *Langmuir* **1994**, *10*, 4142.

Chapter 5

(5) **Photochemical Stabilization of Ultrathin Polymer Films Prepared by Langmuir-Blodgett Technique**
Hayashi, T.; Mabuchi, M.; Mitsuishi, M.; Ito, S.; Yamamoto, M.; Knoll, W. *Macromolecules* **1995**, *28*, 2537.

Chapter 6

(6) **Fluorescence Spectroscopy for a Polymer Monolayer at the Air / Water Interface**
Ito, S.; Oki, S.; Hayashi, T.; Yamamoto, M. *Thin Solid Films*, **1994**, *244*, 1073.

Chapter 7

(7) **Liquid Crystal Formation Control of Azobenzene-Liquid Crystal Mixtures by Photoisomerization of Azobenzene**
Onogi, Y.; Hayashi, T.; Yamamoto, M. *Nippon Kagakukaishi*, **1990**, *3*, 250.

(8) **Liquid Crystal Formation Control of Polymer-Liquid Crystal Mixtures by Photoisomerization of Azobenzene Moiety**
Onogi, Y.; Hayashi, T.; Mizushima, Y.; Yamamoto, M. *Nippon Kagakukaishi*, **1990**, *8*, 815.

Chapter 8

(9) **Phase Transition of Side Chain Liquid Crystalline Copolymers with Photochromic Group**
Hayashi, T.; Kawakami, H.; Doke, Y.; Tsuchida, A.; Onogi, Y.; Yamamoto, M. *Eur. Polym. J.*, **1995**, *31*, 23.

Acknowledgements

The studies presented in this thesis were carried out at the Department of Polymer Chemistry, Graduate School of Engeneering , Kyoto University from 1988 to 1993 under the guidance of Professor Masahide Yamamoto. The author wishes to express his sincere gratitude to invaluable guidance and discussions throughout the course of this work.

Grateful acknowledgement is due to Professor Takeaki Miyamoto, Institute for Chemical Research, Kyoto University, for making the transmission electron microscopy (TEM) available for the work and constant encouragement.

The author wants to express his deep gratitude to Associate Professor Shinzaburo Ito, Department of Polymer Chemistry, Kyoto University for his invaluable guidance and discussions throughout this work. He also wants to express his sincere appreciation to Professor Yoshihiko Onogi, Mukogawa Women's University for his precious guidance and discussions throughout this work.

The author is indebted to Dr. Mutsuo Matsumoto, Institute for Chemical Research, Kyoto University, for his valuable guidance of TEM measurement. The author also indebted to Dr. Akikazu Matsumoto, Department of Applied Chemistry, Osaka City University, for generously providing him with poly (dialkyl fumarate)s.

The author greatly thanks Professor Hitoshi Yamaoka, Department of Polymer Chemistry, Kyoto University, for making the DSC available for his present work.

The author wishes to thank Dr. Akira Tsuchida and Mr. Masataka Ohoka for various helpful discussions and suggestions. The author also wishes to thank to Dr. Yoshinobu Tsujii, Institute for Chemical Research, Kyoto University, for his helpful discussions. The author thanks to Mr. Masayoshi Ohara for the fabrication of TEM samples. A grateful acknowledgement is due to Associate

Professor Yoshiro Yonezawa, Associate Professor Mitsuo Kawasaki, and Dr. Tomoo Sato, Department of Industrial Chemisty, Kyoto University, for their guidance on the Langmuir-Blodgett technique and measurements of ellipsometry. The author wishes to thank Mr. Yoshiharu Honda, Environmenta Preservation Center, Kyoto University, for the measurement of atomic absorption spectroscopy. Thanks are also expressed to Dr. Gregory W. Haggquist for his useful discussion and help.

Finally, the author would like to express his sincere appreciation to all of the colleagues for useful suggestions, particularly to Messrs.Yasuyuki Mizushima, Yasuo Doke, Takayoshi Ueno, Tsuyoshi Okuyama, Satoshi Oki, Hirofumi Kawakami, Kenji Kawano, Masaya Mitsuishi, and Michiaki Mabuchi for their active collaborations in a part of the study.

November, 1995

Takanori Hayashi

Errata

page	line	printed	should read
1	8	system	systems
6	14	Kilstreiter, Leitner	Kilstreiter, and Leitner
10	19	a	an
19	11	electrical	electronic
40	22	In this chapter assumed	In this chapter,
42	7	a LB film	an LB film
43	20	is	are
46	22	theortical	theoretical
62	5	at100℃	at 100℃
66	15	heterogenious	heterogeneous
83	11	a	an
	13	et. al.	et al.
85	4	Under	Below
93	13	highly	high
94	9	demonstrate	demonstrates
96	1	PVO,PVO-P and PVO-A	PVO-P and PVO-A
119	15	transfered	transferred
	26	devided	divided
121	2	functions	function
122	30	values is decreases	values decreases
133	4	4,4'-di-n-hexyloxydiphenyl	4,4'-di-*n*-hexyloxydiphenyl